

**UTILIZING DISTRIBUTED TEMPERATURE SENSORS IN PREDICTING
FLOW RATES IN MULTILATERAL WELLS**

A Dissertation

by

JASSIM MOHAMMED A. ALMULLA

Submitted to the Office of Graduate Studies of
Texas A&M University
in partial fulfillment of the requirements for the degree of

DOCTOR OF PHILOSOPHY

May 2012

Major Subject: Petroleum Engineering

**UTILIZING DISTRIBUTED TEMPERATURE SENSORS IN PREDICTING
FLOW RATES IN MULTILATERAL WELLS**

A Dissertation

by

JASSIM MOHAMMED A. ALMULLA

Submitted to the Office of Graduate Studies of
Texas A&M University
in partial fulfillment of the requirements for the degree of

DOCTOR OF PHILOSOPHY

Approved by:

Chair of Committee,	Ding Zhu
Committee Members,	Gene Beck
	David Schechter
	Mahmoud El-Halwagi
Head of Department,	Dan Hill

May 2012

Major Subject: Petroleum Engineering

ABSTRACT

Utilizing Distributed Temperature Sensors in Predicting Flow

Rates in Multilateral Wells. (May 2012)

Jassim Mohammed A. Almulla, B.S., University of Louisiana at

Lafayette;

M.S., Texas A&M University

Chair of Advisory Committee: Dr. Ding Zhu

The new advancement in well monitoring tools have increased the amount of data that could be retrieved with great accuracy. Downhole pressure and temperature could be precisely determined now by using modern instruments. The new challenge that we are facing today is to maximize the benefits of the large amount of data that is being provided by these tools and thus justify the investment of more capital in such gadgets. One of these benefits is to utilize the continuous stream of temperature and pressure data to determine the flow rate in real time out of a multilateral well. Temperature and pressure changes are harder to predict in horizontal laterals compared with vertical wells because of the lack of variation in elevation and geothermal gradient. Thus the need of accurate and high precision gauges becomes critical. The trade-off of high resolution sensors is the related cost and resulting complication in modeling. Interpreting measured data at real-time to a downhole flow profile in multilateral and horizontal wells for production optimization is another challenge.

In this study, a theoretical model is developed to predict temperature and pressure in trilateral wells based on given flow conditions. The model is used as a forward engine in the study and inversion procedure is then added to interpret the data to flow profiles. The forward model starts from an assumed well flow pressure in a specified reservoir with a defined well structure. Pressure, temperature and flow rate in the well system are calculated in the motherbore and in the laterals. These predicted temperature and pressure profiles provide the connection between the flow conditions and the temperature and pressure behavior.

Then we use an inverse model to interpret the flow rate profiles from the temperature and pressure data measured by the downhole sensors. A gradient-based inversion algorithm is used in this work, which is fast and applicable for real-time monitoring of production performance. In the inverse model, the flow profile is calculated until the one that generates the matching temperature and pressure profiles in the well is identified. The production distribution from each lateral is determined based on this approach.

At the end of the study, the results showed that we were able to successfully predict flow rates in the field within 10% of the actual rate. We then used the model to optimize completion design in the field.

In conclusion, we were able to build a dependable model capable of predicting flow rates in trilateral wells using pressure and temperature data provided by downhole sensors.

DEDICATION

This work is dedicated:

To my grandmother, Aisha, who passed away while I was away pursuing my PhD. She never failed to make me feel special and that is why she will hold a special place in my heart as long as that heart is beating.

ACKNOWLEDGEMENTS

Praise and gratitude be to the Almighty, Allah, the Creator and Governor of the Universe and his Prophet Mohammed, peace be upon him.

Thanks to my parents for being my guiding star all through my life. I would have never achieved anything in my life without them. Thanks to my wife for being so loving and patient while I'm finishing my studies; I love you Salma. Thanks to my kids that had to live away from home and away from their grandparents and friends. Thanks to my brothers and sisters for being so supportive and for all their encouragements and prayers. Thanks to my best friend, Majed Alomrani, for being my backbone in more ways than he knows.

I wish to express my sincere appreciation to Saudi Aramco for giving me this opportunity to achieve my dream by getting such a degree from a prestigious university, Texas A&M.

I would like to thank the chairman of my graduate advisory committee, Dr. Ding Zhu, for her unlimited support without which this research could have never been completed and above all for being the kind person that she is. I, also, would like to thank Dr. David Schechter, Dr. Gene Beck and Dr. Mahmoud El-Halwagi for serving as members of my advisory committee.

Last but not least, I would like to thank Rashad Al Zahrani, Marwan Zarea, Mohammad Tabtabaei, Chen Yang, Keita Yoshioka, Weibo Sui and Fahad Alrashed for their contributions towards my research.

TABLE OF CONTENTS

	Page
ABSTRACT	iii
DEDICATION	v
ACKNOWLEDGEMENTS	vi
TABLE OF CONTENTS	vii
LIST OF FIGURES.....	ix
LIST OF TABLES	xiii
NOMENCLATURE.....	xiv
 CHAPTER	
I INTRODUCTION	1
1.1 Background	1
1.2 Literature Review	3
1.3 Objectives.....	8
II FORWARD MODEL	9
2.1 Introduction	9
2.2 Wellbore Model.....	10
2.2.1 Single-Phase Wellbore Flow Model	11
2.2.2 Single-Phase Wellbore Thermal Model	16
2.2.3 Two-Phase Wellbore Flow Model	21
2.2.4 Two-Phase Wellbore Thermal Model	27
2.3 Reservoir Model.....	28
2.3.1 Single-Phase Reservoir Flow Model.....	29
2.3.2 Two-Phase Reservoir Flow Model.....	32
2.3.3 Reservoir Thermal Model	33
2.4 Coupled Model.....	37
2.4.1 Coupled Pressure Model	37
2.4.2 Coupled Temperature Model	43
2.5 Forward Model Results	45
2.5.1 Introduction	45
2.5.2 Base Case	45

CHAPTER	Page
2.5.3 Case 2	51
2.5.4 Case 3	55
2.5.5 Cases Comparison	60
2.5.6 Sensitivity Analysis	63
III INVERSE MODEL	69
3.1 Introduction	69
3.2 Least-Square Regression	69
3.3 Markov Chain Monte Carlo	71
3.4 Procedure	73
3.5 Inverse Results	74
IV FIELD APPLICATION	80
4.1 Introduction	80
4.2 Field Case	80
4.3 Procedure	84
4.4 Results and Discussion	86
V MULTILATERAL WELL STRUCTURE DESIGN FOR OPTIMAL PRODUCTION	97
5.1 Introduction	97
5.2 Conditions for the Study	98
5.3 Results	99
5.3.1 Case One	99
5.3.2 Case Two	102
5.3.3 Case Three	105
5.3.4 Case Four	107
5.3.5 Case Five	110
5.4 Discussion	112
VI CONCLUSION	113
REFERENCES	116
VITA	124

LIST OF FIGURES

FIGURE	Page
1.1 Multilateral Well Diagram	1
2.1 Forward Model Breakdown	10
2.2 Wellbore Differential Volume Elements.....	11
2.3 Babu and Odeh Physical Model	29
2.4 Radial and Linear Flow	34
2.5 Coupled Model Segmentation Schematic	38
2.6 Schematic of Flow across ICV	40
2.7 Coupled Pressure Model Calculations Flowchart	42
2.8 Well Layout.....	46
2.9 Base Case Pressure Profiles	48
2.10 Base Case Temperature Profiles	49
2.11 Motherbore Pressure Profile for the Base Case	50
2.12 Motherbore Temperature Profile for the Base Case.....	50
2.13 Case 2 Pressure Profiles	52
2.14 Case 2 Temperature Profiles	53
2.15 Motherbore Pressure Profile Case 2.....	54
2.16 Motherbore Temperature Profile Case 2	55
2.17 Case 3 Pressure Profiles	57

2.18	Case 3 Temperature Profiles	58
2.19	Motherbore Pressure Profile Case 3	59
2.20	Motherbore Temperature Profile Case 3	59
2.21	Motherbore Pressure Profiles for all Cases	61
2.22	Motherbore Temperature Profiles for all Cases	62
2.23	Cumulative Production Rates in all Cases	62
2.24	Pressure Profiles in Motherbore with Different Permeabilities	64
2.25	Temperature Profiles in Motherbore with Different Permeabilities	64
2.26	Pressure Profiles in Motherbore	67
2.27	Temperature Profiles in Motherbore	67
3.1	Inverse Model Flowchart	74
3.2	Motherbore Pressure Profile for the Base Case	75
3.3	Motherbore Temperature Profile for the Base Case.....	76
3.4	Flow Rate Distribution for the Base Case	77
3.5	Motherbore Temperature Profiles	78
3.6	Cumulative Production Rates in all Cases	78
4.1	Field Case Well Configuration.....	81
4.2	Lateral 1 Production Test	85
4.3	Lateral 2 Production Test	85
4.4	Lateral 3 Production Test	86
4.5	Temperature Profiles in Lateral 1.....	87
4.6	Temperature Profiles in Lateral 2.....	88

4.7	Temperature Profiles in Lateral 3.....	89
4.8	Temperature Profiles in Motherbore	90
4.9	Lateral 1 Temperature Reading during Production Test.....	92
4.10	Lateral 2 Temperature Reading during Production Test.....	92
4.11	Lateral 3 Temperature Reading during Production Test.....	93
4.12	Pressure Profiles in Laterals.....	95
4.13	Pressure Profile in Motherbore	96
5.1	Case 1 Temperature Profiles in Lateral 1	100
5.2	Case 1 Temperature Profiles in Lateral 2.....	101
5.3	Case 1 Temperature Profiles in Lateral 3.....	101
5.4	Case 1 Temperature Profiles in Motherbore	102
5.5	Case 2 Temperature Profiles in Lateral 1	103
5.6	Case 2 Temperature Profiles in Lateral 2.....	103
5.7	Case 2 Temperature Profiles in Lateral 3.....	104
5.8	Case 2 Temperature Profiles in Motherbore	104
5.9	Case 3 Temperature Profiles in Lateral 1	105
5.10	Case 3 Temperature Profiles in Lateral 2.....	106
5.11	Case 3 Temperature Profiles in Lateral 3.....	106
5.12	Case 3 Temperature Profiles in Motherbore	107
5.13	Case 4 Temperature Profiles in Lateral 1	108
5.14	Case 4 Temperature Profiles in Lateral 2.....	108
5.15	Case 4 Temperature Profiles in Lateral 3.....	109

5.16	Case 4 Temperature Profiles in Motherbore	109
5.17	Case 5 Temperature Profiles in Lateral 1	110
5.18	Case 5 Temperature Profiles in Lateral 2	111
5.19	Case 5 Temperature Profiles in Lateral 3	111
5.20	Case 5 Temperature Profiles in Motherbore	112

LIST OF TABLES

TABLE	Page
2.1 Kutateladze Numbers	25
2.2 CV Values at different ICV Increments	41
2.3 Base Case Data Input	47
2.4 Base Case Results.....	51
2.5 Case 2 Results	55
2.6 Case 3 Results	60
2.7 Varied Permeability Flow Rates	65
2.8 Flow Rates in Varied Lengths Study.....	66
3.1 Flow Rates Distribution of all Cases.....	79
4.1 Field Case Properties.....	83
4.2 Field Rate Test	84
4.3 Temperature Comparison.....	91
4.4 Production Rates Comparison	94
4.5 Pressure Drop in Laterals	95
5.1 Cases Laterals Summary	98
5.2 Cases Production Summary	99

NOMENCLATURE

A	drainage area
A_{pipe}	cross-sectional area of pipe
a	reservoir length
B_o	oil formation volume factor
b	reservoir width
C_H	shape factor
C_n	covariance matrix
C_p	heat capacity
CV	control valve coefficient
D	diameter
D^*	dimensionless diameter
d	vector of observed data
E_{KE}	kinetic energy
E_{VS}	viscous shear energy
e	energy flux vector
F	function
f	friction factor
$f(x)$	objective function
G	sensitivity matrix of forward model
g	acceleration of gravity

$g(x)$	forward model
H	Hessian matrix
H	enthalpy
h	reservoir thickness
I_{ani}	anisotropy ratio
J	Jacobian matrix
J	productivity index
k	permeability
k_h	horizontal permeability
K_{JT}	Joule-Thompson coefficient
K_T	total conductivity
Ku	Kutateladze number
k_v	vertical permeability
k_x	permeability in the x direction
k_y	permeability in the y direction
k_z	permeability in the z direction
M	number of parameters
N	number of data points
N_{Re}	Reynold's number
p	pressure
\bar{p}	average reservoir pressure
p_e	reservoir pressure

p_i	pressure at boundary
p_{valve}	pressure at control valve
p_{wf}	flowing wellbore pressure
q	flow rate
q_g	gas flow rate
q_o	oil flow rate
q_w	water flow rate
r_w	wellbore radius
s	skin factor
s_R	partial penetration skin factor
T	temperature
T_{cal}	calculated temperature
T_I	temperature at boundary
T_{obs}	observed temperature
T_{wall}	temperature at pipe wall
\hat{U}	internal energy
U_{overall}	overall heat transfer coefficient
v	velocity vector
v_g	in-situ gas velocity
v_{sg}	gas superficial velocity
v_{so}	oil superficial velocity

v_{sw}	water superficial velocity
y_i	phase volume factor
γ	pipe open ratio
ρ	density
μ	viscosity
ε	relative pipe roughness
β	thermal expansion coefficient
$\hat{\rho}$	specific density

CHAPTER I

INTRODUCTION

1.1 Background

Distributed temperature sensors (DTS) and pressure sensors are now considered as standard completion requirements when drilling new complex wells in some completions. Fiber optic sensors in particular have become even more popular with its capability of providing temperature and pressure profiles along the well (vertical wells, horizontal wells or multilateral wells mainly the motherbore) rather than at a single point. Advancement of having the laterals covered by fiber optic cables is also in sight for multilateral wells. Fig. 1.1 shows an example of multilateral wells with intelligent completion by permanent downhole monitor sensors. The fiber optic technology has been utilized in field applications for some time. The first reported fiber optic sensor was installed in 1993 in one of Shell's Sleen Field wells (Kragas et al. 2001).

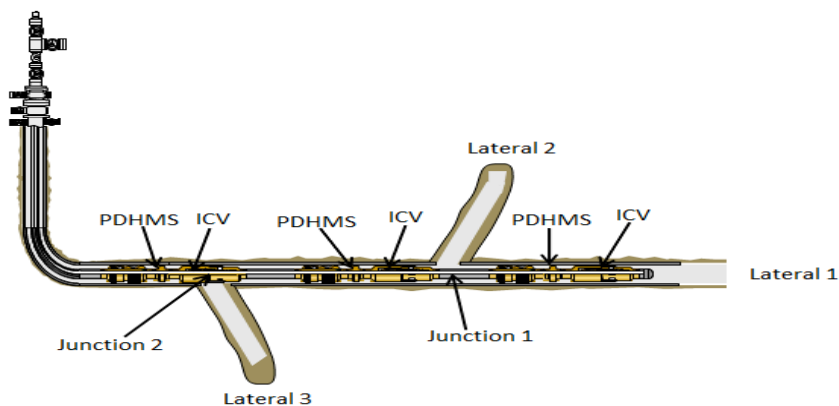


Fig. 1.1 Multilateral Well Diagram

This dissertation follows the style of the *SPE Journal*.

When a light signal is sent down to the fiber optic cable, the reflection of the light wave length is a function of temperature and strain at certain locations. Measuring wave length provides estimation of temperature and pressure and from the temperature and pressure data, downhole flow conditions can be evaluated. This technology is extremely valuable in horizontal and multilateral wells because in such a well, large reservoir contact results in higher level of heterogeneity of contacted formation, and non-uniform distribution of flow. With DTS measurement, it helps engineers understand the flow condition, and therefore optimize production performance.

The new advancements in well monitoring tools have increased the amount of data that could be retrieved with great accuracy. Downhole pressure and temperature could be precisely determined now using modern instruments. The new challenge that we are facing today is to maximize the benefits of the large amount of data that is being provided by these tools and thus justify the investment of more capital in such gadgets. One of these benefits is to utilize the continuous stream of data to determine the flow rate in real time out of a multilateral well.

Temperature and pressure changes are harder to predict in horizontal laterals because of the lack of variation in geothermal temperature, so the need of accurate and high precision gauges is essential. Temperature and pressure could be measured and detected real-time with the modern instruments that are used today in multilateral and horizontal wells.

1.2 Literature Review

Thermodynamic have been studied in oil and gas wells for decades for different purposes. Most of the early work done on temperature prediction has been dedicated to vertical wells.

Nowak (1953) presented one of the earliest temperature studies. He focused on water injection wells and developed models to use temperature logs used to optimize these injection operations. He was able to relate the temperature readings to the thickness of the zones taking the water.

Ramey (1962) expanded on Nowak's work as he developed a predicting model that is capable of handling either a single-phase incompressible fluid or a single-phase ideal gas in vertical wells. Ramey's wellbore temperature equation is the base for many researchers has been widely used in the industry. Hill (1990) extended on the Ramey work and used it in the area of quantitative interpretation of production log to understand flow distribution of injection or production zones in vertical wells. He stated that in order to calculate the wellbore temperature, the temperature distribution in a large portion of the reservoir has to be determined first. The method of estimating fracture height from temperature logs was also introduced in his work. Sagar et al. (1991) then introduced his work which included inclined wellbores.

There are numerous works in horizontal well flow study. Dikken (1990) presented a coupled reservoir and wellbore equations to simulate the flow behavior of horizontal wells. His work concentrated on pressure of wellbore and reservoir in addition

to the effect of well flow rate. His work included the importance of wellbore pressure drop and how it should not be ignored as that would result in errors in flow rate estimations.

Ouyang and Belanger (2006) argued that in order to approximate flow profile using steady-state DTS data, a well should have a deviation of no more than 75° . Izgec et al. (2007) presented a simulator that couples the transient wellbore effects with the semianalytic temperature model to calculate fluid temperature profiles in the wellbore during flowing or shut in conditions.

Yoshioka et al. (2007) showed that it is possible to estimate the flow profiles if the profiles of the pressure and/or temperature are sensitive to inflow profiles by inverting the measured temperature and pressure to a flow distribution. The inversion method is not easy to apply for horizontal wells due to the usually small pressure drop along the well and also due to the small temperature changes caused by the Joule-Thompson effects.

Achnivu et al. (2008) used a forward model to predict flowing pressure and temperature. The inversion method was then used to determine the water and gas entry points along a well. The model was directed towards highly-slanted gas wells with water coning from a bottom water aquifer. They concluded that fluid entries, especially in gas, could be identified using temperature profiles. Still, the mathematical complexity and the advanced well structures represented the greatest challenges that faced the model validation and application.

Sui et al. (2008) showed that in a multilateral vertical well, transient temperature is sensitive to individual layer permeability and skin. Abnormal temperature responses could be interpreted as low productivity which is attributed to low permeability and high skin factor.

Kabir et al. (2008) presented a method to compute total and individual rates independently from temperature. To do that, a model that handles steady-state fluid flow and unsteady-state heat transfers estimates the production rate at a given wellhead pressure and temperature. The same model is then used to calculate the flow profile based on the available temperature profile. Hill et al. (2008) also concluded that fluids with different thermal properties would have different temperatures even at the same depth which makes it possible to differentiate fluid types based on their temperature.

The majority of hydrocarbon-bearing formations are multilayered reservoirs which are formed due to sequential sedimentary depositional processes. When produced from one wellbore, such a production is referred to as comingled production. Reservoir properties might not necessarily be the same in these different layers despite them being in the same “reservoir”. That is the reason many studies have been conducted to develop the appropriate ways to test and analyze multilayer reservoirs.

One of the earliest studies on comingled reservoirs was performed by Lefkovits (1961). In this study, build up curves were used to determine average formation properties. It was also found that permeability and skin play the key role in determining early-time flow rate. The study has two glaring limitations though; first, it was for two layered reservoirs and secondly the method could not be used to determine individual

layer properties. His pioneer work was later extended by others. Tariq and Ramey (1978) introduced the wellbore storage effect into the comingled model. He was one of the first people to introduce the use of the Stehfest (1970) algorithm for numerical inversion of Laplace transforms in the petroleum engineering literature. Sandal et al. (1978) also introduced the Stehfest algorithm around the same time as Tariq.

Multilayer testing that provided individual layer properties was later introduced by Kuchuk and Avestaran (1986a). The technique used is to simultaneously measure wellbore pressure and flow rate at each layer, by changing flow rate and placing a production logging tool (spinner meter) above each layer. He used the logarithmic convolution method and the nonlinear least-square estimation method to estimate layer parameters. A field case study was then introduced by Kuchuck et al. (1986b) that supported his multilayer test approach and showed good results.

Ehlig-Economides and Joseph (1987) introduced an analytical solution for comingled and interlayer cross-flow reservoirs and for even more than two layers. Shah et al. (1988) introduced the step-wise changes in the surface flow rates that made the Ehlig-Economides and Joseph (1987) model more practical.

An improved model for multilayer testing was then introduced by Kuchuk et al. (1991) that was applicable to horizontal wells. Two boundary conditions are considered in this model. The first boundary condition assumed that there is no flow at the top and bottom boundaries. The second assumed a constant pressure at one boundary (either top or bottom) while the other boundary is at no-flow condition. This model has introduced five different flow periods that will be discussed in more detail later on in this study.

In another study, Kuchuk and Habashy (1996) utilized electromagnetics to overcome flow problems in non-homogeneous reservoirs. This solution is general enough to be applied to various testing and fluid flow problems. This study shows the difficulty of multilayer parameter estimation through conventional well tests, and suggested that gas caps should not be always treated as a constant-pressure boundary. A field example of a horizontal well that is completed in a multilayer reservoir was used to illustrate how the model works. Gilbert (1996) provided a detailed field case study that was performed on 9 different North Sea wells. His study showed how pressure transient tests could reveal layer properties that could as a result be used to fully understand reservoir behavior.

Correction plots were designed by Wells and Ehlig-Economides (2005) to estimate average reservoir pressure using data provided by buildup tests. A wide range of horizontal well position and reservoir shape combinations has been developed in this study.

Previously published work has successfully developed a model that determines flow rate in horizontal wells through pressure, Zarea (2010), and temperature, Al Zahrani (2010), data. It also modeled temperature behavior through inflow control valves. These previous studies would be used as a base in the development of interpretation flow profile from temperature data model for multilateral wells.

1.3 Objectives

The objectives of this study is to develop a theoretical model for trilateral wells equipped with ICV's to evaluate downhole temperature, pressure under given conditions, to invert the measured temperature and pressure to downhole flow distribution, and therefore, to monitor and control well production.

It will start from the developed models for horizontal wells with inflow control valves, and extend the model to trilateral wells. Parametric study will be conducted to design and optimize well performance for such a well. Examples will be used to illustrate the procedure to apply the developed model approach.

CHAPTER II

FORWARD MODEL

2.1 Introduction

The forward model consists of two main parts; wellbore model and reservoir model. The forward model is essential in this study in order to help understanding the connection between temperature and pressure behaviors and flow conditions. **Fig. 2.1** provides a schematic that shows the breakdown of all the components that the forward model is made out off.

The models, either wellbore or reservoir, have two main parts. Mass balance provides flow equations, and energy balance provides the temperature response to flow conditions. For example, the wellbore model consists of a wellbore flow model and a wellbore thermal model. The wellbore flow model is governed by mass and momentum balance and used to solve the wellbore fluid velocity and pressure profiles. On the other hand, the wellbore thermal model is governed by energy balance equations and used to solve the wellbore fluid temperature profiles.

Similarly, the reservoir model consists of a reservoir flow model and a reservoir thermal model. The reservoir flow model deals with fluid flow within the reservoir and is solved using multilayer transient testing theory. The reservoir thermal model deals with various subtle thermal effects in the reservoir and is solved using transient energy balance equation.

Coupling all the models together, the integrated model will be able to describe the thermal and flow behavior in a multilateral system.

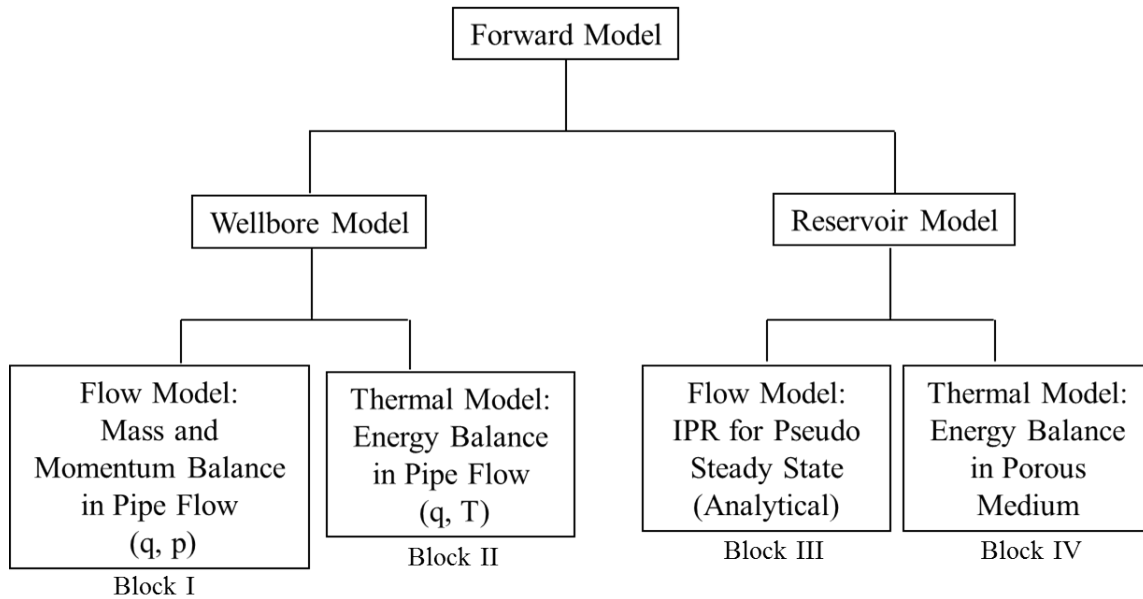


Fig. 2.1 Forward Model Breakdown

2.2 Wellbore Model

Mass, momentum, and energy balance equations over a wellbore differential volume element (Fig. 2.2) will be derived in order to establish the steady-state wellbore flow model and the transient wellbore thermal model. Wellbore models consists of two parts, the flow model (Block I in Fig 2.1) and thermal model (Block II in Fig 2.1). We will start with the flow model and thermal model of the single phase flow then discuss two-phase flow and thermal models.

2.2.1 Single-Phase Wellbore Flow Model

The wellbore flow model developed by Al Zahrani (2010) will be adopted to interpret the single-phase wellbore flowing fluid velocity and pressure profile in the wellbore.

As could be seen from Fig. 2.2, there are two main directions that take place. The first one is the axial direction (v_{in}) while the second one is the radial direction (v_x). As a result, the velocity vector is,

$$v = \begin{pmatrix} v_x \\ v_r \\ v_\theta \end{pmatrix} = \begin{cases} \begin{pmatrix} v_x \\ 0 \\ 0 \end{pmatrix} \text{ anywhere} \\ \begin{pmatrix} 0 \\ v_{in} \\ 0 \end{pmatrix} @ r = r_w \end{cases} \dots\dots\dots 2.1$$

where r_w is the wellbore radius.

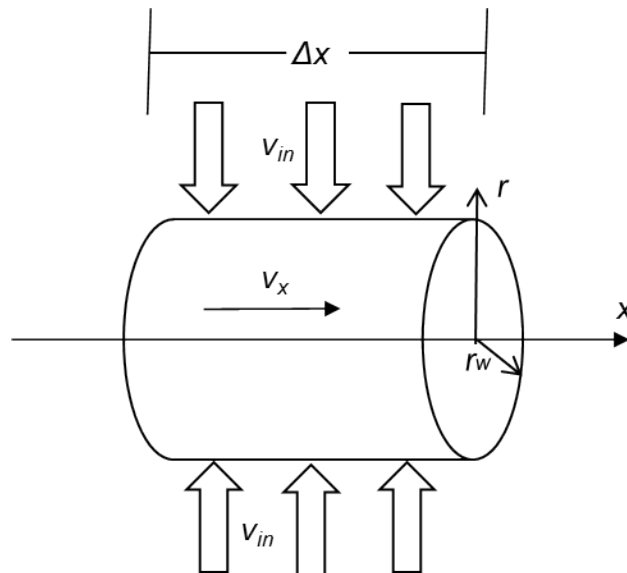


Fig. 2.2 Wellbore Differential Volume Elements

Mass Balance

Conservation of mass can be obtained from the incoming mass flux and outgoing mass flux

$$[\text{Rate of increase of mass}] = [\text{rate of mass in}] - [\text{rate of mass out}] \dots\dots\dots 2.2$$

For the defined system as shown in Fig 2.2, we have

$$\pi r_w^2 (v_x)|_x + 2\pi r_w \Delta x (v_{in}) = \pi r_w^2 (v_x)|_{x+\Delta x} \dots\dots\dots 2.3$$

After dividing by $(\pi r_w^2 \Delta x)$ and rearranging we end up with,

$$\frac{(v_x)|_{x+\Delta x} - (v_x)|_x}{\Delta x} = \frac{2(v_{in})}{r_w} \dots\dots\dots 2.4$$

For the purpose of this study, the wellbore is going to be divided into segments. The subscript, j , is going to refer to a particular segment. Solving for flux at segments, Eq.

2.4 can be written as

$$v_{xj} = v_{xj-1} + \frac{2\Delta x (v_{in})}{r_w} \dots\dots\dots 2.5$$

Momentum Balance

The momentum balance over the volume element is defined as

$$\begin{bmatrix} \text{Rate of} \\ \text{momentum} \\ \text{in} \end{bmatrix} = \begin{bmatrix} \text{rate of} \\ \text{momentum} \\ \text{out} \end{bmatrix} - \begin{bmatrix} \text{external} \\ \text{force on} \\ \text{fluid} \end{bmatrix} \dots\dots\dots 2.6$$

We start with the combined rate of momentum flux which has been introduced by Bird et al. (2002),

$$\Phi = \rho v + p\delta + \tau \dots\dots\dots 2.7$$

We are only interested in the combined rate of momentum flux in two components,

$$\Phi_{xx} = \rho v_x v_x + p\delta + \tau_{xx} \dots\dots\dots 2.8$$

and,

$$\Phi_{rx} = \rho v_x v_r + p\delta + \tau_{rx} \dots\dots\dots 2.9$$

For Newton’s fluids, the shear stress as introduced by Yoshioka (2007),

$$\tau_{xx} = 2\mu \frac{\partial v_x}{\partial x} - \frac{2}{3} \mu \left[\frac{1}{r} \frac{\partial (r v_{in})}{\partial r} + \frac{\partial v_x}{\partial x} \right] = \frac{4}{3} \mu \frac{\partial v_x}{\partial x} \dots\dots\dots 2.10$$

We move to deal with the third term of Eq. 2.6 which represents the external force on the fluid. The only force that we will consider is the gravity as can be seen here,

$$\left[\begin{array}{l} \text{external} \\ \text{force on} \\ \text{fluid} \end{array} \right] = -\pi r_w^2 \Delta x \rho g \sin \theta \dots\dots\dots 2.11$$

As far as this study concerned, the term is negative because the flow is working against the gravity when flowing to the surface as the case in producing wells.

So, by substituting these previous equations back into the momentum balance equation (Eq. 2.6) we end with the following equation,

$$\pi r_w^2 \left(\rho v_x v_x + p - \frac{4}{3} \mu \frac{\partial v_x}{\partial x} \right) \Big|_{x=x} + 2\pi r_w \Delta x (\rho v_x v_r + \tau_{rx}) \Big|_{r=R} = \left(\rho v_x v_x + p - \frac{4}{3} \mu \frac{\partial v_x}{\partial x} \right) \Big|_{x=x+\Delta x} \dots$$

.....2.12

We assume that v_x is zero at the wall of the pipe. As a result, $\rho v_x v_r$ goes to zero as well.

If we divide Eq. 2.12 by $(\pi R^2 \Delta x)$ as well we obtain,

$$\frac{\left(\rho v_x^2 + p - \frac{4}{3} \mu \frac{\partial v_x}{\partial x} \right) \Big|_{x=x}}{\Delta x} + \frac{2}{r_w} (\tau_{rx}) \Big|_{r=r_w} = \frac{\left(\rho v_x^2 + p - \frac{4}{3} \mu \frac{\partial v_x}{\partial x} \right) \Big|_{x=x+\Delta x}}{\Delta x} \dots\dots\dots 2.13$$

To get the differential form of Eq 2.13, the velocity of derivative term would be a second derivative. For simplicity, these terms will be neglected and the following equations is obtained,

$$\frac{(\rho v_x^2 + p) \Big|_{x=x}}{\Delta x} + \frac{2}{r_w} (\tau_{rx}) \Big|_{r=R} = \frac{(\rho v_x^2 + p) \Big|_{x=x+\Delta x}}{\Delta x} \dots\dots\dots 2.14$$

Multiplying by Δx and substituting the subscripts,

$$(\rho v_x^2 + p) \Big|_{j-1} + \frac{2\Delta x}{r_w} (\tau_{rx}) \Big|_{r=r_w} = (\rho v_x^2 + p) \Big|_j \dots\dots\dots 2.15$$

Rearranging the equation to solve for the pressure at the current segment,

$$p_j = p_{j-1} + \rho(v_{x,j-1}^2 - v_{x,j}^2) + \frac{2\Delta x}{r_w} (\tau_{rx}) \Big|_{r=r_w} \dots\dots\dots 2.16$$

We will use the Fanning friction factor to calculate the shear stress (τ_{rx}) on the wall,

$$\tau_{rx} = \frac{-\rho f v_x^2}{2} \dots\dots\dots 2.17$$

By substituting the previous equation into Eq. 2.16, we obtain,

$$p_j = p_{j-1} + \rho(v_{x,j-1}^2 - v_{x,j}^2) - \frac{\Delta x \rho f v_{x,j}^2}{r_w} \dots\dots\dots 2.18$$

The term, f , represents the friction factor. To calculate the friction factor, we will use the correlations presented by Ouyang (1998). For laminar flow,

$$f = f_0 \left(1 + \left(0.04304 N_{Re,w}^{0.6142} \right) \right) \dots\dots\dots 2.19$$

For turbulent flow,

$$f = f_0 \left(1 - \left(29.03 \left(\frac{N_{Re,w}}{N_{Re}} \right)^{0.8003} \right) \right) \dots\dots\dots 2.20$$

For perforated completion,

$$f = f_0 \left(1 - \left(0.0153 N_{Re,w}^{0.3978} \right) \right) \dots\dots\dots 2.21$$

The Reynold's numbers are solved using,

$$N_{Re,w} = \frac{2r_w \rho v_{in}}{\mu} \dots\dots\dots 2.22$$

$$N_{Re} = \frac{2r_w \rho v_x}{\mu} \dots\dots\dots 2.23$$

f_0 is is calculated from Chen's correlation (Economides et al. 1994),

$$f_0 = \left[-4 \log \left\{ \frac{\varepsilon}{3.7065} - \frac{5.0452}{N_{Re}} \log \left[\frac{\varepsilon^{1.1098}}{2.8257} + \left(\frac{7.149}{N_{Re}} \right)^{0.8981} \right] \right\} \right]^{-2} \dots\dots\dots 2.24$$

ε is the relative pipe roughness.

2.2.2 Single-Phase Wellbore Thermal Model

The wellbore thermal model is designed to interpret the behavior of fluid temperature while flowing during a transient test in the wellbore. Similar to the flow model, the thermal model is divided into a radial part and an axial part (Fig 2.2).

Energy Balance

The approach presented by Sui (2009) will be adopted in this section. Conservation of energy equation is used to define the system as follows

$$\left[\begin{array}{c} \text{Rate of} \\ \text{increase} \\ \text{of energy} \end{array} \right] = \left[\begin{array}{c} \text{rate of} \\ \text{energy} \\ \text{in} \end{array} \right] - \left[\begin{array}{c} \text{rate of} \\ \text{energy} \\ \text{out} \end{array} \right] + \left[\begin{array}{c} \text{rate of work} \\ \text{done on system} \\ \text{by external forces} \end{array} \right] + [\text{source}] \dots \dots \dots 2.25$$

To derive the energy balance equation, it is necessary to introduce the combined energy flux vector e . The necessity of the combined flux vector is due to the total energy being transported by three different mechanisms

1. Convection.
2. Molecular mechanisms.
3. Heat.

As a result, the combined energy flux vector is defined be (Bird, 2002) as

$$e = \left(\frac{1}{2} \rho v^2 + \rho \hat{U} \right) v + [\pi \cdot v] + q \dots \dots \dots 2.26$$

\hat{U} is the internal energy, π is the molecular stress tensor, and q is heat. So, the first term of the RHS represents the energy transported by convection, the second term represents the energy transported by molecular mechanisms, and the third term represents the energy transported by heat. The molecular stress tensor π can be divided into two parts:

$\pi = p\delta + \tau$, where p is the normal stress while τ is the shear stress, so

$[\pi \cdot v] = pv + [\tau \cdot v]$. Enthalpy, H , is defined as,

$$H = U + \frac{p}{\rho} \dots\dots\dots 2.27$$

So, the combined energy flux vector can be written in the general form

$$e = \left(\frac{1}{2} \rho v^2 + \rho \hat{H} \right) v + [\tau \cdot v] + q \dots\dots\dots 2.28$$

Breaking Eq. 2.26 to pieces will yield the following,

$$\left[\begin{array}{l} \text{Rate of} \\ \text{increase} \\ \text{of energy} \end{array} \right] = \pi_w^2 \Delta z \frac{\partial}{\partial t} \left(\frac{1}{2} \rho v^2 + \rho \hat{U} \right) \dots\dots\dots 2.29$$

in the above equation, $\frac{1}{2} \rho v^2$ represents the kinetic energy per unit volume while $\rho \hat{U}$

represents the internal energy per unit volume.

$$\left[\begin{array}{l} \text{rate of} \\ \text{energy} \\ \text{in} \end{array} \right] = 2\pi_w \Delta z (e_r)_R + \pi_w^2 (e_z)_z \dots\dots\dots 2.30$$

e_r and e_z represent the combined energy flux components in the radial and vertical directions respectively.

$$\left[\begin{array}{l} \text{rate of} \\ \text{energy} \\ \text{out} \end{array} \right] = \pi r_w^2 (e_z)_{z+\Delta z} \dots\dots\dots 2.31$$

$$\left[\begin{array}{l} \text{rate of work} \\ \text{done on system} \\ \text{by external forces} \end{array} \right] = -\pi r_w^2 \Delta z \rho v g \sin \theta \dots\dots\dots 2.32$$

as the gravity forces are the only one we should take into consideration. The source term is zero.

Now we substitute Eqs. **2.29** to **2.32** into Eq. **2.25** and that will yield,

$$\pi r_w^2 \Delta z \frac{\partial}{\partial t} \left(\frac{1}{2} \rho v^2 + \rho \hat{U} \right) = 2\pi r_w \Delta z (e_r)_R + \pi r_w^2 (e_z)_z - \pi r_w^2 (e_z)_{z+\Delta z} - \pi r_w^2 \Delta z \rho v g \sin \theta \dots\dots\dots 2.33$$

dividing Eq. **2.33** by $\pi r_w^2 \Delta z$ and taking the limit $\Delta z \rightarrow 0$ we get,

$$\frac{\partial}{\partial t} \left(\frac{1}{2} \rho v^2 + \rho \hat{U} \right) = \frac{2(e_r)_{r_w}}{r_w} - \frac{\partial(e_z)}{\partial z} - \rho v g \sin \theta \dots\dots\dots 2.34$$

When we substitute e_r and e_z into the energy balance equation, we end up with,

$$\frac{\partial}{\partial t} (\rho \hat{U}) = \frac{2(\gamma)}{r_w} \rho_l \hat{H}_l v_l - \frac{\partial}{\partial z} (\rho \hat{H} v) - \rho v g \sin \theta \dots\dots\dots 2.35$$

E_{KE} is the kinetic energy and E_{VS} is the viscous shear energy term. We can then expand the transient term to

$$\frac{\partial}{\partial t} (\rho \hat{U}) = \rho \frac{\partial \hat{U}}{\partial t} + \hat{U} \frac{\partial(\rho)}{\partial t} \dots\dots\dots 2.36$$

substituting Eq. **2.27** into Eq. **2.36** to get,

$$\frac{\partial}{\partial t} (\rho \hat{U}) = \rho \frac{\partial \hat{H}}{\partial t} - \frac{\partial p}{\partial t} + \hat{H} \frac{\partial \rho}{\partial t} \dots\dots\dots 2.37$$

Then we go back and substitute Eq. 2.37 into Eq. 2.35

$$\rho \frac{\partial \hat{H}}{\partial t} - \frac{\partial p}{\partial t} + \hat{H} \frac{\partial \rho}{\partial t} = \frac{2\gamma}{r_w} \rho_l \hat{H}_l v_l - \frac{\partial}{\partial z} (\rho \hat{H} v) - \rho v g \sin \theta \dots\dots\dots 2.38$$

From mass balance equation and with manipulation and simplification

$$\rho \frac{\partial \hat{H}}{\partial t} - \frac{\partial p}{\partial t} = \frac{2\gamma}{r_w} \rho_l v_l (\hat{H}_l - \hat{H}) - \rho v \frac{\partial \hat{H}}{\partial z} - \rho v g \sin \theta \dots\dots\dots 2.39$$

In order to evaluate enthalpy, the standard equilibrium thermodynamic formula is used

$$d\hat{H} = \left(\frac{\partial \hat{H}}{\partial T} \right)_p dT + \left(\frac{\partial \hat{H}}{\partial p} \right)_T dp = \hat{C}_p dT + \frac{1}{\rho} (1 - \beta T) dp \dots\dots\dots 2.40$$

so as a result,

$$\frac{\partial \hat{H}}{\partial t} = \hat{C}_p \frac{\partial T}{\partial t} + \frac{1}{\rho} (1 - \beta T) \frac{\partial p}{\partial t} \dots\dots\dots 2.41$$

$$\frac{\partial \hat{H}}{\partial z} = \hat{C}_p \frac{\partial T}{\partial z} + \frac{1}{\rho} (1 - \beta T) \frac{\partial p}{\partial z} \dots\dots\dots 2.42$$

where the thermal expansion coefficient in the above equations, β , is defined as follows,

$$\beta = -\frac{1}{\rho} \left(\frac{\partial \rho}{\partial T} \right)_p = \frac{1}{V} \left(\frac{\partial V}{\partial T} \right)_p \dots\dots\dots 2.43$$

If we let the pressure at the boundary, p_l , be equal to the pressure at the wellbore, p , then the enthalpy difference can be calculated as follows,

$$\hat{H}_l - \hat{H} = \hat{C}_p (T_l - T) + \frac{1}{\rho} (1 - \beta T_l) (p_l - p) = \hat{C}_p (T_l - T) \dots\dots\dots 2.44$$

We substitute Eqs. 2.42, 2.43 and 2.44 into Eq. 2.38 and then divide by $\rho v \hat{C}_p$ to get,

$$\frac{1}{v} \frac{\partial T}{\partial t} - \frac{\beta T}{\rho v \hat{C}_p} \frac{\partial p}{\partial t} = \frac{2\gamma}{r_w} \frac{\rho_l v_l}{\rho v} (T_l - T) - \frac{\partial T}{\partial z} - \frac{(1 - \beta T)}{\rho \hat{C}_p} \frac{\partial p}{\partial z} - \frac{g \sin \theta}{\hat{C}_p} \dots\dots\dots 2.46$$

By substituting the Joule-Thomson coefficient ($K_{JT} = \frac{\beta T - 1}{\rho \hat{C}_p}$) and the exchange heat

flux conduction between wellbore fluid and formation ($q_I = U_T (T_r|_{r=r_{wb}} - T)$), we end

up with the final form of the single-phase wellbore thermal model,

$$\frac{1}{v} \frac{\partial T}{\partial t} - \frac{\beta T}{\rho v \hat{C}_p} \frac{\partial p}{\partial t} = \frac{2\gamma}{r_w} \frac{\rho_l v_l}{\rho v} (T_l - T) = U_T (T_r|_{r=r_{wb}} - T) - \frac{\partial T}{\partial z} + K_{JT} \frac{\partial p}{\partial z} - \frac{g \sin \theta}{\hat{C}_p}$$

.....2.47

This solution of this equation after integration is presented by Al Zahrani (2010) as,

$$T_j - T_{j-1} = \Delta x A_1 \frac{\partial p}{\partial x} + \Delta x A_2 (T_{wall} - T_j) \dots\dots\dots 2.47$$

where,

$$A_1 = K_{JT} \dots\dots\dots 2.48$$

and

$$A_2 = \frac{2}{\rho v C_p r_w} U_T \dots\dots\dots 2.49$$

In Eq. 2.47 the subscript j denotes the segment of interest while j-1 denotes the previous adjacent segment. T_{wall} is the temperature at the pipe wall.

The temperature difference between adjacent segments is determined in the previous equation by the two terms on the right hand side of the equation. The first term represents the Joule-Thompson coefficient multiplied in the pressure drop. The Joule-Thompson coefficient is negative for liquids, while the pressure drop is negative as well

for producing wells. The second term represents the change in temperature caused by incoming fluid which is divided by the specific heat capacity coefficient. The second term then is multiplied by the difference in temperature in the pipe and at the wall of the pipe.

After rearrangement, Eq. 2.47 becomes,

$$T_j = \frac{T_{j-1} + A_1(p_j - p_{j-1}) + \Delta x A_2 T_{wall}}{1 + \Delta x A_2} \dots\dots\dots 2.50$$

2.2.3 Two-Phase Wellbore Flow Model

Similar to the single-phase model, the two-phase wellbore model will be borrowed as well. Yoshioka (2007) has developed a model that can be adapted for the purpose of this study.

Mass Balance

The mass balance for all phases (oil, gas or water) is given by,

$$\frac{d(\rho_i v_i y_i)}{dx} = \frac{2y_{i,I}}{r_w} \rho_i v_{i,I} \dots\dots\dots 2.51$$

where y_i represents the volume factor of phase i . The discrete form as a result will be

$$y_{i,j} v_{i,j} = y_{i,j-1} v_{i,j-1} + \frac{2v_{i,in}}{r_w} \dots\dots\dots 2.52$$

Momentum Balance

The simplest way to estimate pressure profiles and holdup along a well is by assuming the fluid is flowing as a single-phase flow in a homogeneous model referred as drift flux model. It is the model that is preferred to the mechanistic model that is more realistic but is complicated and has its limitations when it comes to flow regime transitions convergence.

Oil-Water Flow

The momentum balance equation is given as,

$$\frac{dp}{dx} = -\frac{\rho_m v_m^2 f_m}{r_w} - \frac{d(\rho_m v_m^2)}{dx} - \rho_m g \sin \theta \dots\dots\dots 2.53$$

where the subscript m denotes the mixture properties. The mixture density is calculated by,

$$\rho_m = \rho_o y_o + \rho_w y_w \dots\dots\dots 2.54$$

Since the flow assumed to be homogeneous and there is no slip velocity between oil and water to be considered, we can calculate the hold up using,

$$y_o = \frac{v_{so}}{v_{so} + v_{sw}} \dots\dots\dots 2.55$$

and

$$y_w = 1 - y_o \dots\dots\dots 2.56$$

v_{sw} is the water superficial velocity while v_{so} is the oil superficial velocity. The mixture density equation is,

$$\rho_m = y_o \rho_o + y_w \rho_w \dots\dots\dots 2.57$$

Jayawardena (2001) introduced a model that we can use to get the phase inversion point,

$$\mu_m = \mu_o (1 - y_w)^{-2.5} \dots\dots\dots 2.58$$

Then we need to use Eqs. 2.22 and 2.23 to calculate the Reynold's number. We will be able to use these equations because we assume a single phase in each reservoir segment. As a result, the pressure drop equation we end up with is,

$$p_j = p_{j-1} + \rho (v_{m,x,j-1}^2 - v_{m,x,j}^2) - \frac{\Delta x \rho f v_{m,x,j}^2}{r_w} \dots\dots\dots 2.59$$

Liquid-Gas Flow

We start with the drift-flux model presented by Shi et al. (2005). First, we need to calculate the superficial velocities of both phases,

$$v_{sg} = \frac{q_g}{A_{pipe}} \dots\dots\dots 2.60$$

and,

$$v_{sl} = \frac{q_o + q_w}{A_{pipe}} \dots\dots\dots 2.61$$

The in-situ gas velocity is calculated using,

$$v_g = v_{sg} + v_m + \frac{(1 - y_g)Ku}{y_g \sqrt{\frac{\rho_g}{\rho_l} + 1 - y_g}} \left(\frac{\sigma_{gl}g(\rho_l - \rho_g)}{\rho_l^2} \right)^{\frac{1}{4}} \dots\dots\dots 2.62$$

y_g is the in-situ gas void fraction and can be calculated using,

$$y_g = \frac{v_{sg}}{v_g} \dots\dots\dots 2.63$$

Ku is the Kutateladze number and is calculated as follows,

$$Ku = \begin{cases} 1.53 \text{ if } y_g < 0.2 \\ Ku(D^*) \text{ from Table 2.1} \dots\dots\dots \end{cases} \dots\dots\dots 2.64$$

D^* is the dimensionless diameter and defined as,

$$D^* = \left(\frac{g(\rho_l - \rho_g)}{\sigma_{gl}} \right)^{\frac{1}{2}} D \dots\dots\dots 2.65$$

D is the pipe diameter.

Table 2.1 Kutateladze Numbers

D*	Ku
2 ≤	0
4	1
10	2.1
14	2.5
20	2.8
28	3.0
50 ≥	3.2

For the liquid-gas flow, the Ouyang and Aziz (2001) model is used. The model is as follows,

$$p_j = p_{j-1} + \Delta x \left[\frac{dp}{dx_f} + \frac{dp}{dx_g} + \frac{dp}{dx_{aW}} + \frac{dp}{dx_{aE}} \right] \dots\dots\dots 2.66$$

$\frac{dp}{dx_f}$ is the pressure drop caused by friction, $\frac{dp}{dx_g}$ is the pressure drop caused by gravity,

$\frac{dp}{dx_{aW}}$ is the pressure drop caused by acceleration due to inflow, and $\frac{dp}{dx_{aE}}$ is the pressure

drop caused by acceleration due to fluid expansion.

In order to calculate the four components of pressure drop in the model, the following parameters need to be calculated first,

$$q_{in,l} = nAv_{sl,in} \dots\dots\dots 2.67$$

$$q_{in,g} = nAv_{sg,in} \dots\dots\dots 2.68$$

$$q_{in,TP} = \frac{\rho_l}{\rho_{TP}} q_{in,l} + \frac{\rho_g}{\rho_{TP}} q_{in,g} \dots\dots\dots 2.69$$

$$q_{in,m} = q_{in,l} + q_{in,g} \dots\dots\dots 2.70$$

$$v_{TP} = \frac{\rho_l}{\rho_{TP}} v_{sl} + \frac{\rho_g}{\rho_{TP}} v_{sg,g} \dots\dots\dots 2.71$$

$$\beta_{aE} = \frac{\rho_{TP} v_m v_{sg}}{p} \dots\dots\dots 2.72$$

$$\rho_{TP} = \rho_l (1 - y_g) + \rho_g y_g \dots\dots\dots 2.73$$

$$\mu_{TP} = \mu_l (1 - y_g) + \mu_g y_g \dots\dots\dots 2.74$$

$$\rho_{in,m} = \rho_l \frac{q_{in,l}}{q_{in,m}} + \rho_g \frac{q_{in,g}}{q_{in,m}} \dots\dots\dots 2.75$$

$$\mu_{in,m} = \mu_l \frac{q_{in,l}}{q_{in,m}} + \mu_g \frac{q_{in,g}}{q_{in,m}} \dots\dots\dots 2.76$$

$$N_{Re,TP} = \frac{\rho_{TP} v_{TP} D}{\mu_{TP}} \dots\dots\dots 2.77$$

$$N_{Re,wall} = \frac{\rho_{in,m} v_{in,m} D}{\mu_{in,m}} \dots\dots\dots 2.78$$

The pressure drop components can be calculated now,

$$\frac{dp}{dx_f} = -\pi R \Delta x f_{TP} \rho_{TP} v_{TP}^2 \dots\dots\dots 2.79$$

The friction factor can be calculated using Eqs. 2.19, 2.20, and 2.21. The only difference is using Eqs. 2.77 and 2.78 to calculate the Reynold's numbers.

$$\frac{dp}{dx_g} = -g\rho_{TP} \sin \theta \dots\dots\dots 2.80$$

$$\frac{dp}{dx_{aW}} = -\frac{1}{\pi R^2} [0.8\rho_{TP}(v_m q_{in,TP} + v_{TP} q_{in,m}) + 0.4\rho_{TP} v_m q_{in,TP}] \dots\dots\dots 2.81$$

$$\frac{dp}{dx_{aE}} = \frac{\beta_{aE}}{(1 - \beta_{aE})} \left[\frac{dp}{dx_f} + \frac{dp}{dx_g} + \frac{dp}{dx_{aW}} \right] \dots\dots\dots 2.82$$

2.2.4 Two-Phase Wellbore Thermal Model

Energy Balance

Yoshioka (2007) presented the approach we will adopt. The energy balance while neglecting the kinetic energy and viscous shear terms for phase i is given by,

$$\rho_i v_i y_i C_{p,i} \frac{dT_i}{dx} = \rho_i v_i y_i C_{p,i} K_{JT,i} \frac{dp_i}{dx} + \frac{2}{r_w} \gamma \rho_{i,l} v_{i,l} y_{i,l} C_{p,i} (T_{i,l} - T_i) - \rho_i v_i y_i g \sin \theta \dots\dots 2.83$$

If we sum the equations of the three phases while assuming that the pressure and temperature are the same for each then we have,

$$\frac{dT}{dx} \sum \rho_i v_i y_i C_{p,i} \dots\dots\dots 2.84 = \frac{dp}{dx} \sum \rho_i v_i y_i C_{p,i} K_{JT,i} + \frac{2}{r_w} (T_l - T) \sum \rho_{i,l} v_{i,l} y_{i,l} C_{p,i} - \sum \rho_i v_i y_i g \sin \theta$$

α_T is the overall heat transfer coefficient in multi-phase flow. Solving for the temperature gradient we end up with,

$$\frac{dT}{dx} = \frac{(\rho v C_p K_{JT})_T}{(\rho v C_p)_T} \frac{dp}{dx} + \frac{2}{r_w} \frac{\alpha_{T,I}}{(\rho v C_p)_T} (T_I - T) - \frac{(\rho v)_T}{(\rho v C_p)_T} g \sin \theta \dots\dots\dots 2.85$$

with

$$\alpha_{T,I} = \gamma (\rho v C_p)_{T,I} + (1 - \gamma) \alpha_T \dots\dots\dots 2.86$$

Similar to what we did with the single-phase model earlier we will introduce these terms to simplify the equation which are borrowed from Al Zahrani (2010),

$$A_3 = \frac{\sum_i (\rho v_j C_p y K_{JT})_i}{\sum_i (\rho v_j C_p y)_i} \dots\dots\dots 2.87$$

$$A_4 = \frac{2}{r_w \sum_i (\rho v_j C_p y)_i} U_T \dots\dots\dots 2.88$$

so we end up with this final discrete form,

$$T_j = \frac{T_{j-1} + A_3 (p_j - p_{j-1}) + \Delta x A_4 T_{wall}}{1 + \Delta x A_4} \dots\dots\dots 2.89$$

which is similar to Eq. 2.50 that was used for the single-phase flow.

2.3 Reservoir Model

Similar to the wellbore model, the reservoir model will consist of two main parts which are the reservoir flow model and the reservoir thermal model.

For the reservoir flow model, two models will be used to the two types of fluid flow that we will be dealing with. For the single-phase slightly-compressible fluid, we will use the Babu and Odeh (1989) model.

2.3.1 Single-Phase Reservoir Flow Model

A reservoir inflow model is used to describe the relationship between flow rate from the reservoir to the wellbore and the wellbore pressure. The model developed by Babu and Odeh (1989) was used in this work.

The reservoir is considered to be box-shaped with a well laying away from the boundaries and parallel to the x-axis as could be seen in **Fig. 2.3**. The well does not need to be fully penetrated. A partial penetration skin factor was added to the inflow equation to count for the flow from each end section of the reservoir where the well is not present.

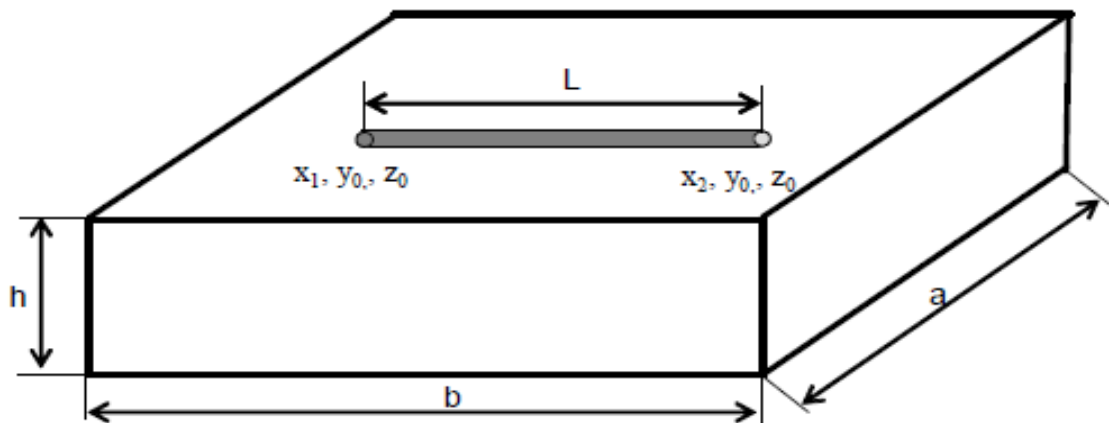


Fig. 2.3 Babu and Odeh Physical Model

The model is modified from Darcy's equation for vertical wells with the well rotated 90° to represent a horizontal well.

So, the Babu and Odeh model is as following

$$q = \frac{\sqrt{k_y k_z} b (\bar{p} - p_{wf})}{141.2 B_o \mu \left[\ln \left(\frac{A^{0.5}}{r_w} \right) + \ln C_H - 0.75 + s_R + s \right]} \dots\dots\dots 2.90$$

In the above equation, A is the drainage area, C_H is the shape factor counting for the non-circular shaped drainage, s_R is the partial penetration skin as mentioned before, and s is any other skin factor.

The shape factor can be determined by using the following equation,

$$\ln C_H = 6.28 \frac{a}{I_{ani} h} \left[\frac{1}{3} - \frac{y_0}{a} + \left(\frac{y_0}{a} \right)^2 \right] - \ln \left(\sin \frac{\pi z_0}{h} \right) - 0.5 \ln \left[\left(\frac{a}{I_{ani} h} \right) - 1.088 \right] \dots\dots\dots 2.91$$

Where I_{ani} is the anisotropy ratio,

$$I_{ani} = \sqrt{\frac{k_H}{k_V}} \dots\dots\dots 2.92$$

The partial penetration skin, S_R, is for non-fully penetrated wellbore (L<b in Fig 2.3). So, S_R is equal to zero when the well is fully penetrating the reservoir. If the well is not fully penetrating the reservoir then there are two conditions that apply:

1. Reservoir is relatively wide (a>b) and the following criteria is met:

$$\frac{a}{\sqrt{k_x}} \geq 0.75 \frac{b}{\sqrt{k_y}} > 0.75 \frac{h}{\sqrt{k_z}} \dots\dots\dots 2.93$$

then,

$$s_R = P_{xyz} + P'_{xy} \dots\dots\dots 2.94$$

and,

$$P_{xyz} = \left(\frac{b}{L} - 1\right) \left[\ln \frac{h}{r_w} + 0.25 \ln \frac{k_y}{k_z} - \ln \left(\sin \frac{\pi z}{h} \right) - 1.84 \right] \dots\dots\dots 2.95$$

$$P'_{xy} = \frac{2b^2}{Lh} \sqrt{\frac{k_z}{k_x}} \left\{ F\left(\frac{L}{2b}\right) + 0.5 \left[F\left(\frac{4x_{mid} + L}{2b}\right) - F\left(\frac{4x_{mid} - L}{2b}\right) \right] \right\} \dots\dots\dots 2.96$$

The function, F , in Eq. 2.36 is defined as follows,

If $(4x_{mid} + L)/2b$ and $(4x_{mid} - L)/2b$ are equal to or less than 1 then F is calculated by the following equation,

$$F\left(\frac{L}{2b}\right) = -\left(\frac{L}{2b}\right) \left[0.145 + \ln\left(\frac{L}{2b}\right) - 0.137\left(\frac{L}{2b}\right)^2 \right] \dots\dots\dots 2.97$$

With the argument $(L/2b)$ replaced by either $(4x_{mid} + L)/2b$ or $(4x_{mid} - L)/2b$. On the other hand, if $(4x_{mid} + L)/2b$ and $(4x_{mid} - L)/2b$ is greater than 1 F is calculated using the following equation,

$$F(x) = (2 - x) \left[0.145 + \ln(2 - x) - 0.137(2 - x)^2 \right] \dots\dots\dots 2.98$$

where x can be replaced by either $(4x_{mid} + L)/2b$ or $(4x_{mid} - L)/2b$.

x_{mid} is the midpoint of the well and can be easily calculated,

$$x_{mid} = \frac{x_1 + x_2}{2} \dots\dots\dots 2.99$$

2. Reservoir is relatively long ($a < b$) then the following criteria is met:

$$\frac{b}{\sqrt{k_x}} \geq 1.33 \frac{a}{\sqrt{k_y}} > \frac{h}{\sqrt{k_z}} \dots\dots\dots 2.100$$

In this case,

$$s_R = P_{xyz} + P_y + P_{xy} \dots\dots\dots 2.101$$

where,

P_{xyz} is the same as defined in Eq. 2.35.

$$P_y = \frac{6.28b^2}{ah} \frac{\sqrt{k_x k_z}}{k_y} \left[\left(\frac{1}{3} - \frac{x_{mid}}{b} + \frac{x_{mid}^2}{b^2} \right) + \frac{L}{24b} \left(\frac{L}{b} - 3 \right) \right] \dots\dots\dots 2.102$$

and

$$P_{xy} = \left(\frac{b}{L} - 1 \right) \left(\frac{6.28a}{h} \sqrt{\frac{k_z}{k_x}} \right) \left(\frac{1}{3} - \frac{y_0}{a} + \frac{y_0^2}{a^2} \right) \dots\dots\dots 2.103$$

if neither of these two conditions apply, then the Babu and Odeh model is not applicable.

2.3.2 Two-Phase Reservoir Flow Model

Since the relationship between relative permeability and pressure is hard to obtain analytically, most commonly used two-phase analytical flow models for reservoir inflow are empirical correlations. The most popular one is Vogel's equation (1968) for vertical wells, and many horizontal well models use Vogel's as a start point. As presented by Kamkom and Zhu (2005) for a vertical well, the oil flow rate is correlated to the maximum open flow potential as,

$$\frac{q_o}{q_{o,max}} = 1 - 0.2 \left(\frac{p_{wf}}{\bar{p}} \right) - 0.8 \left(\frac{p_{wf}}{\bar{p}} \right)^2 \dots\dots\dots 2.104$$

where q_o is the oil rate, $q_{o,max}$ is the maximum oil rate, p_{wf} is the flowing bottom hole pressure, and \bar{p} is the average reservoir pressure. The maximum oil rate could be

achieved when the flowing bottom hole pressure is equal to zero and a single-phase oil flow equation is used to calculate the maximum oil rate, $q_{o,\max}$.

For horizontal wells, the maximum productivity index can be calculated by setting wellbore flowing pressure, p_{wf} , to zero, and using the Babu and Odeh's model,

$$J = \frac{q_o}{(\bar{p} - p_{wf})} = \frac{b\sqrt{k_y k_z}}{141.2B_o\mu \left[\ln\left(\frac{A^{0.5}}{r_w}\right) + \ln C_H - 0.75 + s_R + s \right]} \dots\dots\dots 2.105$$

and

$$q_{o,\max} = \left(\frac{J\bar{p}}{1.8} \right) \dots\dots\dots 2.106$$

These equations will calculate the oil rate, and if we know the gas-oil ratio (GOR) then the gas rate can be easily calculated as follows,

$$q_g = q_o(GOR) \dots\dots\dots 2.107$$

2.3.3 Reservoir Thermal Model

Yoshioka (2007) presented a simple reservoir thermal model. In his model, the fluid and rock properties are assumed to be constant and the reservoir is box-shaped as in the Babu and Odeh model.

Yoshioka showed that the reservoir temperature differential equation based on energy balance can be expressed as,

$$\rho C_p (\vec{u} \cdot \vec{\nabla} T) - \beta T (\vec{u} \cdot \vec{\nabla} p) - K_T \nabla^2 T + \vec{u} \cdot \vec{\nabla} p = 0 \dots\dots\dots 2.108$$

The first term of LHS of Eq. **2.110** represents the thermal energy transported by convection. The second term represents the thermal energy change caused by fluid expansion. The third term is the thermal energy transported by heat conduction. Finally, the fourth term is the viscous dissipative heating. These equations can be solved analytically. If we assume that the heat transfer in the system can be divided to two parts, a linear flow part and a radial flow part, as shown in Fig **2.4**, then for a radial flow system, the solution is

$$T_r = \frac{1}{\beta} + c_0 r^{m_0} + c_1 r^{m_1} \dots\dots\dots 2.109$$

while the temperature equation for a linear flow system is,

$$T_l = \frac{1}{\beta} + c_2 e^{m_2} + c_3 e^{m_3} \dots\dots\dots 2.110$$

Fig. 2.4 helps explaining the difference between the two flow types.

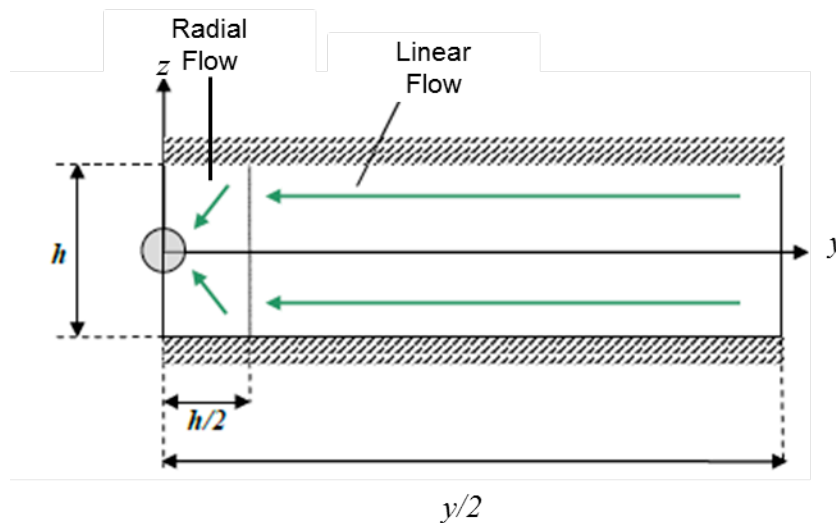


Fig. 2.4 Radial and Linear Flow

To be able to use Eqs. **2.109** and **2.110**, the variables in those equations needed to be calculated using the following equations,

$$c_0 = \frac{\theta_3 + \theta_4}{\psi_1 + \psi_2} \dots\dots\dots 2.111$$

$$c_1 = \frac{\theta_1 + \theta_2}{\psi_1 + \psi_2} \dots\dots\dots 2.112$$

$$c_2 = \frac{l_3 + l_4}{\psi_1 + \psi_2} \dots\dots\dots 2.113$$

$$c_3 = \frac{l_1 + l_2}{\psi_1 + \psi_2} \dots\dots\dots 2.114$$

$$m_0 = \frac{q}{4\pi L} \left[\frac{\rho C_p}{K_T} + \sqrt{\left(\frac{\rho C_p}{K_T} \right)^2 + \frac{4\mu\beta}{kK_T}} \right] \dots\dots\dots 2.115$$

$$m_1 = \frac{q}{4\pi L} \left[\frac{\rho C_p}{K_T} - \sqrt{\left(\frac{\rho C_p}{K_T} \right)^2 + \frac{4\mu\beta}{kK_T}} \right] \dots\dots\dots 2.116$$

$$m_2 = \frac{q}{4hL} \left[\frac{\rho C_p}{K_T} + \sqrt{\left(\frac{\rho C_p}{K_T} \right)^2 + \frac{4\mu\beta}{kK_T}} \right] \dots\dots\dots 2.117$$

$$m_3 = \frac{q}{4hL} \left[\frac{\rho C_p}{K_T} - \sqrt{\left(\frac{\rho C_p}{K_T} \right)^2 + \frac{4\mu\beta}{kK_T}} \right] \dots\dots\dots 2.118$$

where K_T is the total conductivity of the rock and the fluid saturated in the rock, β is coefficient of isobaric thermal expansion, μ is viscosity, ρ is density, and C_p is the specific heat capacity.

$$\theta_1 = e^{\frac{h}{2}(m_3+m_2)} \frac{h}{2} r_w^{m_0} (m_3 - m_2) (K_T m_0 - U_{overall} r_w) (\beta T_0 - 1) \dots \dots \dots 2.119$$

$$\theta_2 = \left(\frac{h}{2}\right)^{m_0} (\beta T_{well} - 1) U_{overall} r_w \left[e^{\frac{h}{2}m_3 + \frac{Y}{2}m_2} \left(\frac{h}{2}m_3 - m_2\right) + e^{\frac{h}{2}m_2 + \frac{Y}{2}m_3} \left(\frac{-h}{2}m_2 - m_3\right) \right] \dots \dots \dots 2.120$$

$$\theta_3 = e^{\frac{h}{2}(m_3+m_2)} \frac{h}{2} r_w^{m_1} (m_3 - m_2) (-K_T m_1 + U_{overall} r_w) (\beta T_0 - 1) \dots \dots \dots 2.121$$

$$\theta_4 = \left(\frac{h}{2}\right)^{m_1} (\beta T_{well} - 1) U_{overall} r_w \left[e^{\frac{h}{2}m_2 + \frac{Y}{2}m_3} \left(\frac{h}{2}m_1 - m_1\right) + e^{\frac{h}{2}m_3 + \frac{Y}{2}m_2} \left(\frac{-h}{2}m_3 - m_1\right) \right] \dots \dots \dots 2.122$$

$U_{overall}$ is the overall heat transfer coefficient including inflow effect.

$$\psi_1 = \beta r_w^{m_1} \left(\frac{h}{2}\right)^{m_1} (K_T m_1 - U_{overall} r_w) \left[e^{\frac{h}{2}m_2 + \frac{Y}{2}m_3} \left(\frac{h}{2}m_2 - m_0\right) + e^{\frac{h}{2}m_3 + \frac{Y}{2}m_2} \left(\frac{-h}{2}m_3 + m_0\right) \right] \dots \dots \dots$$

\dots \dots \dots 2.123

$$\psi_2 = \beta r_w^{m_0} \left(\frac{h}{2}\right)^{m_1} (K_T m_0 - U_{overall} r_w) \left[e^{\frac{h}{2}m_2 + \frac{Y}{2}m_3} \left(\frac{h}{2}m_3 - m_1\right) + e^{\frac{h}{2}m_3 + \frac{Y}{2}m_2} \left(\frac{-h}{2}m_2 + m_1\right) \right] \dots \dots \dots$$

\dots \dots \dots 2.124

$$l_1 = r_w^{m_0} e^{\frac{h}{2}m_2} (-K_T m_0 + U_{overall} r_w) (\beta T_0 - 1) \left(\frac{h}{2}\right)^{m_1} \left(\frac{h}{2}m_2 - m_1\right) \dots \dots \dots 2.125$$

$$l_2 = \left(\frac{h}{2}\right)^{m_0} \left(e^{\frac{h}{2}m_2} r_w^{m_1} \left(\frac{-h}{2}m_2 + m_1\right) (-K_T m_1 + U_{overall} r_w) (\beta T_0 - 1) \right) \dots \dots \dots 2.126$$

$$+ \left(\frac{h}{2}\right)^{m_0} \left(e^{\frac{Y}{2}m_2} U_{overall} r_w \left(\frac{h}{2}\right)^{m_1} (\beta T_{well} - 1) (m_1 - m_0) \right)$$

$$l_3 = r_w^{m_1} e^{\frac{h}{2}m_2} (K_T m_0 + U_{overall} r_w) (\beta T_0 - 1) \left(\frac{h}{2}\right)^{m_1} \left(\frac{h}{2}m_2 + m_1\right) \dots \dots \dots 2.127$$

$$l_4 = \left(\frac{h}{2}\right)^{m_0} \left(e^{\frac{h}{2} m_2} r_w^{m_1} \left(\frac{h}{2} m_2 + m_0\right) (-K_T m_1 + U_{overall} r_w) (\beta T_0 - 1) \right) \dots\dots\dots 2.128$$

$$- \left(\frac{h}{2}\right)^{m_0} \left(e^{\frac{Y}{2} m_3} U_{overall} r_w \left(\frac{h}{2}\right)^{m_1} (\beta T_{well} - 1) (m_1 - m_0) \right)$$

2.4 Coupled Model

In the previous section, we discussed the flow and thermal equations. In Fig 2.1, the flow problem in the wellbore (Block I) will be solved by Eq. 2.18 for single-phase and Eq. 2.82 for two-phase. The thermal problem of the wellbore (Block II) will be solved by Eq. 2.50 for single-phase flow and Eq. 2.89 for two-phase flow. The reservoir flow problem (Block III) will be solved using Eq. 2.90 for single-phase flow and Eq. 2.106 for two-phase flow. The last block (Block IV) is the reservoir thermal problem that will be solved using Eq. 2.109 for radial flow and Eq. 2.110 for linear flow in the reservoir.

In this section, we will couple the models developed to generate a method to estimate flow rate, pressure and temperature in trilateral well systems as shown in Fig. 1.1.

2.4.1 Coupled Pressure Model

After establishing the wellbore and reservoir models, the next step is to couple those models together in order to calculate the pressure and temperature profiles in each lateral. To solve the problem, we treat each lateral as an individual producer, and we

segment each lateral into several sections to calculate flow, pressure and temperature as shown in Fig. 2.5.

The following assumptions are followed in the coupled model:

1. Stable flow: flow in the reservoir and wellbore is assumed to be stable.
2. Isolated laterals: each lateral is draining from an isolated reservoir well.
3. Isolated reservoir segments: there is no cross-flow between adjacent reservoir segments. Each segment flows separately into the wellbore.

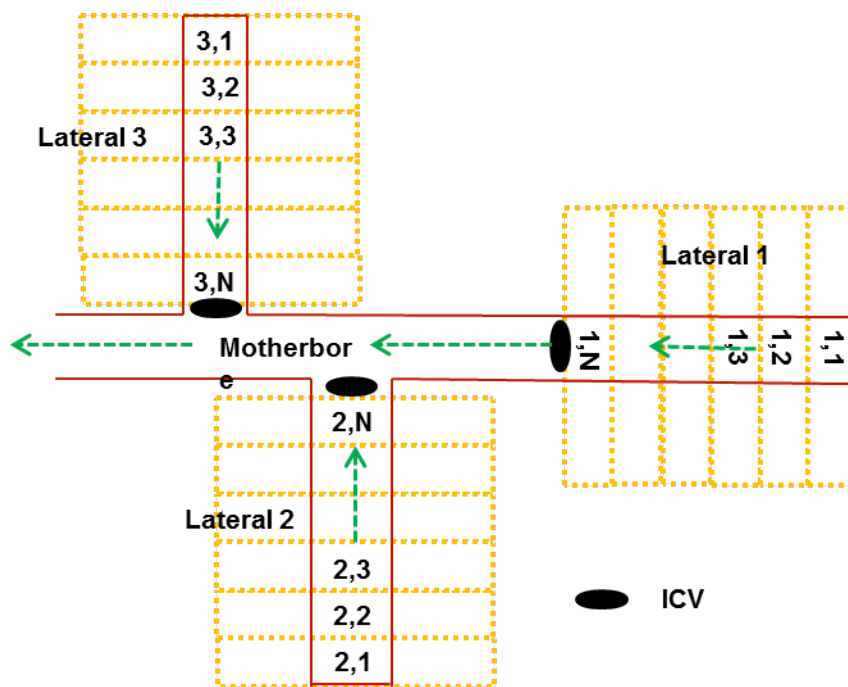


Fig. 2.5 Coupled Model Segmentation Schematic

The solution for the coupled model starts with calculating the pressure and flow rate in each lateral. To do so, we divide each lateral and corresponding reservoir into

equal segments, as can be seen in **Fig 2.5**. We start with an assumed wellbore flowing pressure for the first segment of the lateral (segment 1,1). Then, the flow rate is calculated in the lateral using the Babu and Odeh model that we have introduced earlier. In case of multiphase flow, we use the Vogel's correlation with Kamkom and Zhu's (2005) modification.

Once obtained flow rate from segment, we then calculate the pressure drop over this first segment inside the wellbore, $p_{1,2}$. Next, we move to the next segment and calculate the flowing pressure in the segment by the following equation,

$$p_{wf,2} = p_{wf,1} - \Delta p_{1,2} \dots\dots\dots 2.129$$

The flow rate of the next segment is then calculated using the new flowing bottomhole pressure alongside the new drawdown pressure. The same process is repeated for all segments until we reach the heel. The flow rate of the lateral is equal to the sum of all the flow rates of the segments. Once at the heel, we calculate the pressure drop to figure out the pressure at the junction. We proceed then to the next lateral and repeat the same process. Notice that the two junction pressures have to be equal for a multilateral well to produce. In case the junction pressures are not equal, we have to assume a different bottomhole pressure for the second lateral to recalculate the flow profile. Once they are equal, we move to the third and last lateral. Finally, the wellhead pressure is obtained by calculating the pressure drop between the last junction and the surface pressure. The detailed approach was presented by Kamkom and Zhu (2005).

We need to account for the pressure drop across the inflow control valves (ICV's). When ICV's are installed, they control the flow rate from the lateral to the main

wellbore. As a result, additional pressure drop needs to be considered. An ICV acts like a surface choke, when the fluid is forced through the small opening, momentum energy of fluid changes. Fig. 2.6 shows a combination of an ICV at a junction with a multilateral well.

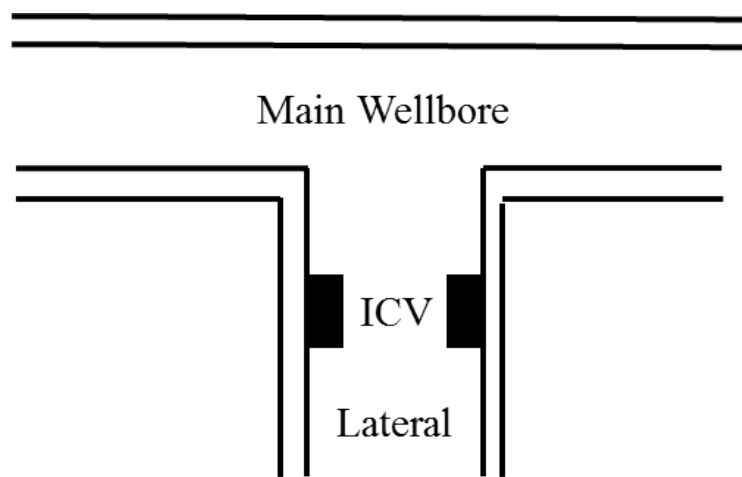


Fig. 2.6 Schematic of Flow across ICV

The pressure drop through ICV depends strongly on the structure of the ICV. For certain types of ICV, equations are provided by vendors. We use one example to show how to couple ICV as a part of the system as shown by Al Zahrani (2010).

The valve is designed to open at set ten different increments. The pressure drop is calculated by the following equation,

$$\Delta p_{valve} = \left(\frac{q}{CV} \right)^2 \bar{\rho} \dots\dots\dots 2.130$$

The term CV is a coefficient that is set to each increment as shown in Table 2.2. $\hat{\rho}$ is the specific density of the fluid. Notice that the pressure drop through ICV, Δp_{valve} , is proportional to the second power of flow rate, q^2 .

Table 2.2 CV Values at different ICV Increments

Valve Increment	CV gpm/psi ^{1/2}
1	1.1
2	2.4
3	4.4
4	6.8
5	9.4
6	14.3
7	25.4
8	42.4
9	105
10	175

After calculating the pressure drop across the ICV, we start the correction process with the first lateral. The pressure across the ICV is set to be equal to the pressure at the heel of lateral 1, $p_{1,N}$, minus the pressure drop across the ICV, Δp_{valve} .

$$p_1 = p_{1,N} - \Delta p_{valve} \dots \dots \dots 2.131$$

After we calculated the pressure drop between all adjacent segments, we calculate the pressure drop between adjacent segments in the wellbore after across the ICV until we get to the first junction. For simplicity we can call that pressure $p_{L1,J1}$. Once we are at the junction we calculate the pressure profile at lateral 2 and the pressure drop across the ICV and call that pressure $p_{L2,J1}$. $p_{L1,J1}$ and $p_{L2,J1}$ should be equal or close enough within an acceptable tolerance. Otherwise, pressure calculation is repeated for L2 until we reach that acceptable tolerance. Once that is achieved, we advance to L3 and the same process is repeated. A flowchart of the process can be seen in Fig 2.7.

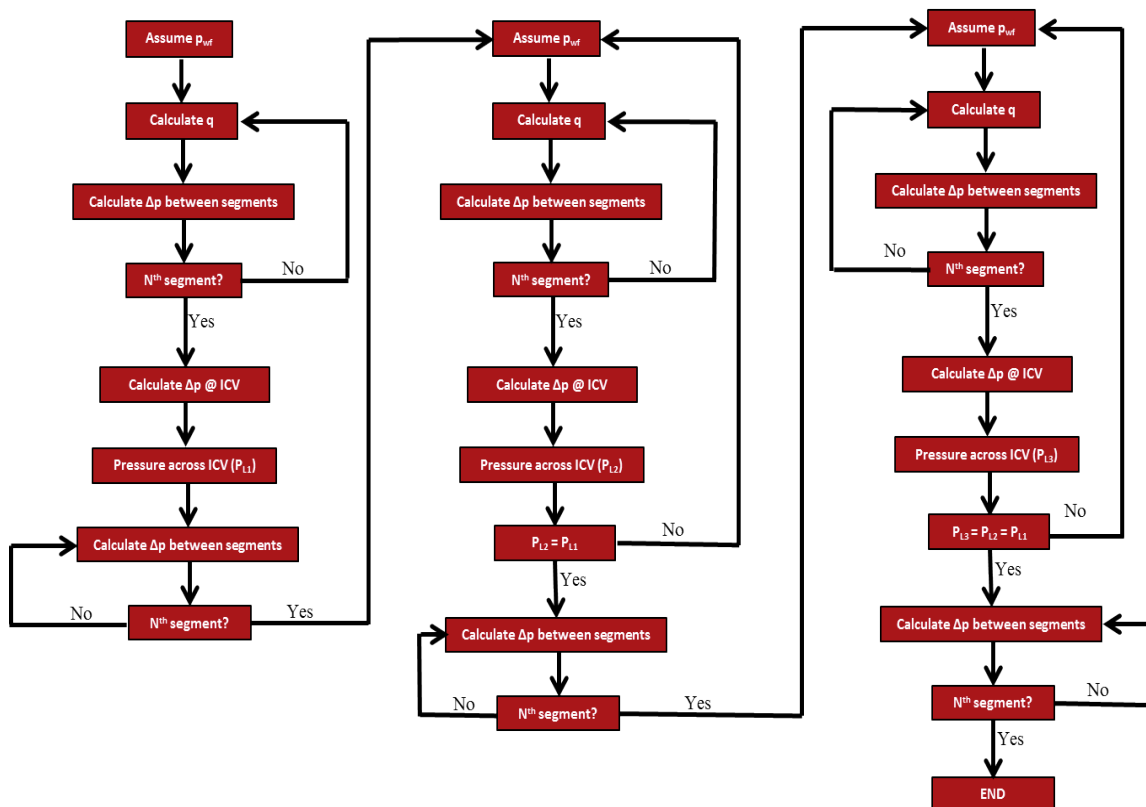


Fig. 2.7 Coupled Pressure Model Calculations Flowchart

2.4.2 Coupled Temperature Model

After establishing the pressure profile in each lateral, the temperature profiles need to be calculated. The process is similar to the one used in the previous section in pressure calculation in which we start with the bottom most lateral (L1) going from the toe to the heel.

All the equations needed for these calculations have been presented already in the previous sections. The single-phase wellbore thermal equation is

$$T_j = \frac{T_{j-1} + A_1(p_j - p_{j-1}) + \Delta x A_2 T_{wall}}{1 + \Delta x A_2} \dots\dots\dots 2.50$$

The two-phase wellbore thermal equation that we derived and will use is

$$T_j = \frac{T_{j-1} + A_3(p_j - p_{j-1}) + \Delta x A_4 T_{wall}}{1 + \Delta x A_4} \dots\dots\dots 2.89$$

While the reservoir thermal profile equation is

$$T = \frac{1}{\beta} + c_0 r^{m_0} + c_1 r^{m_1} \dots\dots\dots 2.109$$

When we calculate the first segment of each lateral, we assume no heat influx at wellbore. As a result, the boundary condition for the outer boundary will be the reservoir temperature while there will be no heat influx at the inner boundary. So, we can calculate the reservoir inflow temperature and assume it is equal to the wellbore temperature. We then assume a temperature profile in the wellbore that we need to estimate inflow temperature at each segment using Eq. 2.109. Then we use Eqs. 2.50 or 2.89 to recalculate the wellbore temperature. These values are then compared with the

assumed temperatures. If they converge to within an acceptable tolerance, the process is finalized. If not, then the process is repeated with different assumptions until the acceptable tolerance is achieved. The process is then repeated until we reach the last segment.

Similar to the pressure calculation, the temperature calculations need to be corrected due to the pressure drop caused by flowing through the ICV's. The main factor that we need to take into account is the Joule-Thompson effect. So, to adjust the temperature profile the following equation is used

$$\Delta T_{valve} = K_{JT} \Delta P_{valve} \dots \dots \dots 2.135$$

The equation used for multiphase is

$$\Delta T_{valve} = \frac{\sum_i (\rho v_x C_p y K_{JT})_i}{\sum_i (\rho v_x C_p y)_i} \Delta P_{valve} \dots \dots \dots 2.136$$

Once ΔT_{valve} is determined, the temperature at the first segment of the motherbore across the valve can be determined using the following equation

$$T = T_{L1,N} + \Delta T_{valve} \dots \dots \dots 2.137$$

Where the subscript $L1,N$ signifies the N^{th} (last) segment of Lateral 1. So, if the change in temperature was negative then the temperature in the first segment of the motherbore will decrease and vice versa. For subsequent segments of the motherbore, we use Eq. **2.50** for single-phase flow or Eq. **2.89** for two-phase flow. Given that there is no inflow, the inflow terms of these equations are not needed.

2.5 Forward Model Results

2.5.1 Introduction

In this section, we will show some results of the forward model. We will start with a base case that has a common condition as the ones in the field. The model introduced in the previous section will be applied to calculate temperature, pressure and flow rate profiles. Then we will show two more cases, one with water production from one of the laterals, and the other with flow controlled by ICV installation.

A sensitivity analysis is then performed to see the effect of changing the studied parameters on well performance as well as to check the dependability of the program. The two parameters that will be studied compared to the base case are permeability and lengths of laterals.

2.5.2 Base Case

In this case, the well has a main wellbore with three laterals. Lateral 1 is an extension of the main bore, and laterals 2 and 3 are branched off from the main bore. The configuration of the well is shown in Fig. **2.8**. The three laterals have the same length, and the three reservoirs have the same properties. The data used for the base case is shown in Table **2.3**.

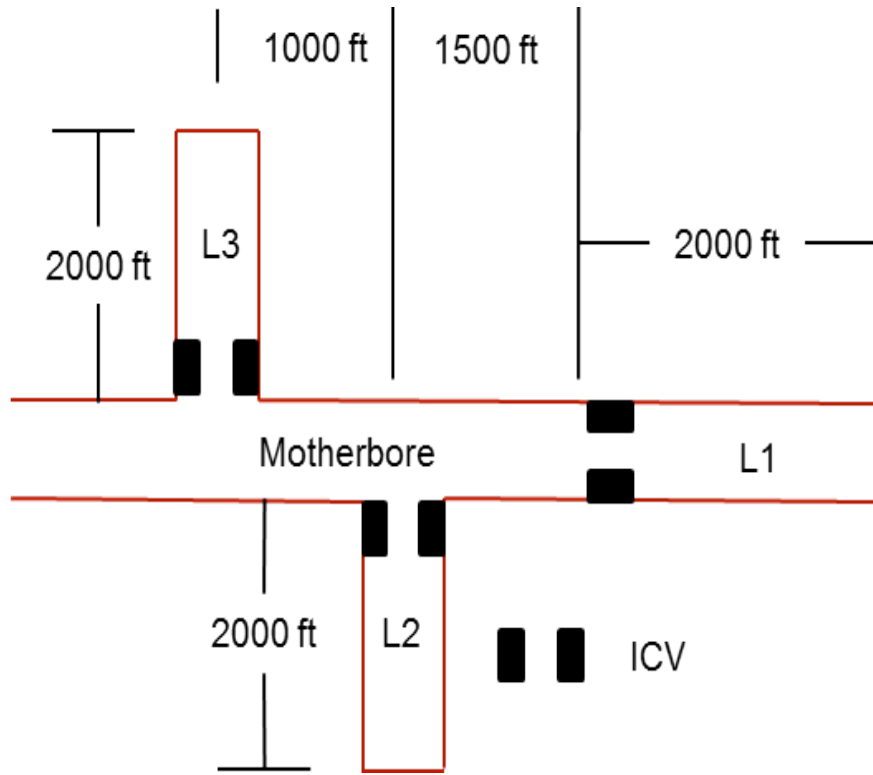


Fig. 2.8 Well Layout

Table 2.3 Base Case Data Input

Reservoir Width, a	3000 ft
Reservoir Length, b	3000 ft
Reservoir Thickness, h	50 ft
Well Length, L	2000 ft/lateral
Wellbore Diameter, D	6 in
Reservoir Pressure, p_e	2800 psi
Wellbore Flowing Pressure, p_{wf}	2700 psi
Reservoir Temperature, T	180°F
Total Conductivity, K_T	2 Btu/hr-ft-F
Horizontal Permeability, k_H	400 mD
Vertical Permeability, k_V	10 mD
Oil Density, ρ	43 lb _m /ft ³
Water Density, ρ_w	63.044 lb _m /ft ³
Oil Viscosity, μ	0.63 cP
Water Viscosity, μ_w	0.48 cP
Specific Heat Capacity, C_P	0.504 Btu/lb _m -F
Water Specific Heat Capacity, $C_{P,w}$	1.002 Btu/lb _m -F

The simulation was used to calculate the flow rate from each lateral, the total flow rate from the well, the pressure and temperature in the lateral and main wellbore. The total flow rate is 27,431 bbl/d, with lateral 1 producing 9008 bbl/d, lateral 2 producing 9131 bbl/d and lateral 3 producing 9292 bbl/d, as summarized Table 2.4.

Fig. 2.9 shows pressure distribution in all three laterals. As expected, all the laterals show a decrease in pressure due to the frictional pressure drop. We notice that the pressure drop increases as we get closer to the heel because of the increase in fluid inflow which in turn increases the frictional pressure drop. Having the same conditions for all laterals, same production rates were to be expected. However, the slight

difference in pressure among the laterals explains the difference in production rate out of each lateral.

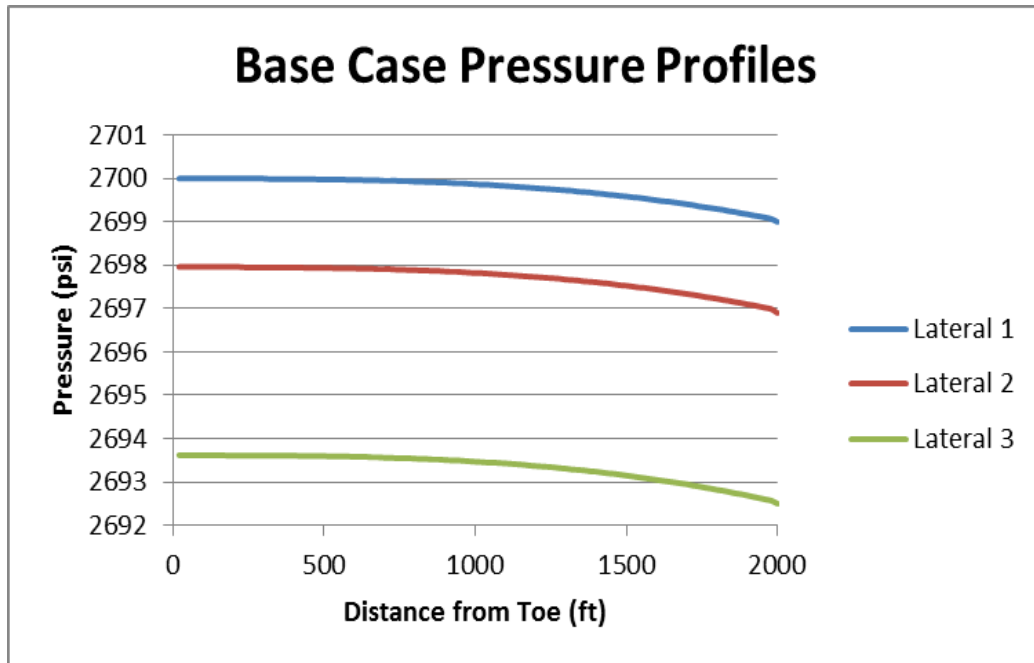


Fig. 2.9 Base Case Pressure Profiles

Temperature distribution in all laterals is shown in Fig. 2.10. All laterals show an increase in temperature as flow moves away from the toe. This phenomenon is caused by frictional heating. The magnitude of temperature in each profile reflects favorably with flow rate from each lateral.

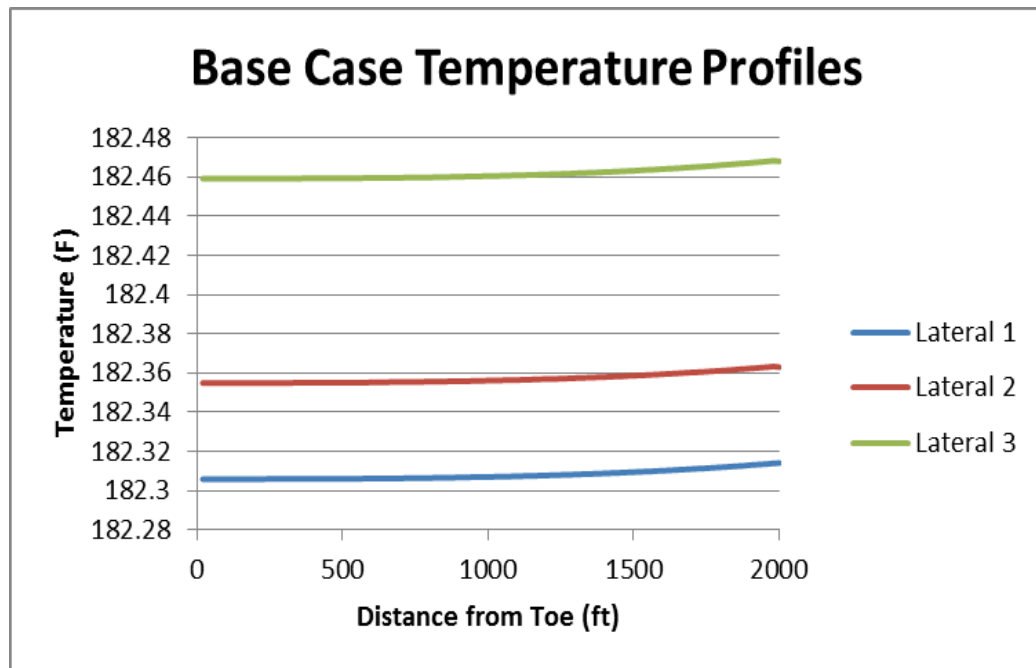


Fig. 2.10 Base Case Temperature Profiles

The following two figures (Figs. 2.11 and 2.12) show the pressure and temperature distribution in the motherbore. Entry points of laterals 2 and 3 are easily identified on both temperature and pressure curves. Both curves behaved as expected, with the decrease in pressure is associated with an increase in temperature as a result of the frictional forces as was shown in the individual lateral profiles. Notice that the slope changes on both curves whenever across an entry point along the motherbore. This provides valuable information for inversion. The slope is directly related to the flow rate. The higher the rate, the higher the absolute value (negative for pressure, positive for temperature) of the slope; leaves us the possibility to interpret the flow profile from the pressure and temperature data.

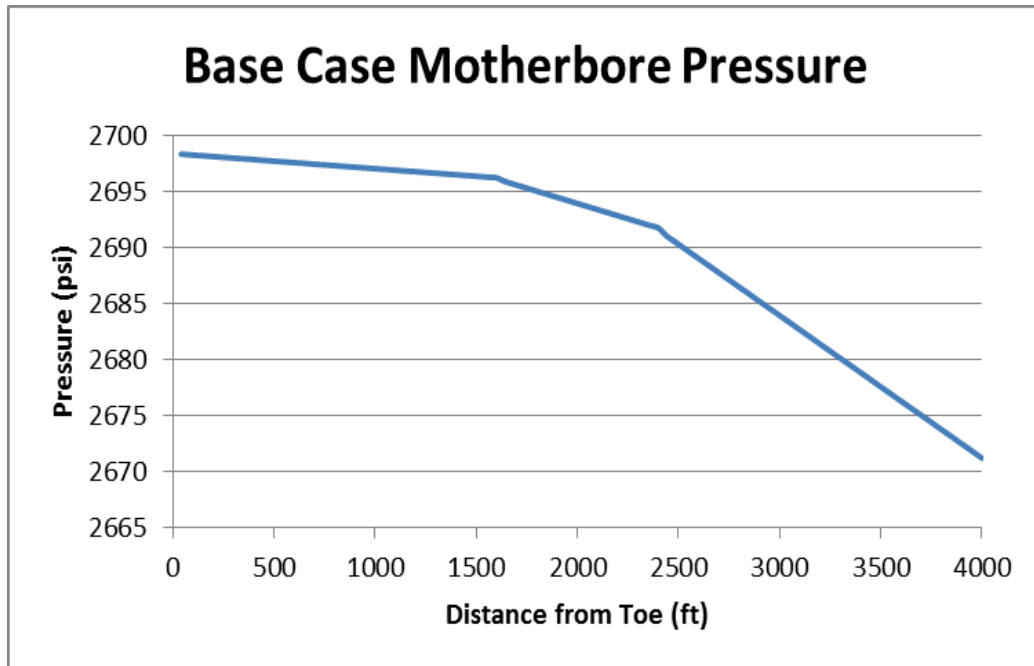


Fig. 2.11 Motherbore Pressure Profile for the Base Case

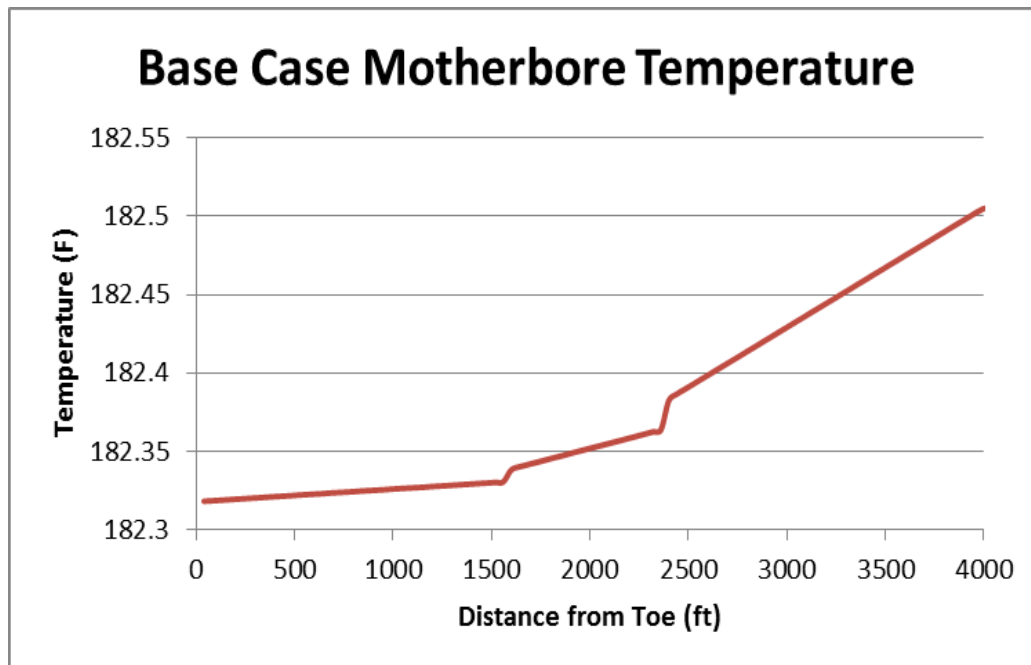


Fig. 2.12 Motherbore Temperature Profile for the Base Case

Table 2.4 summarizes the results of the base case run,

Table 2.4 Base Case Results

	q_o	q_w	q_g	Δp_{fric}	ΔT
L1	9,008	0.0	0.0	0.96	0.0083
L2	9,131	0.0	0.0	0.99	0.0086
L3	9,292	0.0	0.0	1.08	0.0094
Total	27,431				

2.5.3 Case 2

In this case, water is introduced into the system. We want to examine the effect of water production on temperature and pressure profiles, and seek the feasibility of identifying water from the temperature and pressure data. The well configuration is kept the same from the base case as shown in Fig 2.9 as well as the input data as shown in Table 2.3. Water is produced solely from lateral 2.

We have added about 13% of water to the total liquid production. When holding p_{wf} at the toe of lateral 1 equal to 2700 psi, the total flow rate is 27,383 bbl/d, with lateral 1 producing 9008 bbl/d oil, lateral 2 producing 9002 bbl/d liquid (5112 bbl/d of oil, and 3890 bbl/d of water) and lateral 3 producing 9373 bbl/d oil. Producing water had no effect on lateral 1 production as it produced the same rate as in the base case. This was not the case with laterals 2 and 3, as both laterals showed a decrease in production rates.

Fig 2.13 shows the pressure profiles of all laterals. It behaves similarly to the pressure profiles of the base case. The only noticeable difference is that the pressure drop in lateral 2 is greater (1.89 psi) than in the base case (0.99 psi).

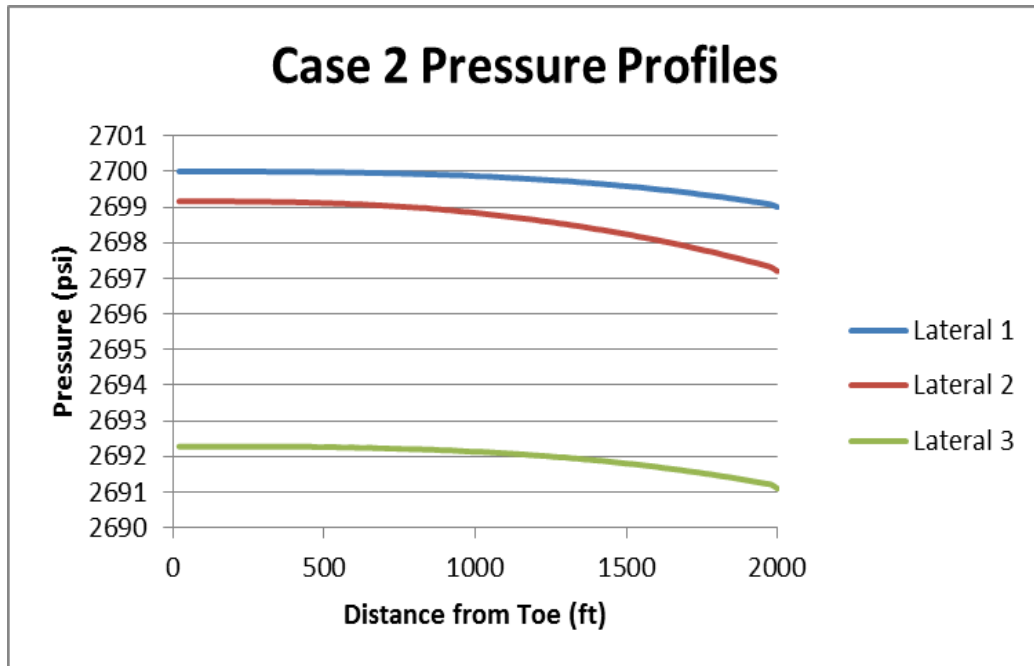


Fig. 2.13 Case 2 Pressure Profiles

Fig 2.14 shows the temperature distribution in all laterals. Laterals 1 and 3 temperature curves show a similar behavior as in the base case. On the other hand, lateral 2 shows a drop in temperature compared to the base case caused by the water production. The feature definitely can help us to identify the zone that is producing water.

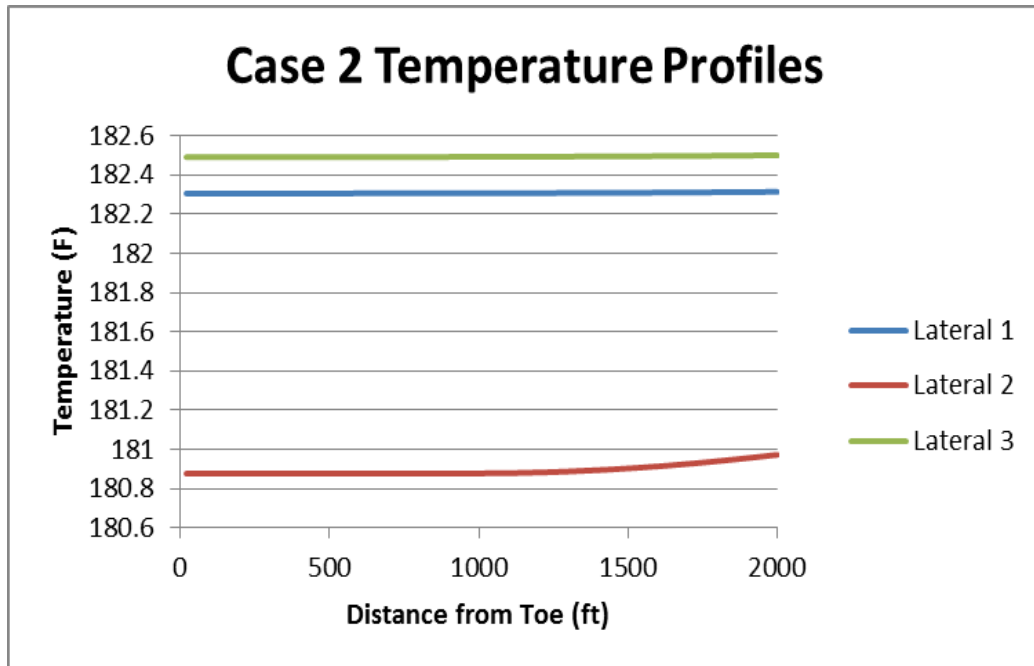


Fig. 2.14 Case 2 Temperature Profiles

Fig 2.15 shows the pressure distribution in the motherbore. From the figure, one can not see any change compared to the base case as the change in pressure between the two cases is minimal.

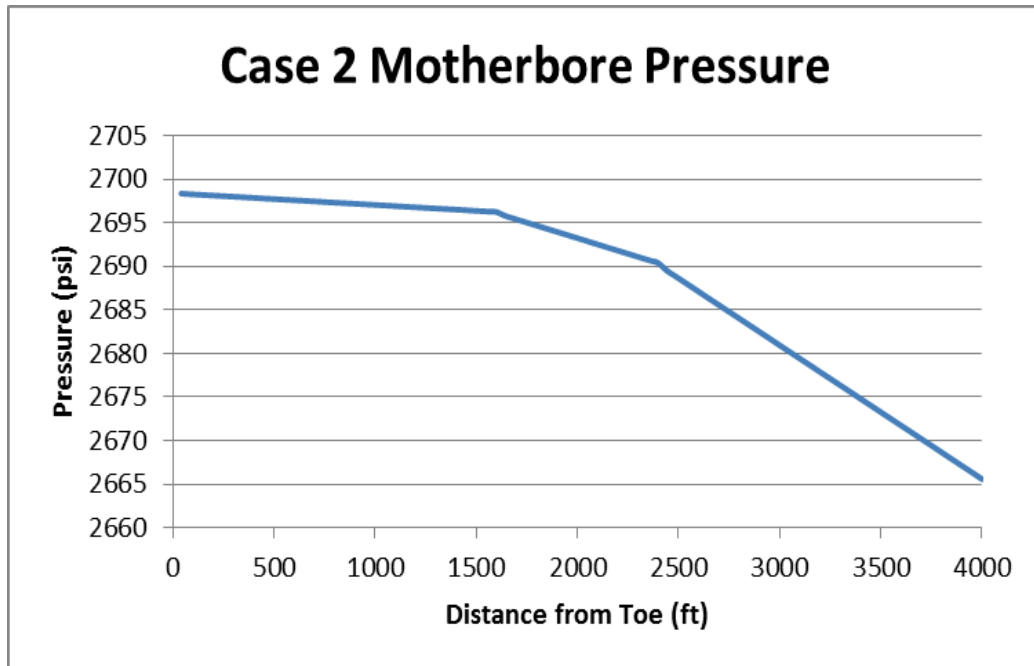


Fig. 2.15 Motherbore Pressure Profile for Case 2

That is not the case when the temperature distribution of the motherbore is plotted in Fig 2.16. The water produced by lateral two is showing an obvious cooling effect as it enters the motherbore. The temperature rises again as only oil from lateral 3 enters the motherbore. Comparing the base case, we can certainly locate water entry in a multilateral well from the measured temperature in the motherbore.

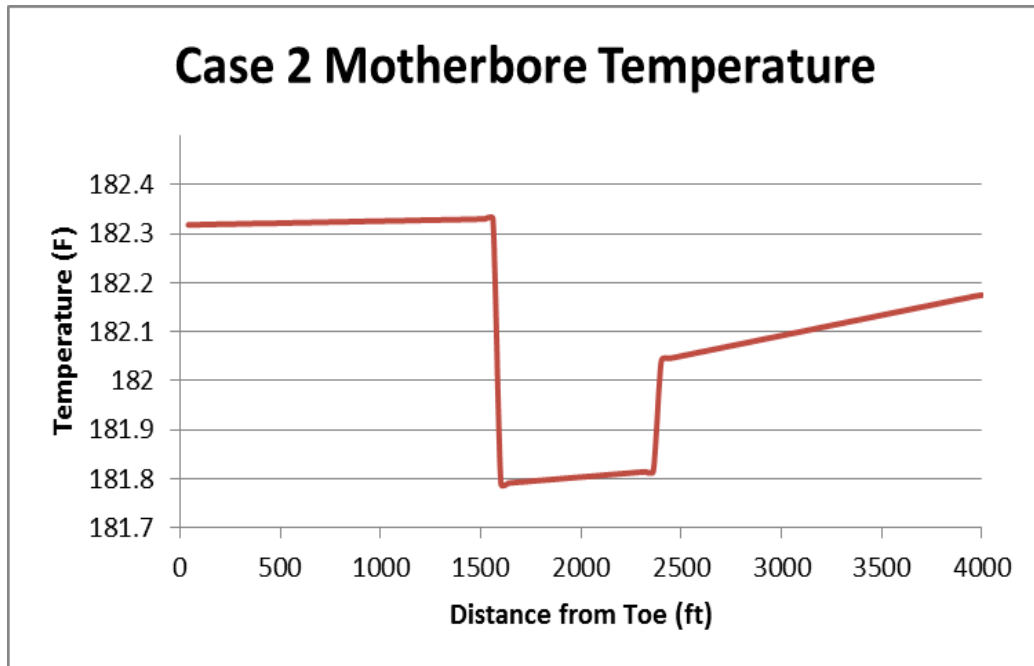


Fig. 2.16 Motherbore Temperature Profile for Case 2

Table 2.5 summarizes the results of case 2 run,

Table 2.5 Case 2 Results

	q_o	q_w	q_g	Δp_{fric}	ΔT
L1	9,008	0.0	0.0	0.96	0.0083
L2	5,112	3,890	0.0	1.89	0.0966
L3	9,373	0.0	0.0	1.11	0.0096
Total	23,493	3,890			

2.5.4 Case 3

In this case, we ICV to control water production. All of the input were kept the same from case 2. Water is produced from lateral 2 as well. The only difference is that lateral

2 is choked back by an installed ICV. This will allow us understand how ICV can be used to improve production when dealing with water producing zones. This will also show if the other laterals are affected by the choking process.

When keeping the p_{wf} at the toe of lateral 1 at 2700 psi, the total flow rate is 25,718 bbl/d, with lateral 1 producing 9008 bbl/d oil, lateral 2 producing 7272 bbl/d liquid (4892 bbl/d oil, and 2380 bbl/d water) and lateral 3 producing 9438 bbl/d. once again, producing water had no effect on lateral 1 production as it produced the same rate as in previous two cases. Lateral 2 produced less due to the ICV choking the rate back. The total fluid rate (oil and water) was reduced from lateral 2. That drop in rate in lateral 2 led to lateral 3 producing more than in the previous two cases. That proves the effectively of ICV's choking back water producing laterals in reducing the amount of water produced as well as help improving the rate of other laterals in the well.

Figure 2.17 below shows the pressure distribution of all laterals. The three curves do not show any abnormal behavior for the conditions stated. Laterals 1 and 3 pressure distribution are almost identical to the ones experienced in case 2. There an obvious shift by 2.09 psi in lateral 2 compared to case 2 due to the choke back effect.

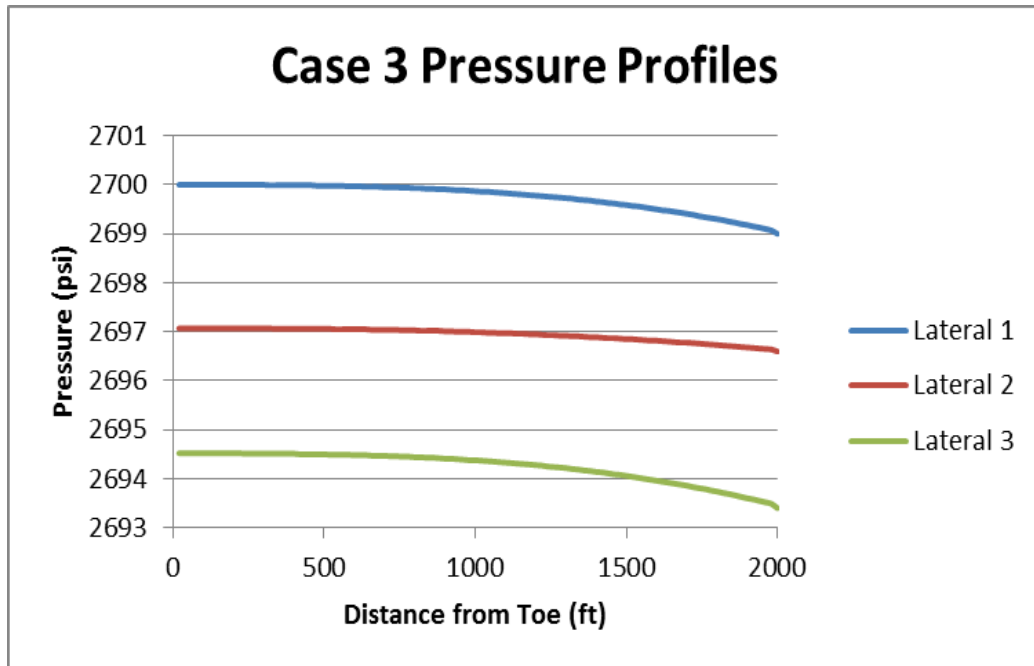


Fig. 2.17 Case 3 Pressure Profiles

Fig 2.18 shows the temperature distribution of all laterals in case 3. Laterals 1 and 3 show a similar temperature behavior to what was observed in case 2 with a slight increase in temperature in lateral 3 due to the increase in rate, which leads to an increase in temperature caused, by the increase in friction.

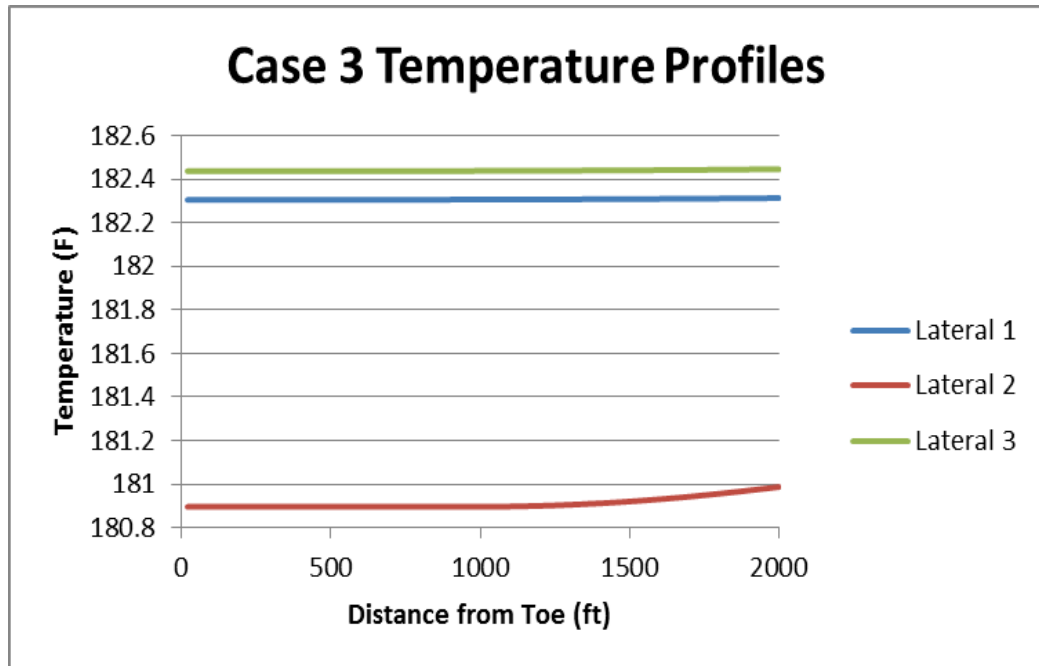


Fig. 2.18 Case 3 Temperature Profiles

The pressure behavior in the motherbore as shown in Fig 2.19 is similar to case 2. The pressure drop shown by the curve is as expected. On the other hand, Fig 2.20 once again helps showing the shift in temperature cause by the reduced rate of water produced. The cooling effect when the flow from lateral two gets into the motherbore is still obvious, but it is “warmer” than what was shown in Fig 2.16 that displayed the temperature profile of the motherbore in case 2.

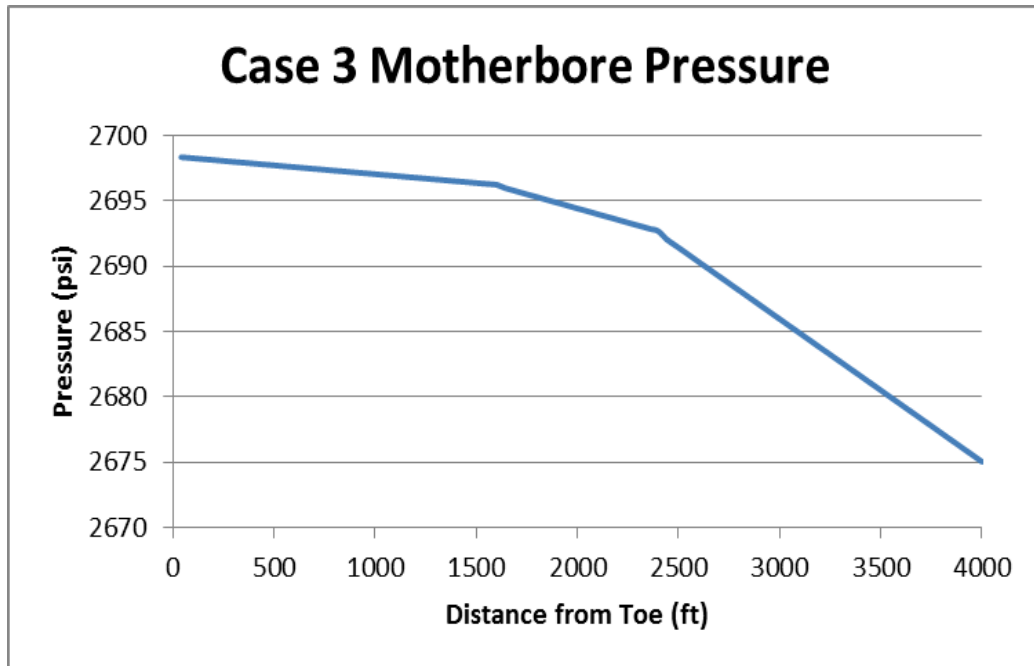


Fig. 2.19 Motherbore Pressure Profile for Case 3

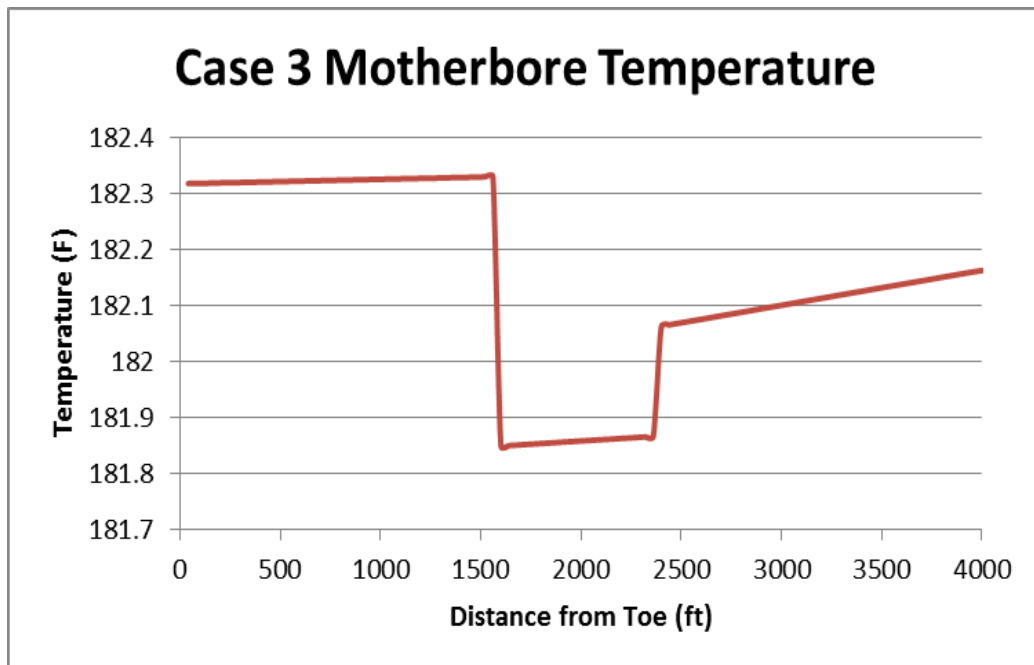


Fig. 2.20 Motherbore Temperature Profile for Case 3

Table 2.6 summarizes the results of case 3 run,

Table 2.6 Case 3 Results

	q_o	q_w	q_g	Δp_{fric}	ΔT
L1	9,008	0.0	0.0	0.96	0.0083
L2	4,892	2,380	0.0	0.44	0.0920
L3	9,438	0.0	0.0	1.06	0.0092
Total	23,338	2,380			

2.5.5 Cases Comparison

In Figs. 2.21, 2.22 and 2.23 we plotted the pressure distribution, the temperature distribution and cumulative production rates in the motherbore of all cases. This helps comparing the results of each case.

Figure 2.21 shows the pressure profile in the motherbore. It shows that in the first part of the well (Lateral 1) the pressure drop for all three cases are exactly the same. From the junction of lateral 2, the pressure profile starts deviating from each other. For case 2, the pressure drop is higher than the base case. The main attribution is the water production from lateral 2. For case 3, the pressure drop in the main bore is lower than the base case because the ICV choked back the production rate. The shape of the three curves is similar but the slop is different depending on the flow profile. The entry point of water could be identified from the curves.

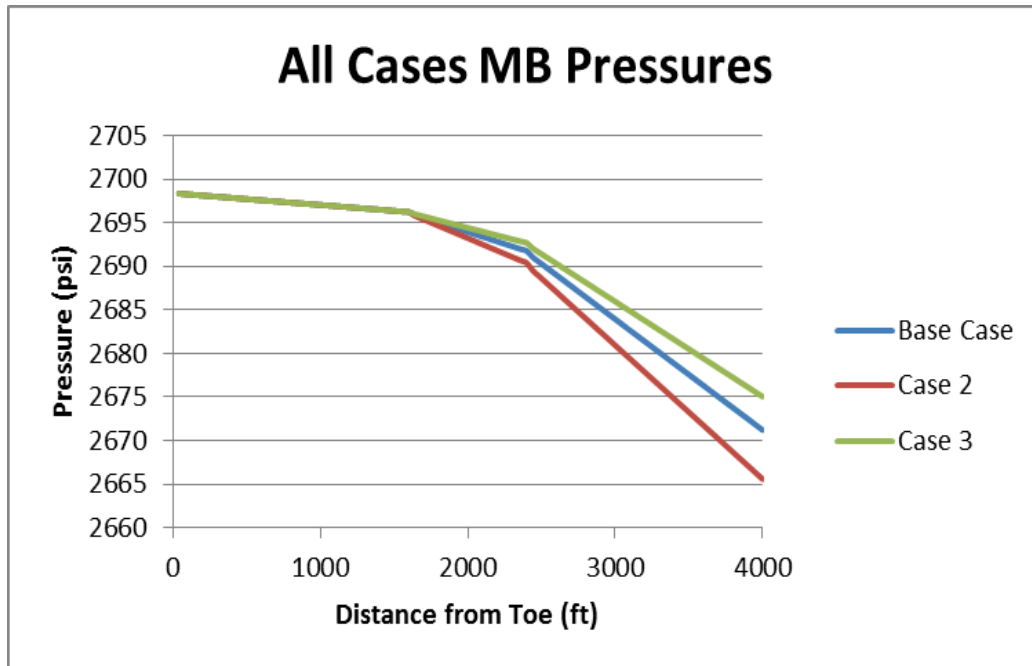


Fig. 2.21 Motherbore Pressure Profiles for all Cases

Figure 2.22 shows the temperature comparison of all three cases. It is interesting to see that the cooling effect caused by water production in lateral 2 in cases 2 and 3 is obvious when the curves are compared to the temperature distribution of the base case. These curves confirm that temperature curve shape is more clear an identification of water entry. When the water is choked back by ICV, the cooling part is moving towards the original temperature curve. This can also tell us if the ICV is working or not.

Figure 2.23 is the flow rate profiles for all these scenarios. All these profiles start with the same p_{wf} at the toe of lateral 1. Realized that in inversion, when these profiles are identified, the calculated temperature and pressure will match the ones, serve as observed in Figs 2.23 and 2.24.

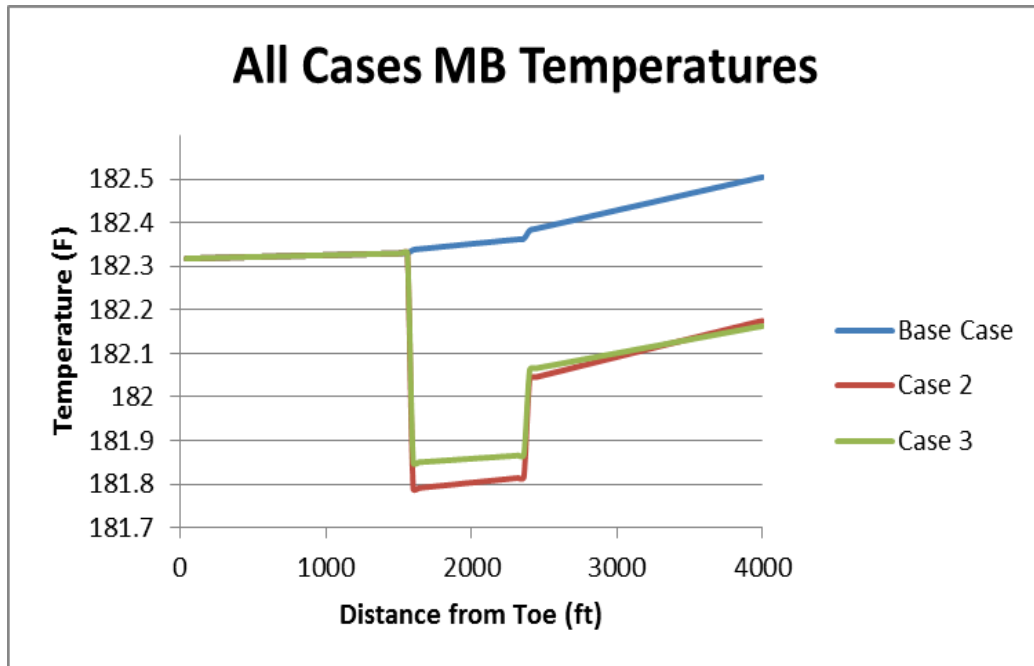


Fig. 2.22 Motherbore Temperature Profiles for all Cases

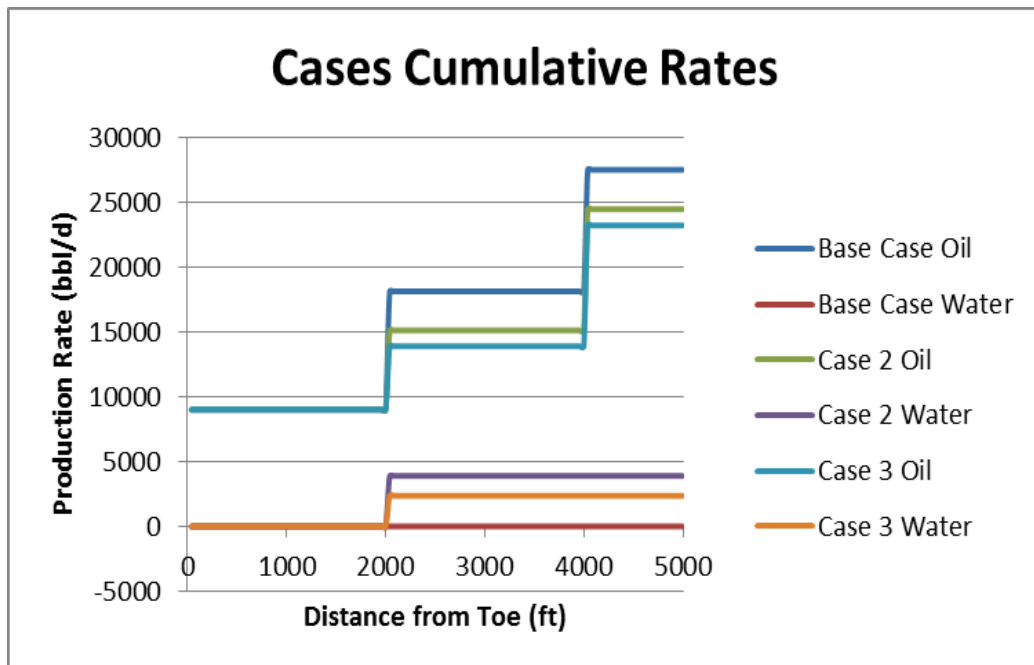


Fig. 2.23 Cumulative Production Rates in all Cases

2.5.6 Sensitivity Analysis

Two parameters were further evaluated in this study. Permeability is the first one examined in the sensitivity analysis. The horizontal permeability in the base case is 400 mD. For the sake of comparison, different values of horizontal permeability were tested while holding all other parameters constant to examine the effect of permeability on flow, temperature, and pressure behavior. The values of horizontal permeability used in the study are 100 and 50 mD.

Fig. 2.24 shows the pressure distribution in the motherbore at different horizontal permeability. We could see that pressure drop increases because of higher production rates in higher permeability case. At high permeability, entry points of each lateral are easily identified as there is a noticeable change in pressure at each entry point. When permeability becomes smaller, the pressure drop in the wellbore becomes subtle, and locating fluid entry becomes difficult.

Those entry points are also identified from temperature data shown in Fig. 2.25.

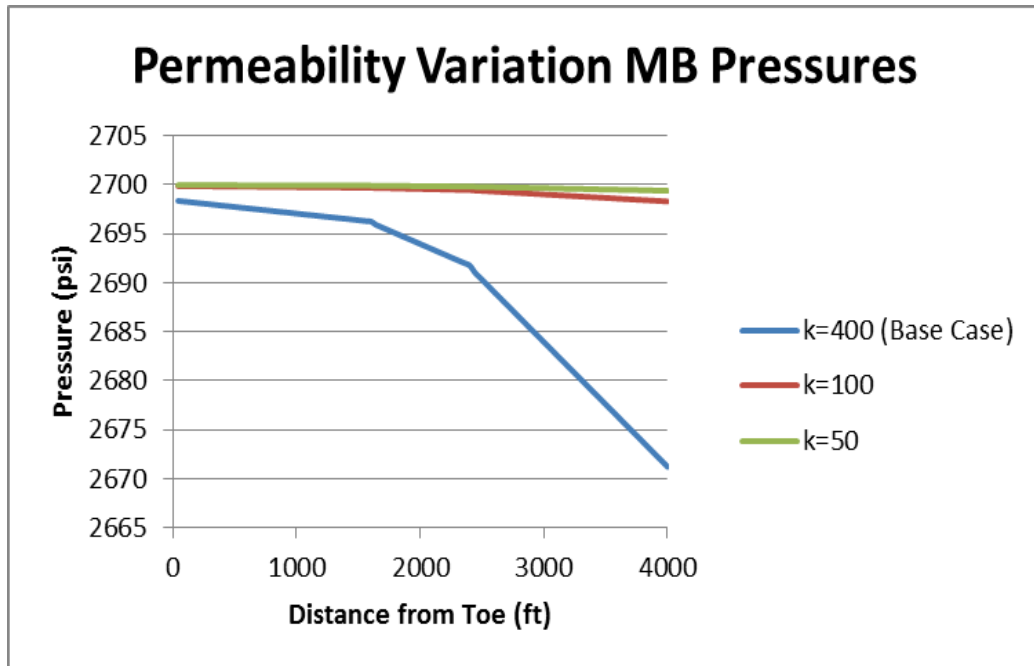


Fig. 2.24 Pressure Profiles in Motherbore with Different Permeabilities

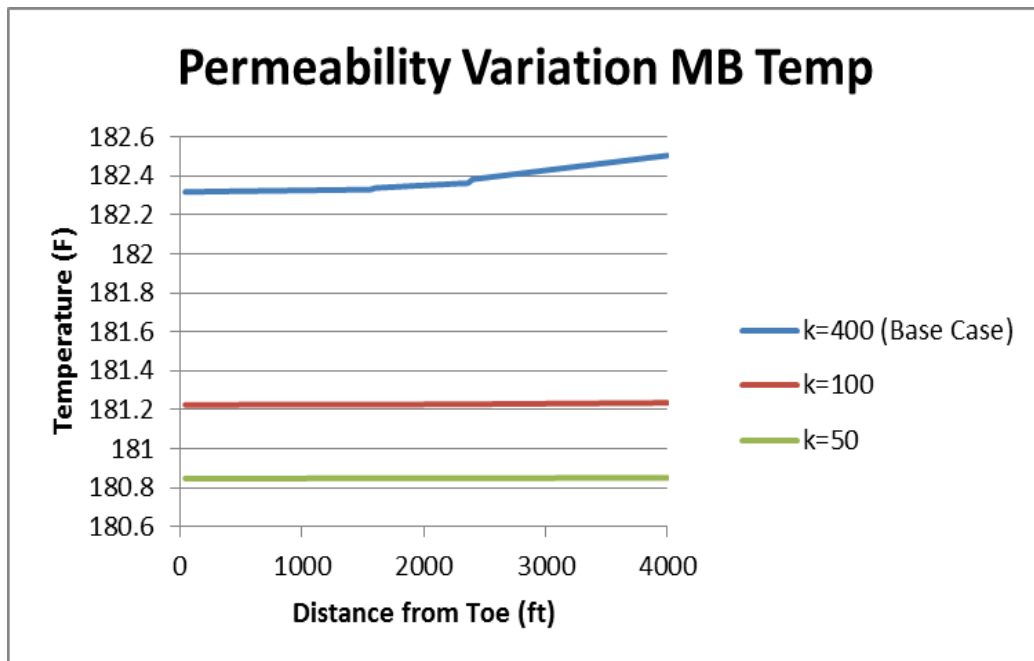


Fig. 2.25 Temperature Profiles in Motherbore with Different Permeabilities

As expected, the production rate varied accordingly to the change in horizontal permeability. This change in permeability also caused a significant change in pressure and temperature profiles, as seen in the previous two figures. Table 2.7 summarizes the total oil production rates in each case.

Table 2.7 Flow Rates in Permeability Study

k_H (mD)	q_T (bbl/d)
400	27,431
100	14,375
50	10,611

The second part of the sensitivity analysis deals with varied lateral lengths. While the lengths of laterals 1 and 3 were changed, the total lateral length was kept the same to have a better comparison between the two cases. The three laterals in the base case have an equal length of 2,000 ft, with a total lateral length of 6,000 ft. The lengths of laterals of the second case are 2,500 ft for lateral 1, 2,000 ft for lateral 2, and 1,500 ft for lateral 3, and a total length of 6,000 ft as well.

The total production of the second case is 26,798 bbl/d which is close to the original case (27,431 bbl/d). There is no significant change in the motherbore pressure or temperature profiles compared to the base case as can be seen Figs 2.26 and 2.27.

It is noticed in Fig 2.26, the average drop in pressure between the base case and the varied lengths case is only about 3 psi. The lower pressure which also can be interpreted as a higher pressure drop in the latter case is related to the slightly lower production. Since lateral 1 has longer length compared with the base case, more fluid

comes into the motherbore from lateral 1, causing a slope change from the toe of the motherbore. Table 2.8 summarizes the flow rate distribution of each case.

Table 2.8 Flow Rates in Varied Lengths Study

	Base Case	Varied Lengths
L1	9,008	10,527
L2	9,131	9,275
L3	9,292	6,996
Total	27,431	26,798

Temperature profiles in the motherbore for both cases can be seen in Fig 2.27. As in the previous case, the entry points are clearly identifiable with the sudden change in temperature at each entry point. The average difference in temperature between the two cases was 0.028°F. The varied lengths case showed a slightly warmer profile overall which was not expected as it had a lower production rate.

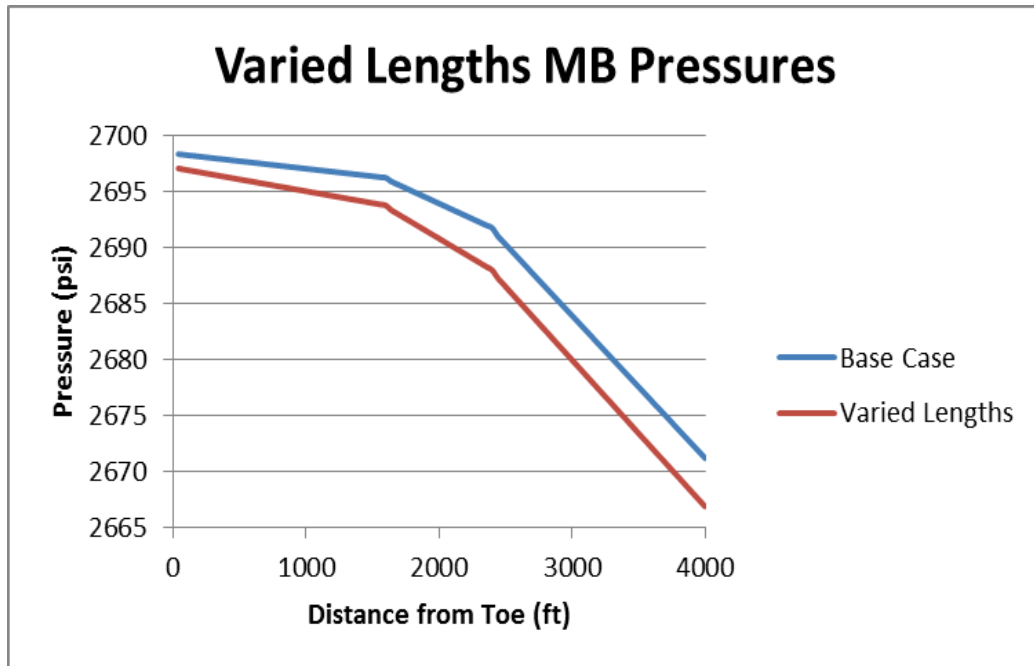


Fig. 2.26 Pressure Profiles in Motherbore

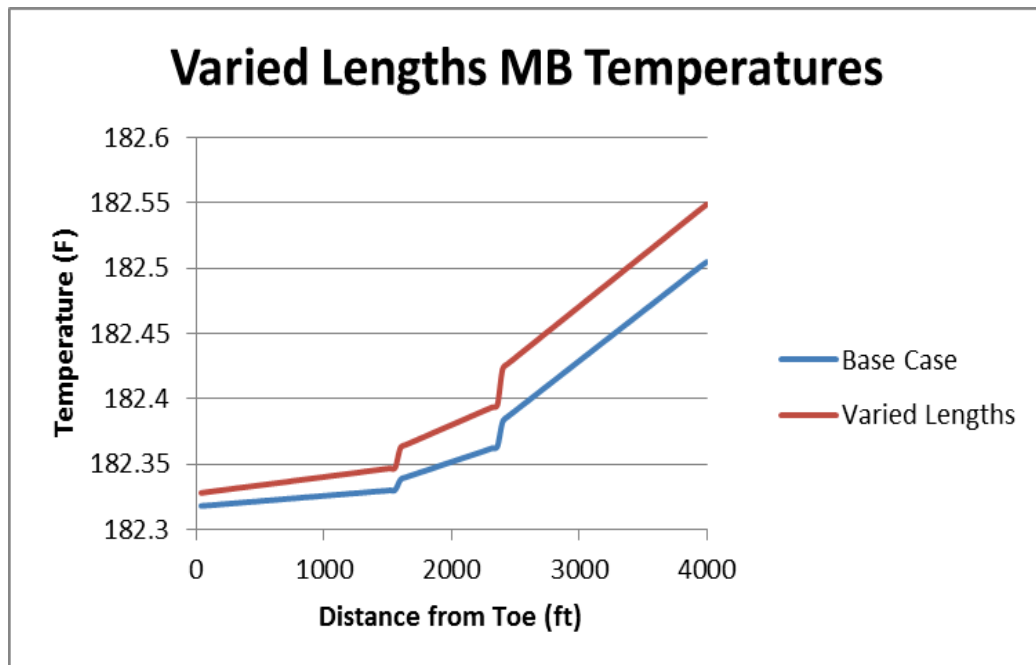


Fig. 2.27 Temperature Profiles in Motherbore

Forward model results have showed encouraging signs of temperature and pressure responses to flow conditions. As behavior of temperature and pressure profiles were as expected and sensitivity analysis reaffirmed initial findings.

In order to use the model to interpret flow rate from temperature and pressure, an inverse model is needed. An inverse model would allow us to calculate flow rate, q , from temperature and pressure readings provided by downhole sensors. Next chapter is dedicated to establishing a reliable inverse model.

CHAPTER III

INVERSE MODEL

3.1 Introduction

In the previous section, the forward model has been introduced to account for temperature and pressure responses in the wellbore during production. The forward model helped us identify the factors that could affect the temperature and pressure responses. Going forward, an inverse model is introduced to estimate laterals flow rates using temperature and pressure data provided by PDHM's.

3.2 Least-Square Regression

The inverse model problem is considered as a nonlinear least-square regression problem. The method is applied by an objective function that calculates the discrepancy between measured and simulated data. The solution is found by minimizing the objective function as much as possible.

A general form of an objective function is as follows (Oliver et al., 2008),

$$f(x) = \frac{1}{2}(d - g(x))^T C_n^{-1}(d - g(x)) \dots \dots \dots 3.1$$

where x is the parameters vector, d is the vector of the observed data, C_n is the covariance matrix that take into account measurement errors and different units of different types of data, and $g(x)$ is the forward model.

To simplify the objective function, we introduce the variable e which is defined as,

$$e = C_n^{-\frac{1}{2}}(d - g(x)) \dots \dots \dots 3.2$$

so, Eq. 3.1 becomes,

$$f(x) = \frac{1}{2} e^T e \dots \dots \dots 3.3$$

For the purpose of this study, the wellbore temperature distribution is the observed data while the flow rate is the calculated data that is estimated from calculated temperature readings. As a result, the objective function becomes

$$f(x) = \sum_{i=1}^N (T_{obs} - T_{cal})^2 \dots \dots \dots 3.4$$

N is the number of data points along the wellbore, T_{obs} is the measured data, and T_{cal} is the calculated data.

The reason behind the need of an inverse model is to guess the flow rate and then use the forward model to simulate wellbore temperature profiles during these flow rates. This process continues until a desirable match between measured and calculated data is reached.

3.3 Markov Chain Monte Carlo

The MCMC method used in this study obtains a Markov chain by sampling from a proposal distribution. The distribution is uniform due to the equal probability of all the samples (Tabtabaei, 2011). To construct the algorithm, the following steps are followed:

1. Process starts with assuming a flow profile in the targeted lateral (q_n). The profile is assumed to be uniform unless otherwise known.
2. Forward model is used to calculate temperature profile of the wellbore (T_n).
3. Objective function (f_n) is calculated using Eq. 3.4.
4. New flow profile (q_{n+1}) is generated using the proposal distribution.
5. Forward model is run again using (q_{n+1}) to calculate a new temperature profile (T_{n+1}).
6. New objective function (f_{n+1}) is calculated via Eq. 3.4.
7. The Metropolis-Hastings criterion (Metropolis et al., 1953) is used to accept the guess of flow rate (q_{n+1}) as

$$\rho(x_n, x_{n+1}) = \min\left(1, \frac{q(x_n | x_{n+1})\pi(x_{n+1})}{q(x_{n+1} | x_n)\pi(x_n)}\right) \dots\dots\dots 3.5$$

where in this case,

$$x_n = q_n \dots\dots\dots 3.6$$

$$\pi(x_n) = e^{-f_n} \dots\dots\dots 3.7$$

Since a uniform probability distribution is assumed, then

$$q(x_{n+1} | x_n) = q(x_n | x_{n+1}) \dots\dots\dots 3.8$$

As a result, Eq. 3.5 becomes

$$\rho(q_n, q_{n+1}) = \min\left(1, \frac{e^{-f_{n+1}}}{e^{-f_n}}\right) \dots\dots\dots 3.9$$

8. If the new calculated flow rates are not within an acceptable range, then we repeat steps 2 to 7 to update the flow rate profile until the temperature profile history is matched. Otherwise, a new q_{n+1} need to be generated in step 4 from the proposal distribution and the whole process is repeated to get to that acceptable range.

To overcome the computational expense associated with using the MCMC method, the algorithm is modified to increase the convergence rate. In this study, a modified MCMC algorithm introduced by Ma et al. (2008) will be used. The modified algorithm is called random walk MCMC algorithm which is based on “perturbing” the current flow rate profile. So, the way it works is by guessing the flow rates from the independent uniform distribution, and then the new flow rate is generated based on the initial guess as in the following equation,

$$q_{n+1} = q_n \pm \Delta q_n \dots\dots\dots 3.10$$

Later we will discuss this process in more details explaining the factors determining whether Δq_n should have a positive or a negative sign. Δq_n is set at 10% for this study.

As a result,

$$\Delta q_n = 0.1q_n \dots\dots\dots 3.11$$

So, this last constraint in Eq. 3.10 needs to be satisfied in step 4 in order for the new flow rate generated from the uniform distribution to be accepted.

3.4 Procedure

The ultimate goal of this study is to enable engineers to monitor well performance real-time. In order to achieve that goal, a fast inversion procedure is desired that can be used with the inversion logarithm that have been described earlier (MCMC).

The inverse model was developed using C++ and is designed to invert the correct flow rate distribution from T_{obs} . The procedure starts with an initial guess of p_{wf} at the first segment of the toe of lateral 1. The forward model is then run using the guessed value of p_{wf} to calculate the flow rate and temperature profiles in the laterals. After that the following function is defined,

$$f(p_{wf}) = \sum_{i=1}^N (T_{obs} - T_{cal})^2 \dots\dots\dots 3.12$$

The gradient, $f'(p_{wf})$, is then calculated. The value of p_{wf} is updated each time during the iteration. The new value of p_{wf} is dependent on the value of the gradient. If the gradient is positive then,

$$p_{wf, new} = p_{wf} - \Delta p \dots\dots\dots 3.13$$

On the other hand, if $f'(p_{wf})$ is negative then,

$$p_{wf, new} = p_{wf} + \Delta p \dots\dots\dots 3.14$$

The forward model is run each time p_{wf} is updated until the following condition is satisfied,

$$\frac{f^{n+1} - f^n}{f^n} \leq \varepsilon \dots\dots\dots 3.15$$

Once the condition is satisfied, the process is stopped and the final p_{wf} value is considered the inverse p_{wf} at the toe of lateral one and it is used to calculate the new q .

To better understand the process, Fig 3.1 is a flowchart for the inverse model iteration process.

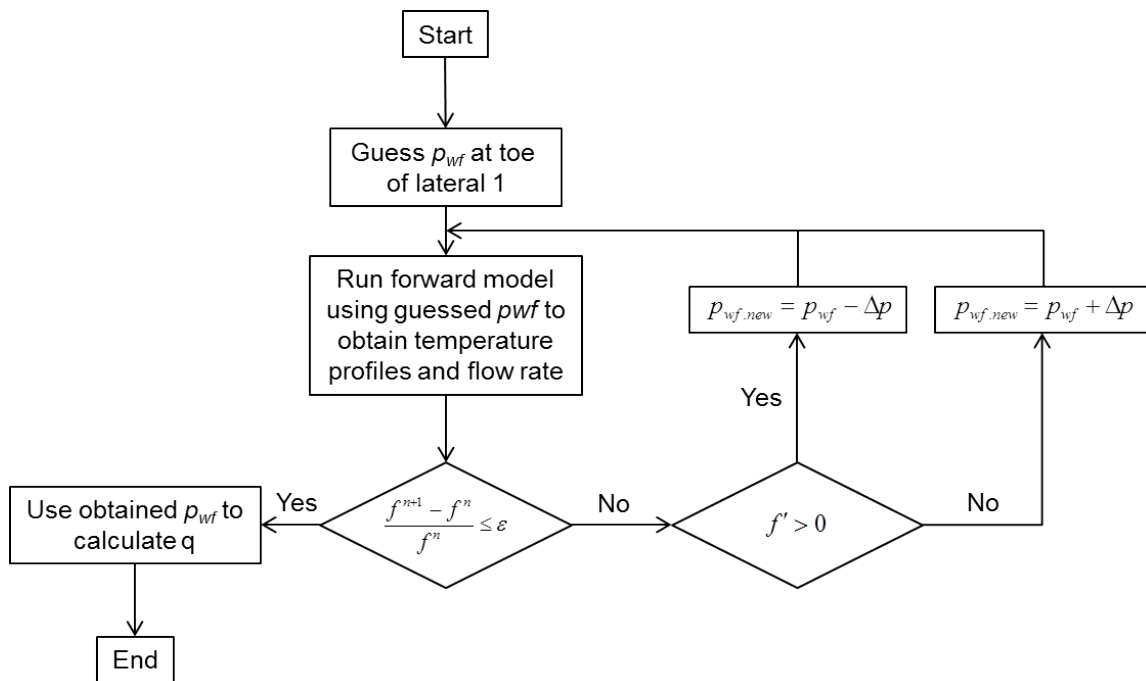


Fig. 3.1 Inverse Model Flowchart

3.5 Inversion Results

In this section, the results of the inverse model will be presented. The base case in the forward model section is going to be used to illustrate how the inversion procedure works.

The trilateral well that was used as the base case in the last chapter will be used again to test the inverse model. All reservoir, fluid, and wellbore properties are kept the same (Table 2.3). The observed data of the well will be first generated by the forward model. And then, we randomly assume a flow profile, and use the forward model to generate calculated data. The inverse model is used to update the flow profile until the calculated temperature matches the observed temperature.

The initial guess of p_{wf} was 2700 psi at the first segment of the toe of lateral 1. The model then used Eqs. 2.90, 2.59, and 2.129 to calculate flow rates out of each segment in the lateral. Eqs. 2.130 and 2.131 were then used to account for the pressure drop across the ICV. The process was repeated for the other laterals to generate the flow profiles. Fig. 3.2 shows the pressure distribution in the motherbore.

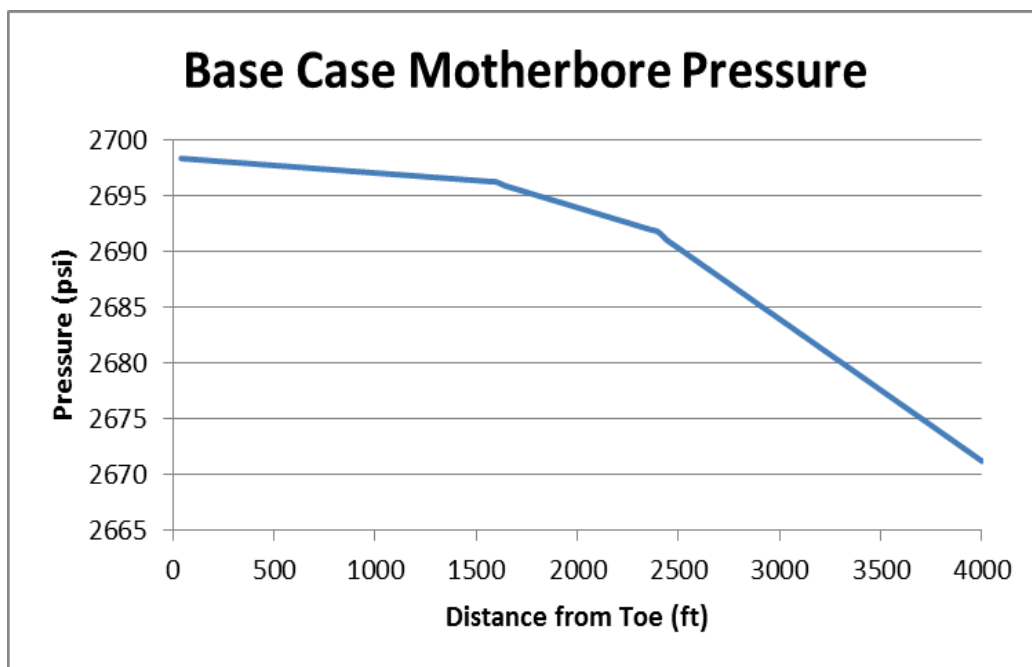


Fig. 3.2 Motherbore Pressure Profile for the Base Case

The temperature profiles were then calculated using Eqs. 2.50 and 2.109. The temperature drop was calculated using Eqs. 2.135 and 1.37. The single-phase equations were used because the system contains only oil. Fig 3.3 shows the temperature distribution in the motherbore of the base case.

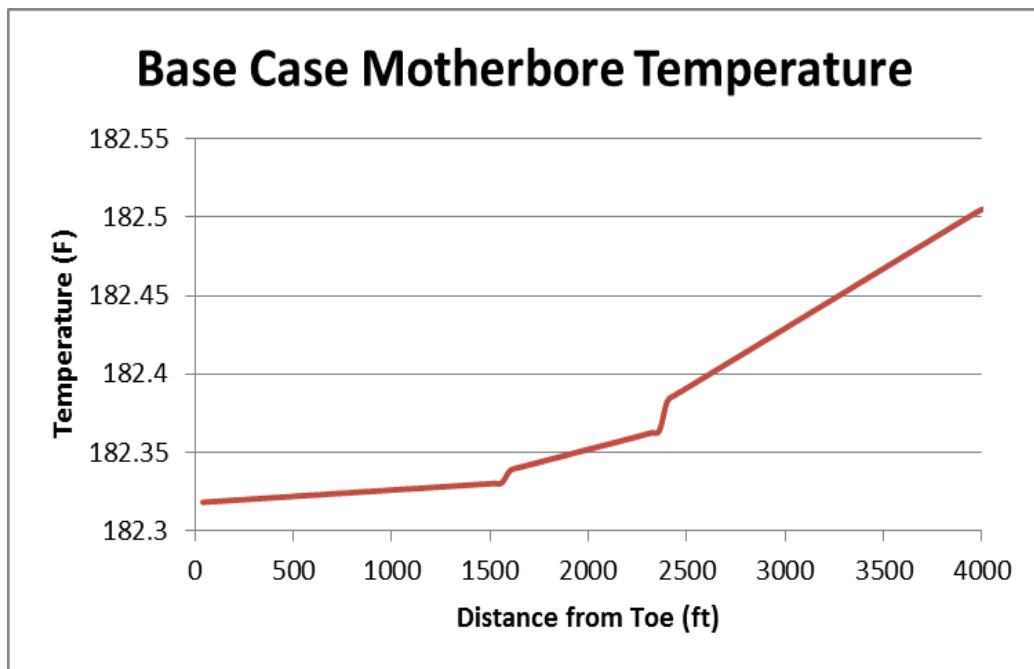


Fig. 3.3 Motherbore Temperature Profile for the Base Case

The total flow rate of the base case is 27,431 bbl/d. The flow rate distribution is in Fig 3.4.

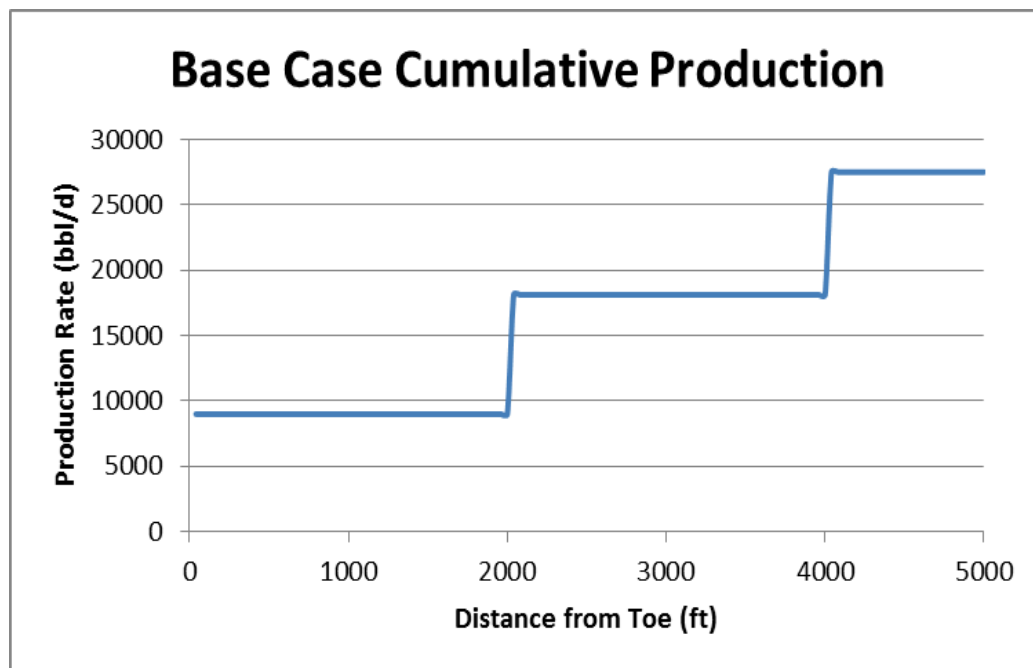


Fig. 3.4 Flow Rate Distribution for the Base Case

A new p_{wf} of 2500 psi was then assumed to start the inversion process. The inverted p_{wf} calculated by the model was 2703 psi. The total flow rate was 26,959 bbl/d. Lateral 1 flow rate was 8827 bbl/d, lateral 2 was 8943 bbl/d and lateral 3 was 9189 bbl/d.

Another p_{wf} of 2750 psi was then assumed and inverted to compare results. The inverted p_{wf} was found to be 2701 psi. The total flow rate was 27,646 bbl/d. Lateral 1 flow rate was 9132 bbl/d, lateral 2 was 9165 bbl/d and lateral 3 was 9349 bbl/d.

Figs. 3.5 and 3.6 show the inverted and the observed temperature profiles in the motherbore and cumulative flow rates distributions of all cases respectively. On the other hand, Table 3.1 shows the flow distribution of all cases.

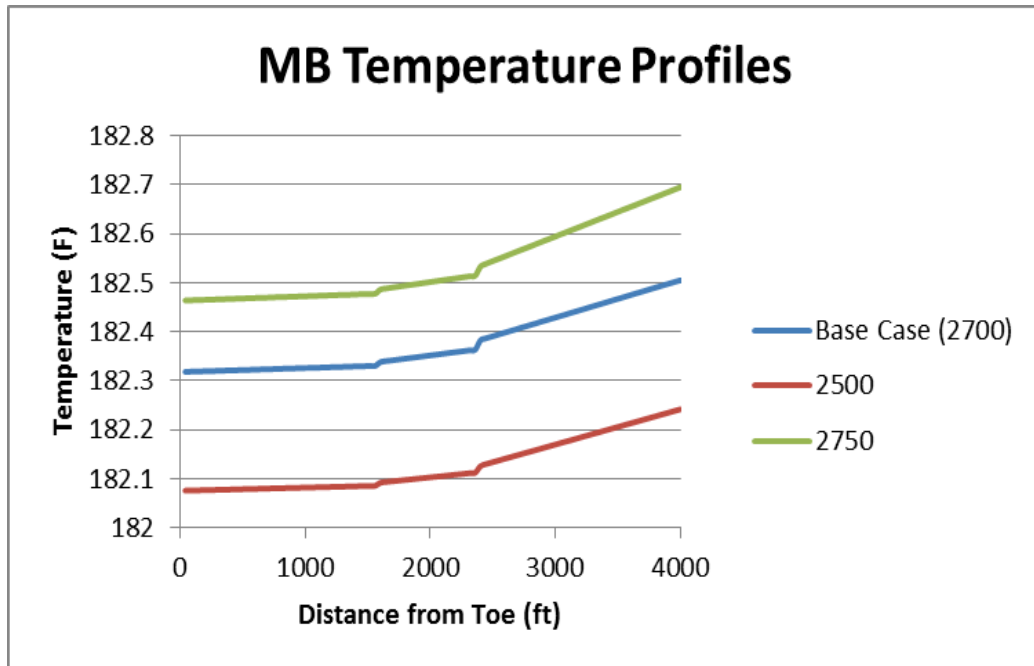


Fig. 3.5 Motherbore Temperature Profiles

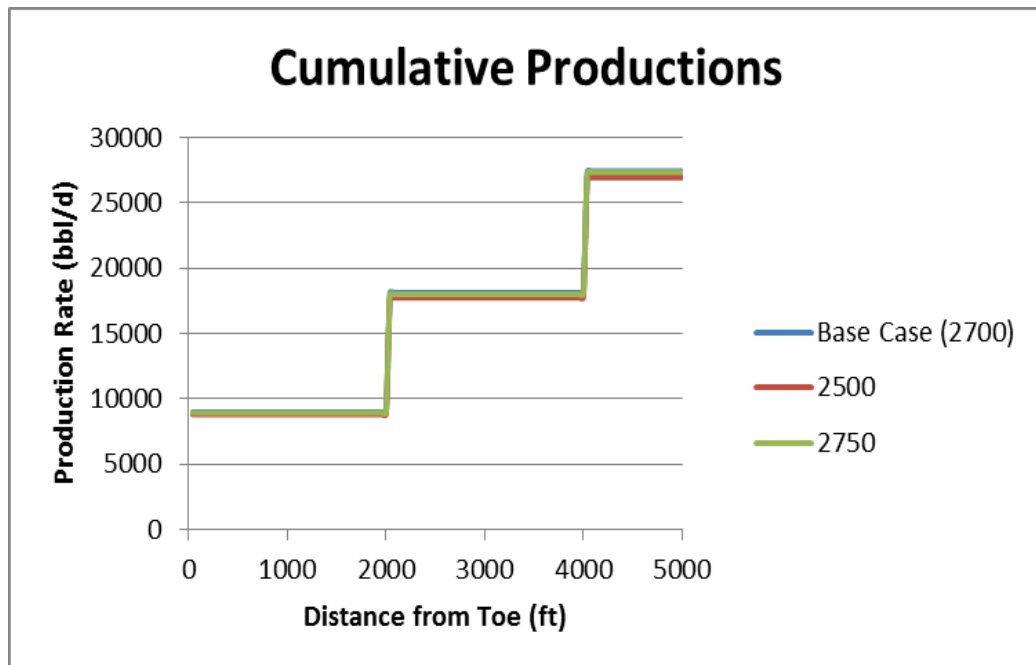


Fig. 3.6 Cumulative Production Rates in all Cases

Table 3.1 Flow Rates Distribution of all Cases

Lateral	Base Case q_o	2500 q_o	2750 q_o
1	9008	8827	9132
2	9131	8943	9165
3	9292	9189	9349
Total	27431	26959	27646

CHAPTER IV

FIELD APPLICATION

4.1 Introduction

The final objective of this study is to investigate the feasibility of application of the developed model, algorithm and method in field conditions. All calculations and results that have been presented in the study so far were computer simulated. Results have been encouraging but to ensure its efficiency, the model needs to be tested with real field data.

In this chapter, a practical test of the model will be presented. In which a comparison of results between field data and model findings will take place. Results will be analyzed and improvements will be recommended if possible.

4.2 Field Case

A trilateral well that is completed similarly to the way this study is geared toward has been selected. The well has sensors and ICV's installed at each lateral. The structure of the well is shown in Fig **4.1**.

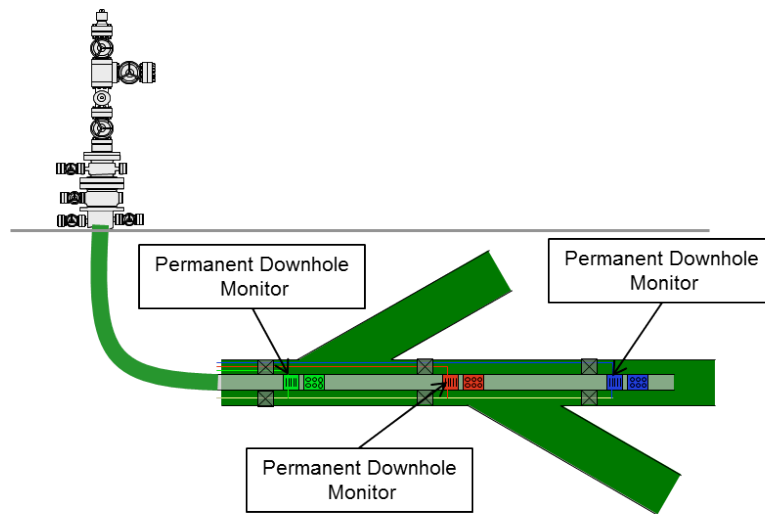


Fig. 4.1 Field Case Well Configuration

The three open-hole laterals are drilled, one is an extension to the motherbore, the other two are branches from the motherbore. Lateral 1 which extends out of the motherbore is 4,423 ft long. Laterals 2 and 3 are sidetracked out of the motherbore. Lateral 2 is 4,753 ft while lateral 3 is 4,802 ft. As a result, the total reservoir exposure provided by the laterals is 13,978 ft. The three laterals were drilled in the same zone so the reservoir and fluid properties are assumed to be the same for all laterals. All the properties used in the model are included in Table 4.1.

It should be noted as can be seen from Fig 4.1 that the temperature and pressure readings are provided by three fixed points “above” each lateral. The data will be used at those three locations and there is no actual measurement that is taking place inside the

laterals. The measurements are taking place just outside the laterals as the fluids get into the motherbore.

A production test was performed on the well in 2011. The test was performed to measure production rates from each lateral, in addition to, the total production from the well. There is no other means of accurately determining flow rates in this well. In order to perform the test, production from each lateral is isolated and metered. All three laterals are then put on production so the total flow rate can be determined. Temperature and pressure are determined by sensors downhole while production rate is observed by multiphase flow meter.

The process is time consuming which leads to high cost. In addition to the cost of running the test itself, there is a hidden cost of production lost during the test. Individual lateral testing means production from the other two laterals has to be stopped. Furthermore to ensure accurate testing each lateral needs to be flown for an extended amount of time so the flow would be stable.

Table 4.1 Field Case Properties

Reservoir Width, a	65000 ft
Reservoir Length, b	65000 ft
Reservoir Thickness, h	235 ft
Lateral 1 Length, L	4423 ft
Lateral 2 Length, L	4753 ft
Lateral 3 Length, L	4802 ft
Wellbore Diameter, D	6 in
Reservoir Pressure, p_e	2800 psi
Wellbore Flowing Pressure, p_{wf}	2390 psi
Reservoir Temperature, T	187°F
Total Conductivity, K_T	2 Btu/hr-ft-F
Horizontal Permeability, k_H	340 mD
Vertical Permeability, k_V	27 mD
Oil Density, ρ	47.5 lb _m /ft ³
Water Density, ρ_w	63.044 lb _m /ft ³
Oil Viscosity, μ	0.89 cP
Water Viscosity, μ_w	0.48 cP
Specific Heat Capacity, C_P	0.507 Btu/lb _m -F
Water Specific Heat Capacity, $C_{P,w}$	1.002 Btu/lb _m -F

As mentioned before, the well has sensors installed in the wellbore at each junction. As a result, the pressure and temperature is determined real-time when fluid flows pass the sensors from each lateral into the motherbore. It would have been more beneficial if there were means of measuring pressure and temperature in the laterals as well. We would be able to compare the pressure and temperature profiles in the laterals generated by the model with the ones provided by such sensors. Unfortunately, the technology to do so was not available as of yet, for this case.

4.3 Procedure

The forward model is used first to generate temperature profiles in the laterals. Field properties that are provided in Table 4.1 are used to run the forward model. The resulting temperature profiles are then used in the inverse model as the reference temperature. The inverse model in turn will generate the calculated temperature profiles and p_{wf} at the first segment of lateral one. The resulting p_{wf} is then used in calculating flow rates out of each lateral similar to what was shown in the previous chapter.

After running the production test, the following production rates as shown in Table 4.2 were tested in the field:

Table 4.2 Field Rate Test

Lateral	Production Rate
1	6586 bbl/d
2	9200 bbl/d
3	9305 bbl/d

These rates are the actual production rates from each lateral as reported after the production test using a multiphase flow meter. Figs. 4.2, 4.3, and 4.4 are test results that show flow rates readings during the duration of testing of each lateral. As can be seen, in each test the flow rate shows a sudden spike when put on production. It takes around 2 hours for the flow rate to stabilize. After the stabilization period is over, flow rate seems to be consistent for an extended period of testing time.

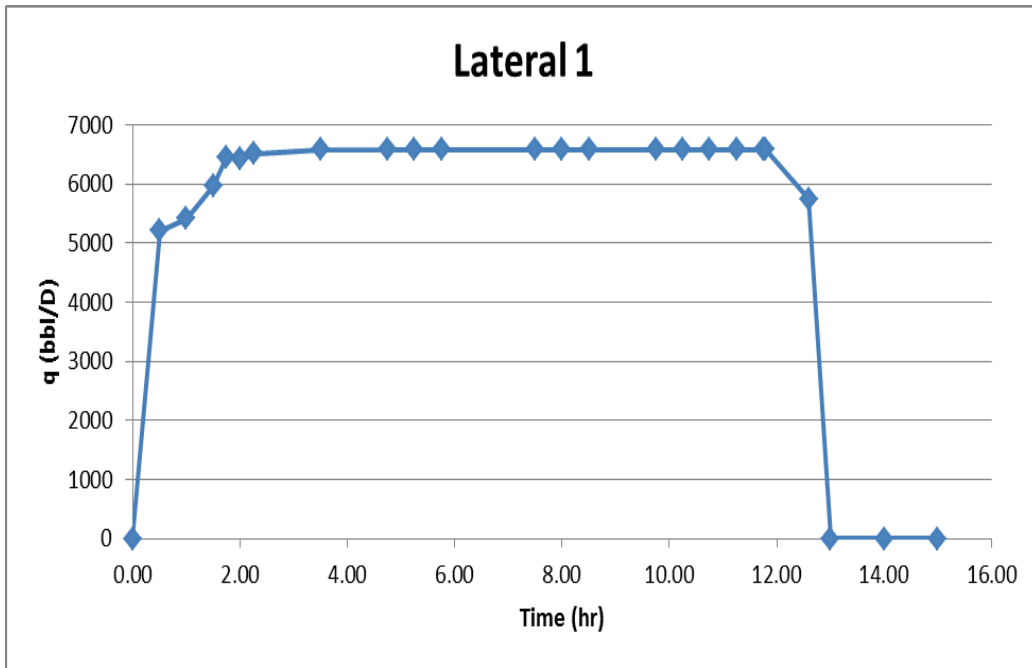


Fig. 4.2 Lateral 1 Production Test

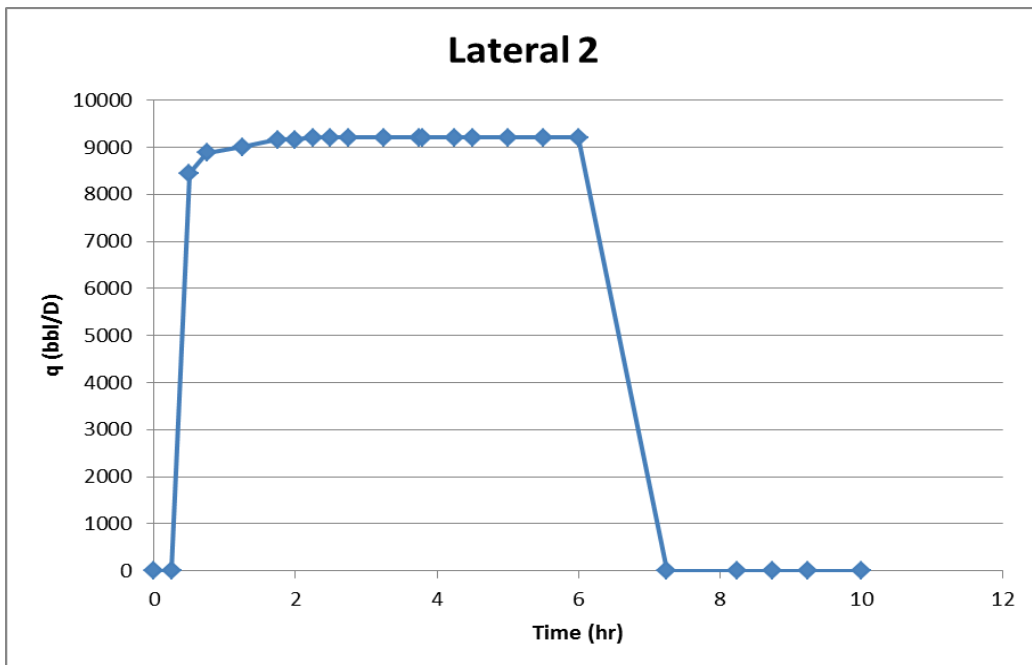


Fig. 4.3 Lateral 2 Production Test

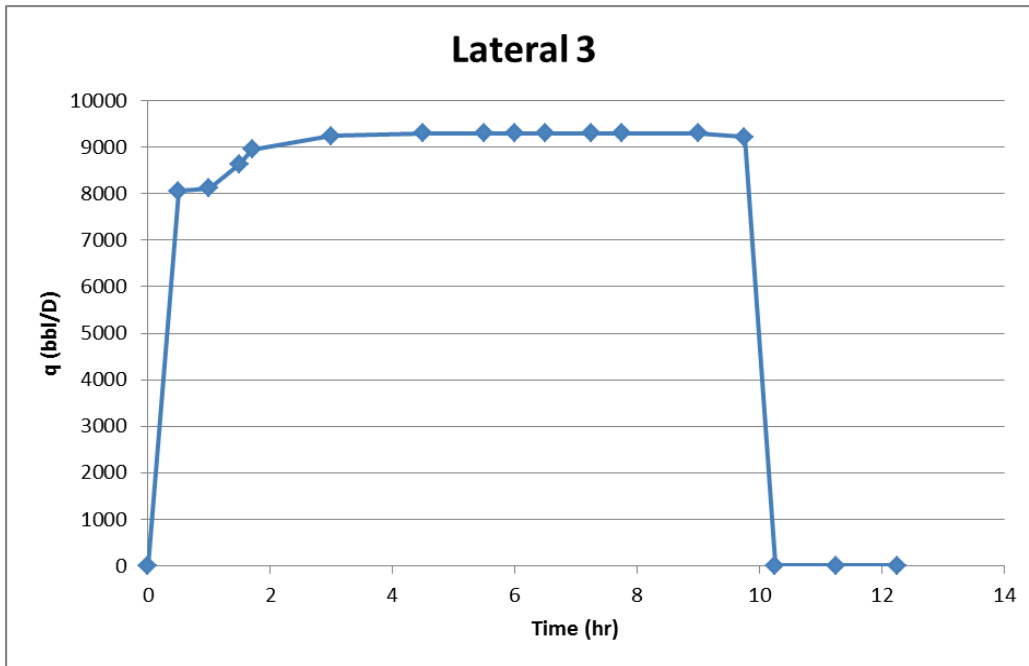


Fig. 4.4 Lateral 3 Production Test

In order to determine the accuracy of the model, the above mentioned metered rates are then compared to the flow rates generated by the model. If the results are deemed close within an acceptable tolerance then the model can be implemented in the field.

4.4 Results and Discussion

The model was able to simulate temperature profiles for each lateral in addition to the motherbore. Fig 4.5 shows the temperature profiles of calculated and observed temperatures in lateral one in addition to the temperature reading provided by sensors in the well. A similar behavior is showing by the two profiles.

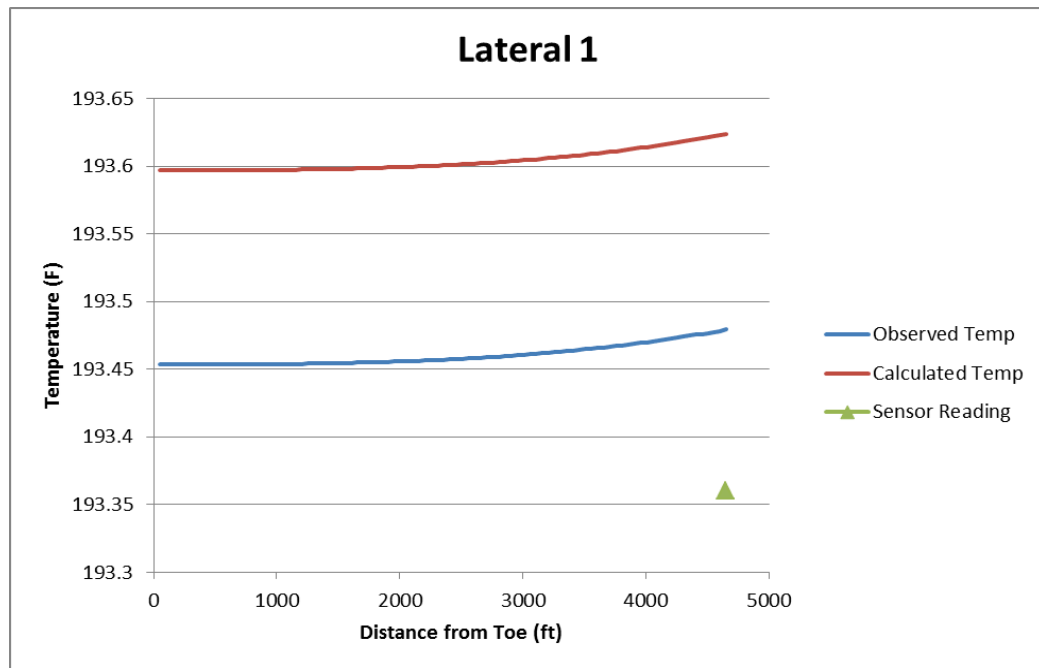


Fig. 4.5 Temperature Profiles in Lateral 1

Similar trends are shown by laterals 2 in Fig 4.6 below. The increase in temperature is noticeable in both laterals however the magnitude in increase is slightly higher in lateral two. This is attributed to the higher production rate in lateral two compared to lateral one. It is worth noting that the overall range of temperatures in the laterals is close enough to within acceptable tolerance levels.

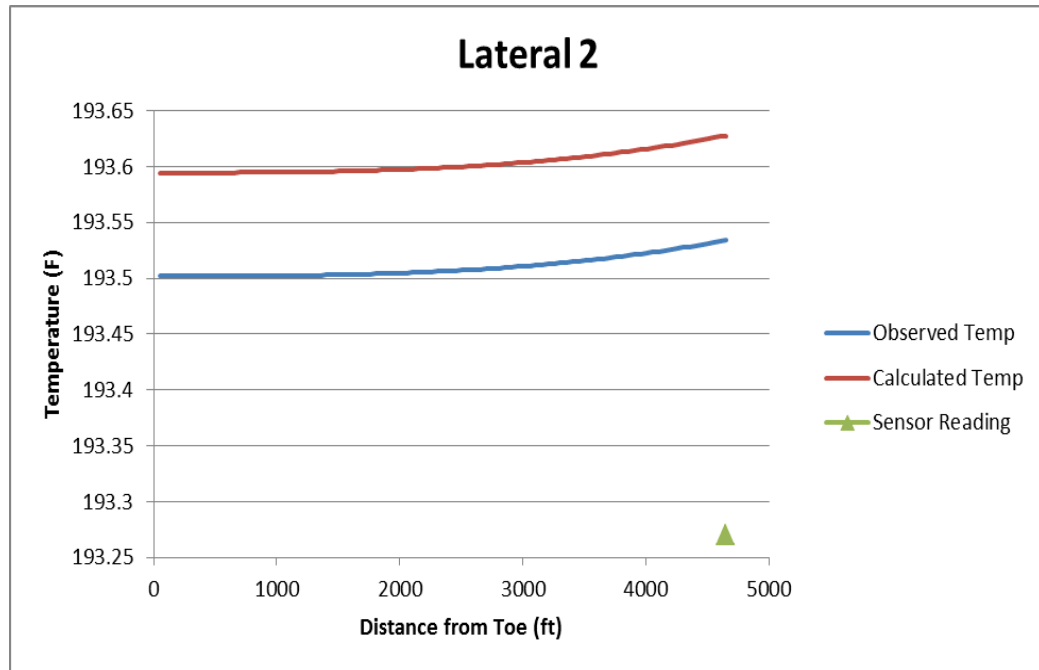


Fig. 4.6 Temperature Profiles in Lateral 2

The magnitude of increase in temperature is even more noticeable in lateral three as can be seen in Fig 4.7. Temperature trends in the motherbore in Fig 4.8 reacted as expected with laterals' entry points clearly noticeable on curves (reference and calculated).

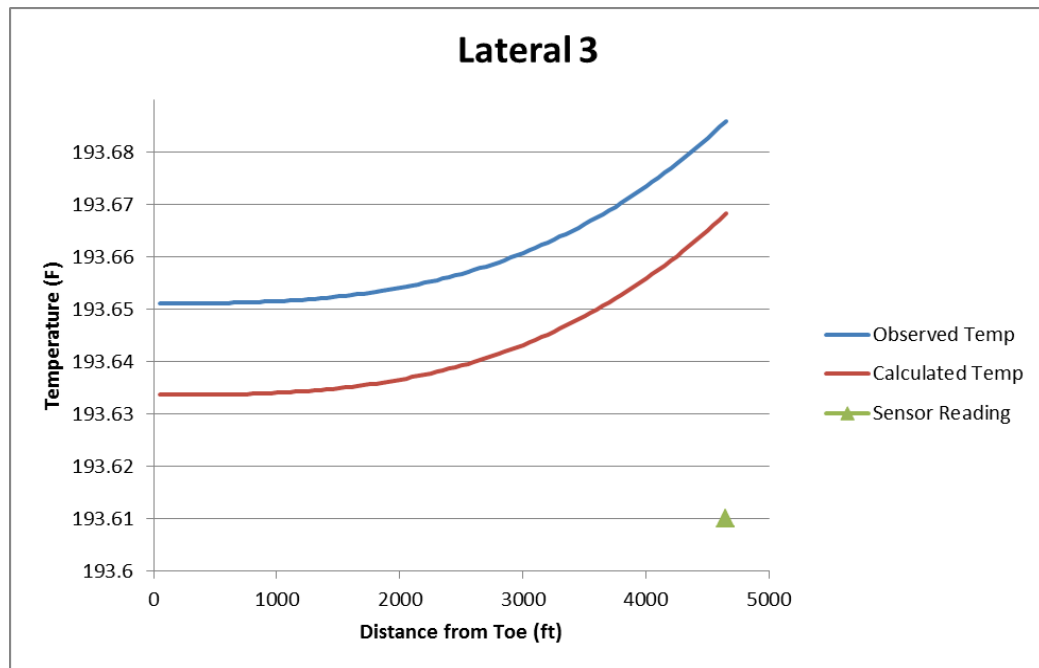


Fig. 4.7 Temperature Profiles in Lateral 3

Temperature results were satisfactory. The average difference between the observed and calculated temperature curves were 0.0725°F or 0.038% . As mentioned before, the sensors provide pressure and temperature readings at a single point. That reading is provided at the entry of each lateral into the motherbore. As a result, there is no way of comparing temperature profiles inside the laterals.

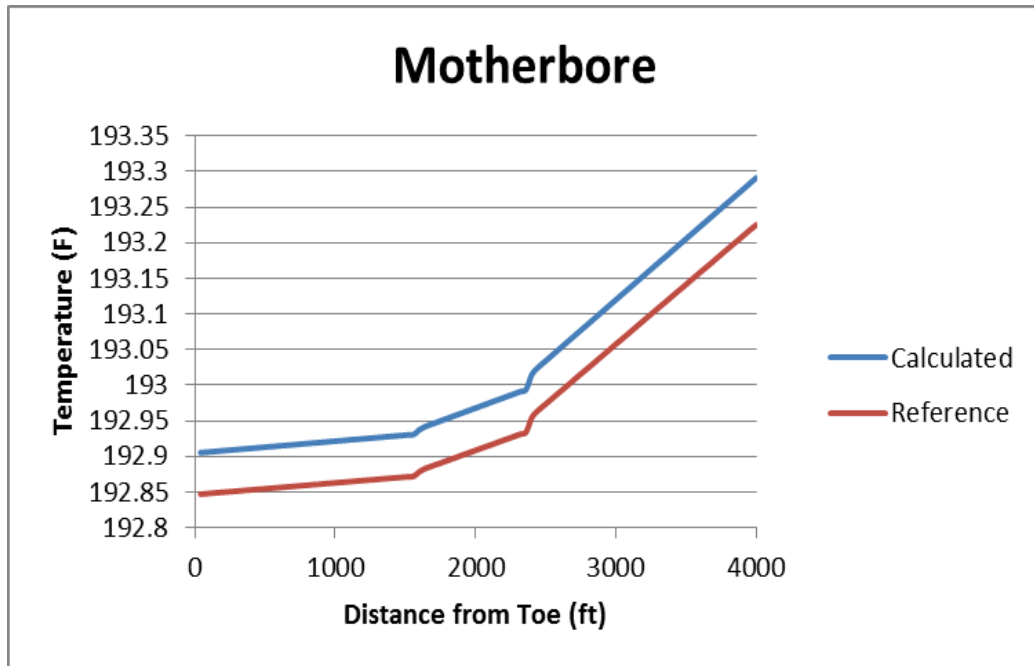


Fig. 4.8 Temperature Profiles in Motherbore

The only meaningful comparison is to compare the sensors temperature reading with the last value provided by inverse model of each profile. Because of the lack of sensors inside the lateral, the last temperature reading in each lateral profile is assumed to be in the last segment and as a result the closest one to the sensor.

That will help determining how close the inverted temperature profiles are to the true temperature measured by the sensors. Table 4.3 summarizes that comparison in all three laterals.

Table 4.3 Temperature Comparison

Lateral	Metered (°F)	Calculated (°F)	Difference (°F)
1	193.36	193.62	0.26
2	193.27	193.63	0.36
3	193.61	193.67	0.06

As can be seen from the table and the figures above, the temperatures generated by the model are within acceptable range compared to the one metered in the field during the production test. The difference in temperature between the meter reading and the calculated temperature in laterals 1 was 0.26°F, in lateral 2 was 0.36°F, and in lateral 3 was 0.06°F.

To compare temperature behavior downhole generated by the model and measured by the sensor, we plotted the meter temperature reading during the test of each lateral against the calculated temperature (Figs. 4.9, 4.10, and 4.11). The measured temperature shows as symbols, and calculated temperature are presented in solid lines.

Because the temperature model is a steady state model, so is the flow model (pseudo-steady state, but the pressure draw down was held constant during test), the temperature profile was constant. For the figures we can see that we are not able to capture the transient behavior at the start of the test, as well as when the test is shut down. The transient period is presented in dotted line.

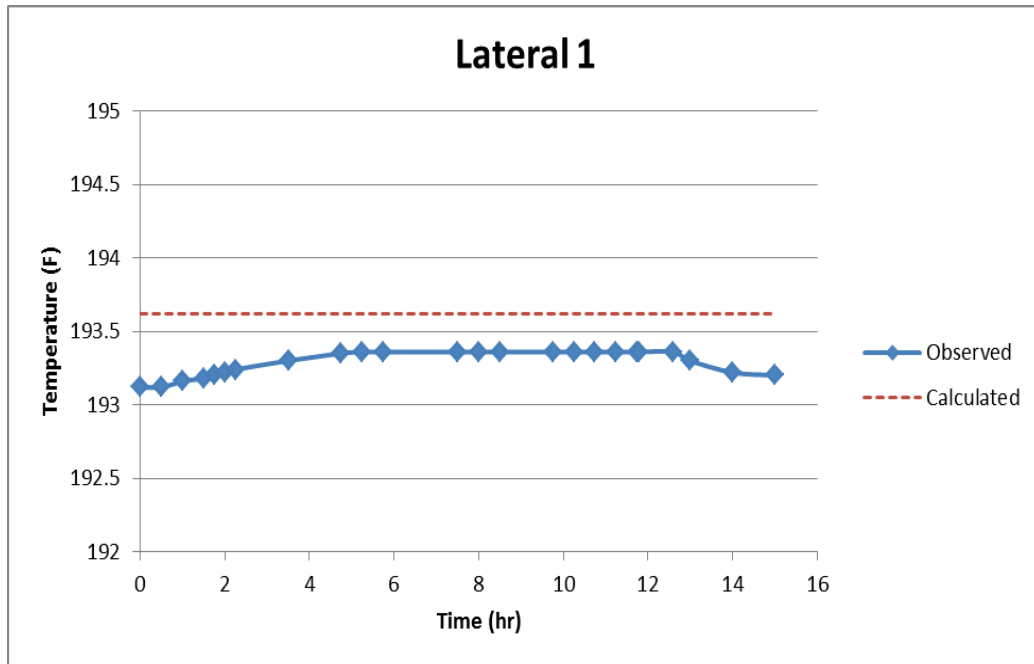


Fig. 4.9 Lateral 1 Temperature Reading during Production Test

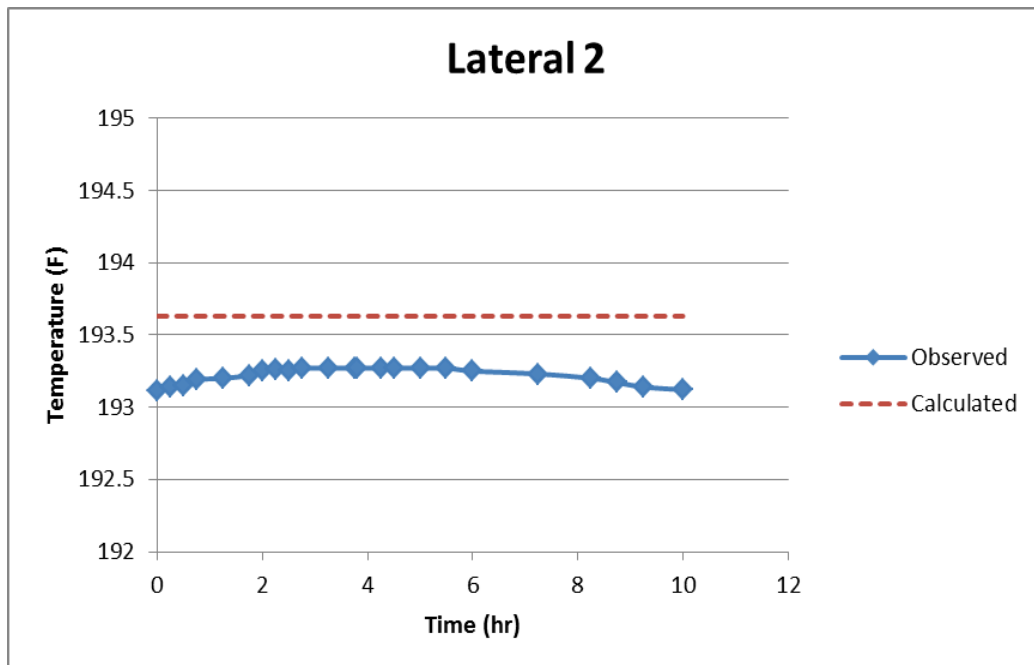


Fig. 4.10 Lateral 2 Temperature Reading during Production Test

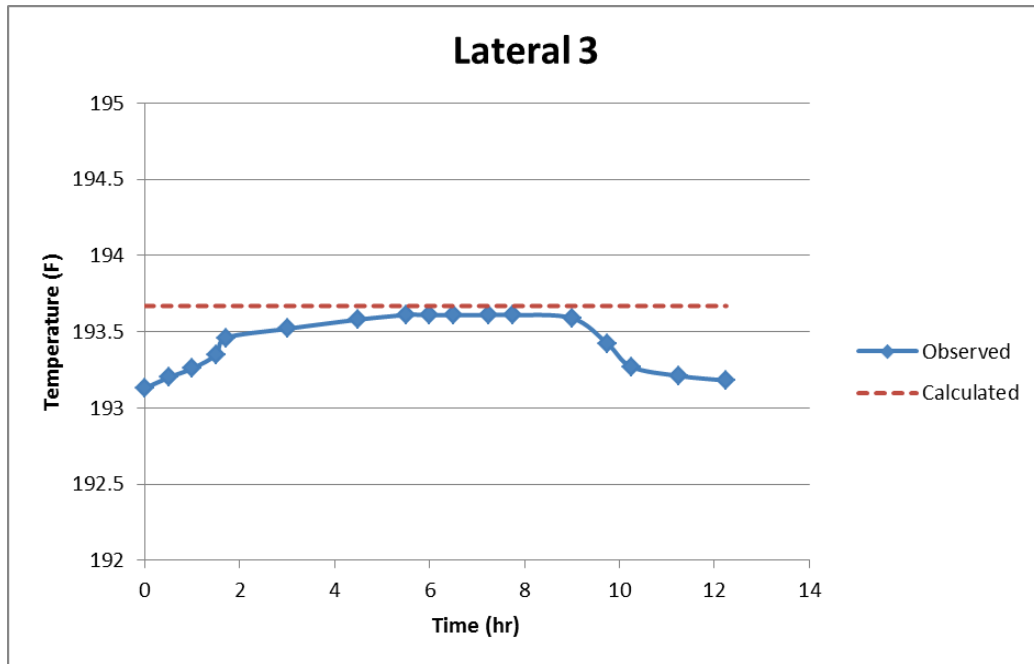


Fig. 4.11 Lateral 3 Temperature Reading during Production Test

The model-generated temperature readings are accurate enough for the scope of this study. For future work, it is worth looking into how accurate they can be compared to actual temperature readings inside the laterals when the technology to install sensors inside the laterals is available.

Flow rates results were encouraging as well. In lateral 1, the model calculated the flow rate to be 8654 bbl/D which is 2068 bbl/D higher than the value provided by the production test of 6586 bbl/D. That is an increase of 31.4% than the actual rate. Flow rates in laterals two and three were more accurate. The simulated flow rates were higher by 1.9% for lateral two and 4.1% for lateral three. The complete production rates can be found in Table 4.4. Total production of the well according to the production test was

25091 bbl/D compared to 27719 bbl/D as per the model. That is an average difference of 10% which is the cutoff point as set per the study.

Production rate simulation using this method is expected to have a better accuracy if the observed temperature profiles used were actually metered downhole instead of being simulated by the forward model.

Another factor that can have a major effect on results accuracy is the accuracy of the reservoir/wellbore/fluid properties that are provided to be tested with this model. The model assumes perfect conditions while it is not usually perfect in the field especially when it comes to the well conditions. Unfortunately, only one set of data was available for this study.

Table 4.4 Production Rates Comparison (bbl/d)

Lateral 1		Lateral 2		Lateral 3	
Calculated	Metered	Calculated	Metered	Calculated	Metered
8654	6586	9376	9200	9689	9305

Although the inverse model is not capable of producing pressure profiles as well, the pressure profiles of the laterals shown in Fig 4.5 were produced by the forward model to give a general idea of the expected pressure behavior in the well.

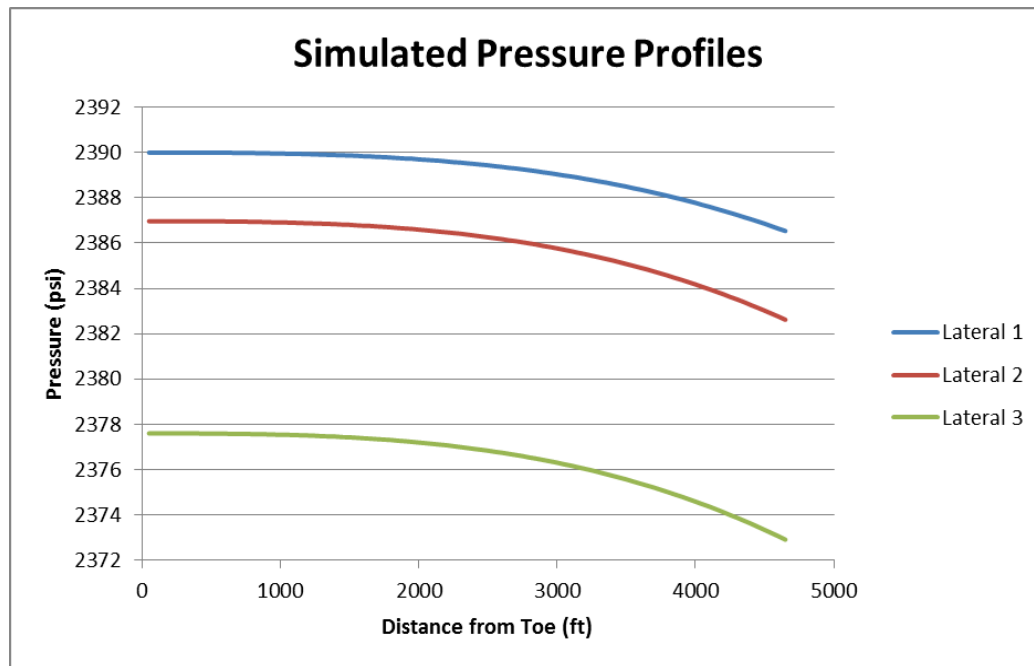


Fig. 4.12 Pressure Profiles in Laterals

Table 4.5 shows the pressure drops calculated by the forward model across each lateral:

Table 4.5 Pressure Drop in Laterals

Lateral	Pressure Drop
1	4.29 psi
2	5.39 psi
3	5.81 psi

The pressure figures seem reasonable given the length of the laterals compared to the base run that was discussed earlier.

The motherbore pressure profile shows an expected behavior as well with a slight drop in pressure along the motherbore as can be seen in Fig 4.6. Entry points are visible as well with a noticeable increase in pressure each time flow enters the motherbore.

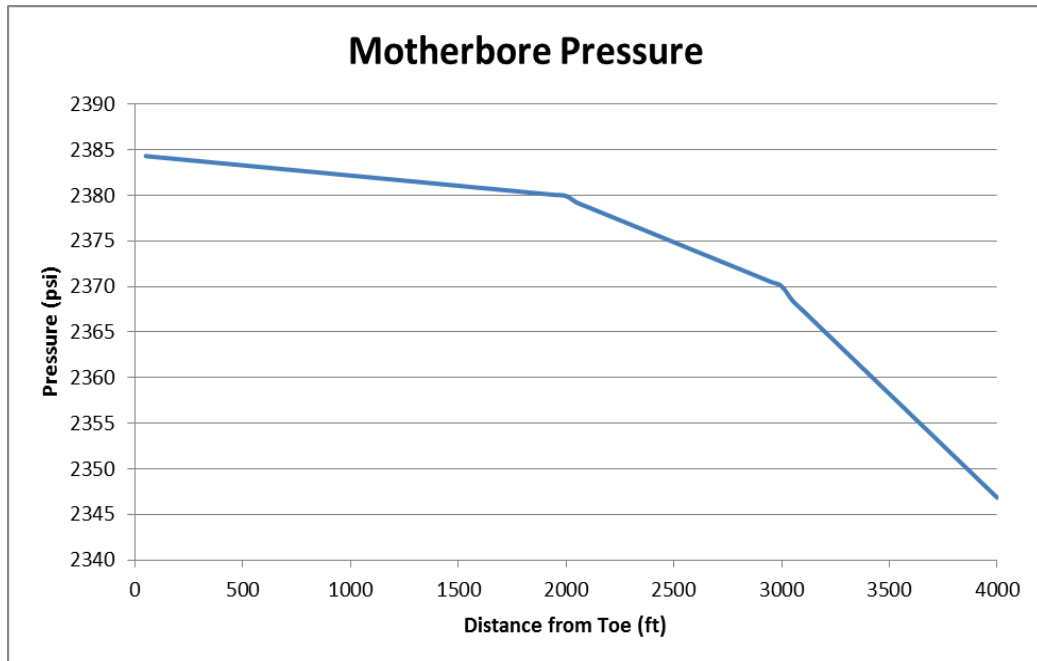


Fig. 4.13 Pressure Profile in Motherbore

CHAPTER V

MULTILATERAL WELL STRUCTURE DESIGN FOR OPTIMAL PRODUCTION

5.1 Introduction

The ultimate goal of this study is to develop a procedure and tools to optimize production of trilateral wells in the field. As have been presented in the previous chapter, the model can estimate temperature profiles of laterals, and therefore, more importantly to estimate production distribution in trilateral wells when necessary data are available.

In this chapter, using the field data that were presented in the previous chapter different trilateral well designs will be analyzed to determine the best scenario for the given conditions. Five different cases have been studied. For each case, the model will generate the temperature curves in each lateral and estimate flow rate. The performance for each case is compared to decide the best way to complete a trilateral well in the given field.

The actual design that was presented in the previous chapter will be the base design for this parametric study. So, the other cases can be considered modifications to the basic well design.

5.2 Conditions for the Study

The five cases that will be tested in this study are listed below:

1. Extending all laterals by 2000 ft.
2. Shortening all laterals by 2000 ft.
3. Extending lateral 1 by 2000 ft while keeping other laterals constant.
4. Extending lateral 2 by 2000 ft while keeping other laterals constant.
5. Extending lateral 3 by 2000 ft while keeping other laterals constant.

The length of the motherbore and the spacing between the laterals were kept the same in all cases. Table 5.1 summarizes the different lengths of each case.

Table 5.1 Cases Laterals Summary

Case	Lateral Length (ft)			Total
	Lateral 1	Lateral 2	Lateral 3	
Base Case	4423	4753	4802	13978
1	6423	6753	6802	19978
2	2423	2753	2802	7978
3	6423	4753	4802	15978
4	4423	6753	4802	15978
5	4423	4753	6802	15978

5.3 Results

All cases have been run successfully. The simulated production rates show logical reflection to what is anticipated by each case. A complete summary of results is in Table 5.2.

Table 5.2 Cases Production Summary

Case	Production Rate (q) bbl/d			Total
	Lateral 1	Lateral 2	Lateral 3	
Base Case	8654	9376	9689	27719
1	12579	13466	14232	40277
2	4705	5360	5499	15564
3	12579	9699	10161	32439
4	8610	12970	9772	31352
5	8610	9334	13379	31323

In all cases, increasing lateral lengths increased production rates and vice versa. Temperature profiles showed similar behavior generally in all cases. In all cases, the motherbore temperature profile exhibited a similar behavior in which it was easy to determine entry points of laterals. Each case will be discussed in more detail next.

5.3.1 Case One

In the first case, all laterals have been extended. The length of each lateral was increased by 2000 ft. That is the first logical “optimization” option. It is always assumed that

drilling longer laterals means higher production rates. That is not always the case. With longer laterals, the pressure drop within laterals increase which decreases the amount of fluid that can be flowed to surface. As a result, all these possibilities need to be addressed while designing the lateral length.

However, in this case all three laterals produced more with the extended lengths. The total production rate of the well is 40,277 bbl/d compared to the original simulated field case of 27,719 bbl/d. That is a total production increase of 45.3%. If this case is compared to what the well actually produced per the production test than the increase in production is actually 60.5%.

Figures 5.1 to 5.4 show the temperature distribution in all laterals.

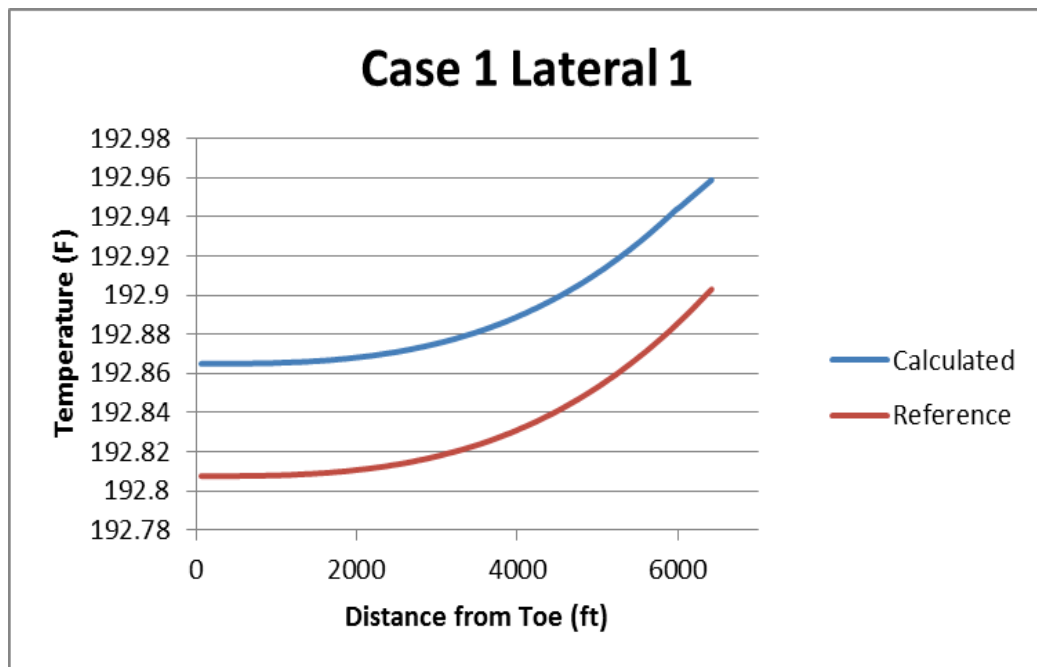


Fig. 5.1 Case 1 Temperature Profiles in Lateral 1

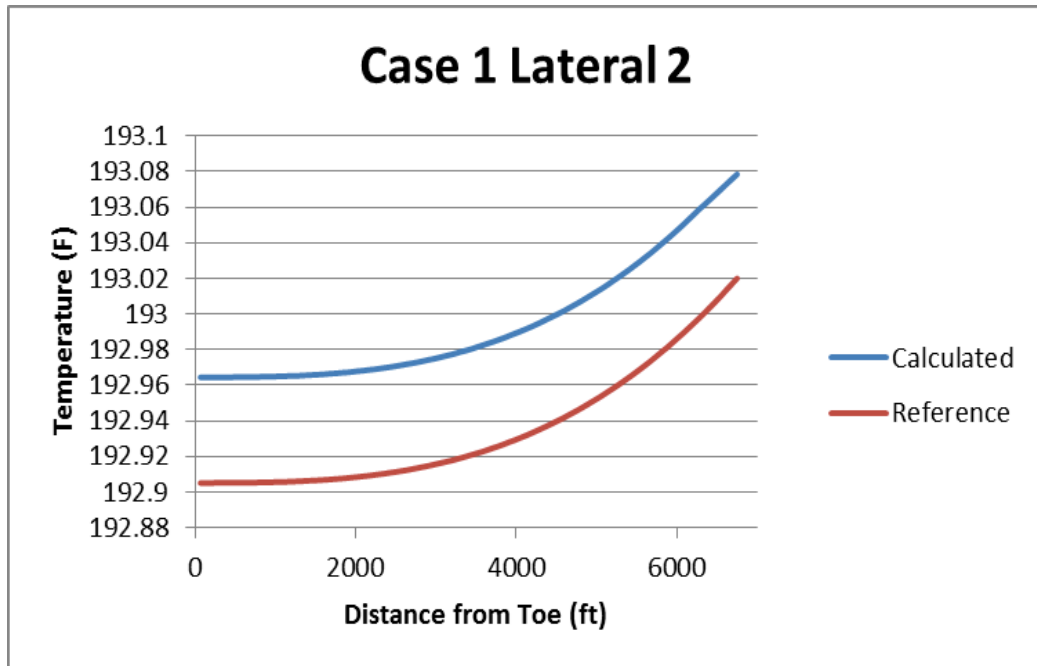


Fig. 5.2 Case 1 Temperature Profiles in Lateral 2

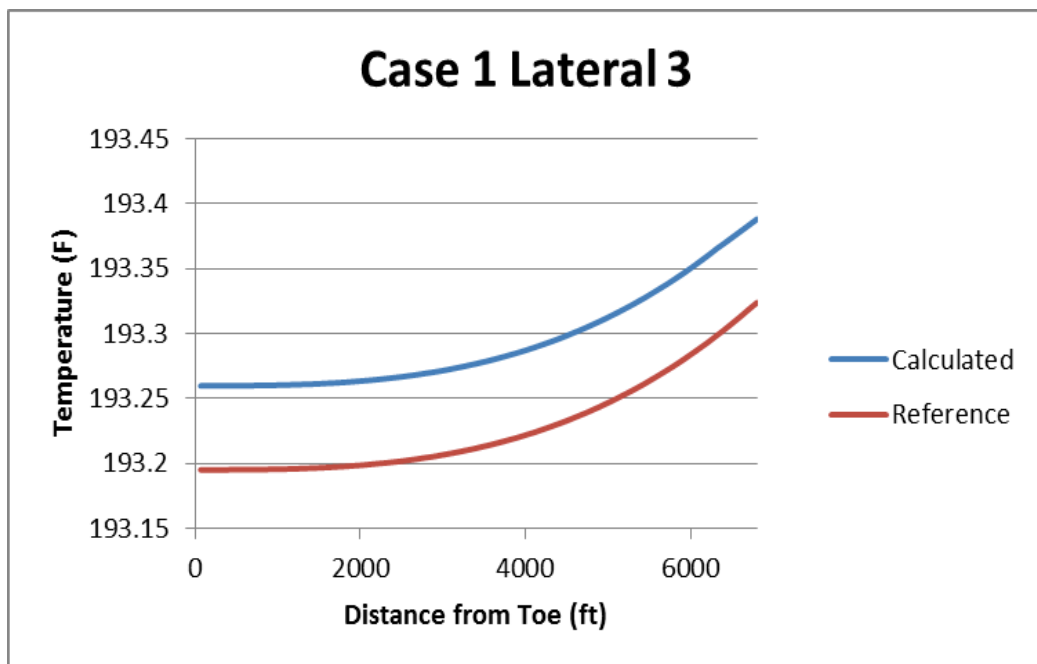


Fig. 5.3 Case 1 Temperature Profiles in Lateral 3

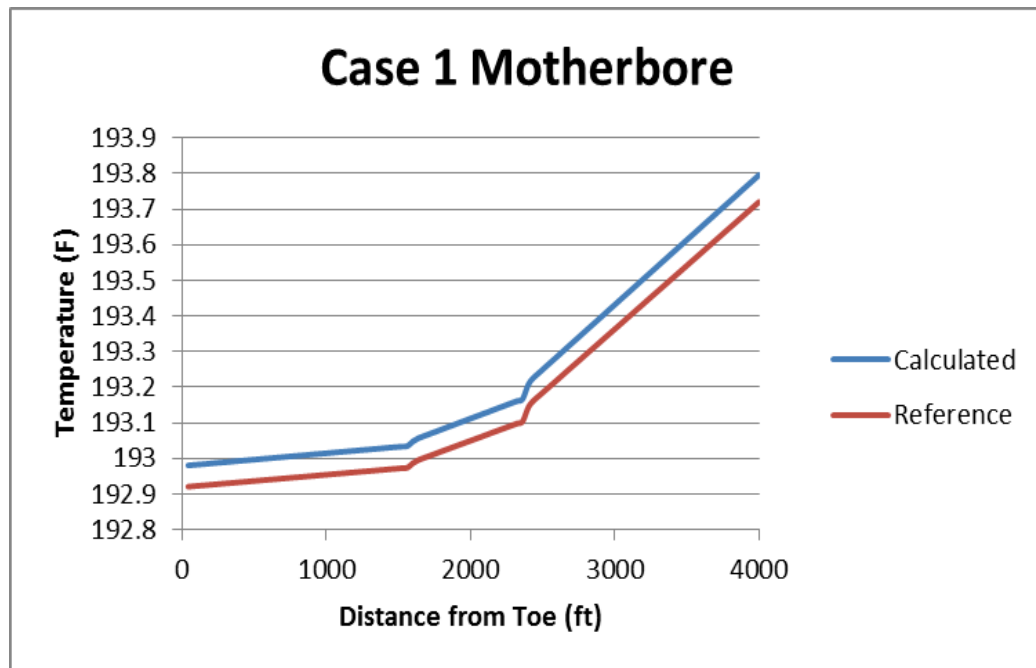


Fig. 5.4 Case 1 Temperature Profiles in Motherbore

5.3.2 Case Two

In case two, all the laterals were shortened by 2000 ft. A drop in rate was noticed as expected. A total production rate of 15,564 bbl/d is estimated by the model for this case. That is a logical decrease in rate given the lost reservoir exposure with the shortened laterals.

What is noticeable in this case was the small change in temperature inside the laterals as can be seen in figures 5.5 to 5.8.

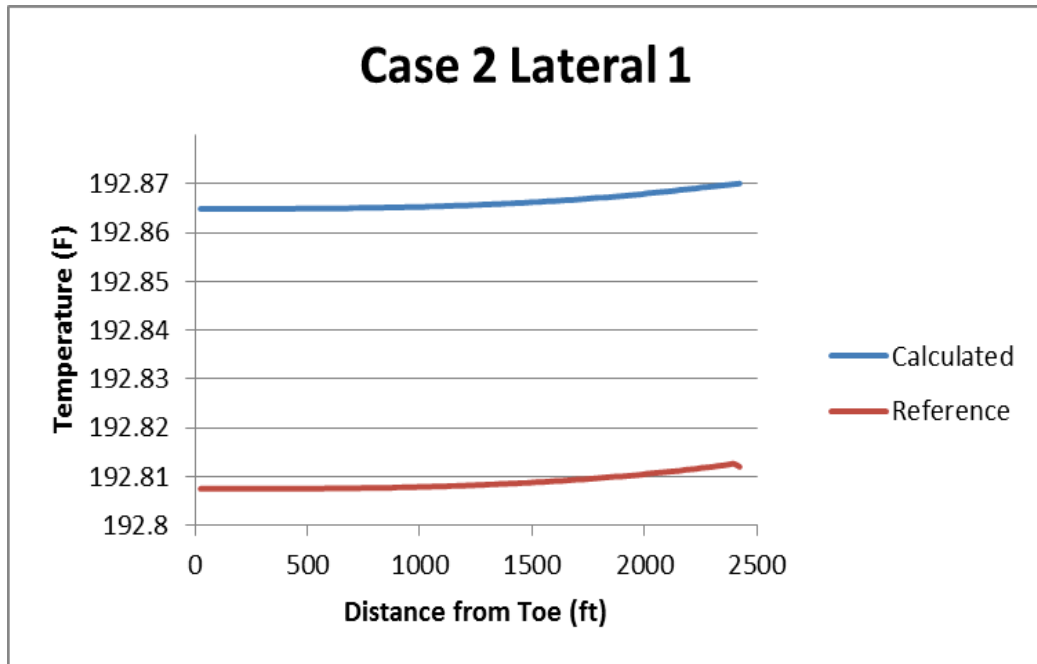


Fig. 5.5 Case 2 Temperature Profiles in Lateral 1

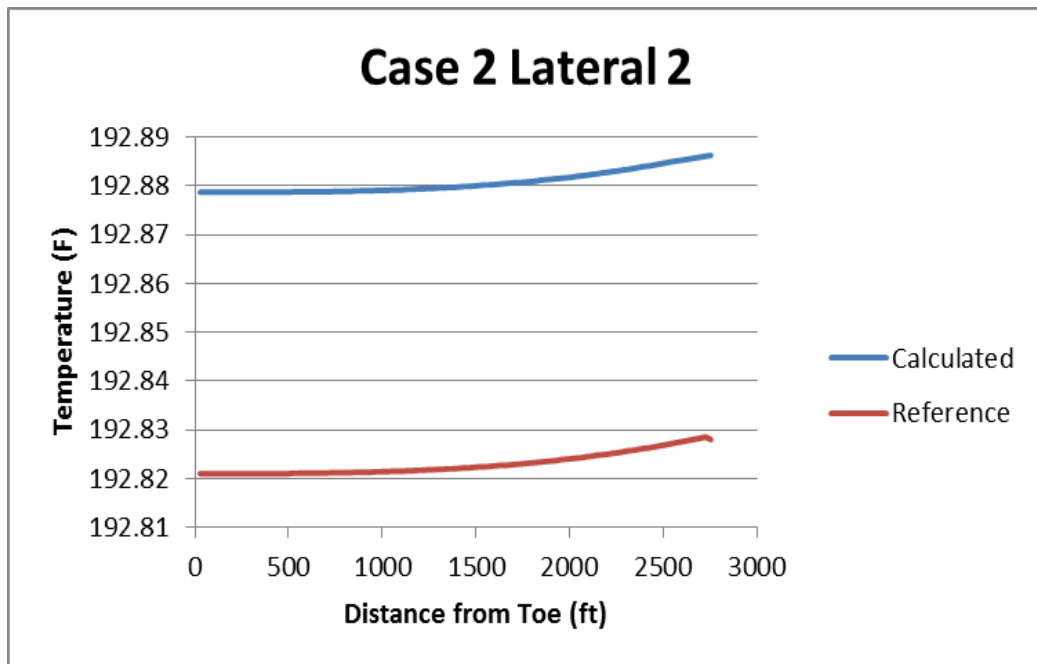


Fig. 5.6 Case 2 Temperature Profiles in Lateral 2

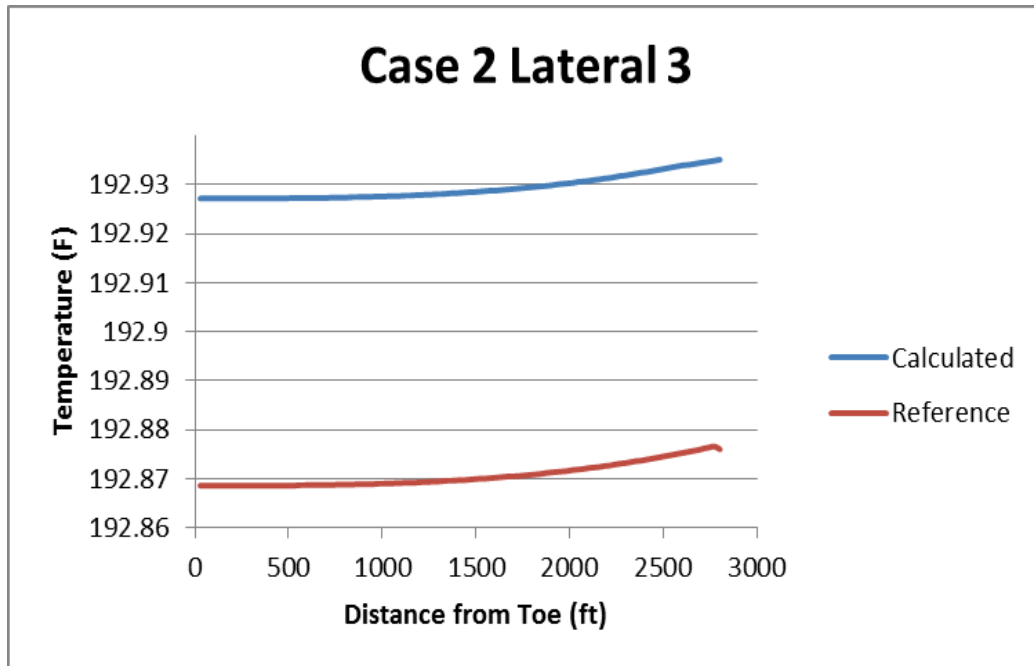


Fig. 5.7 Case 2 Temperature Profiles in Lateral 3

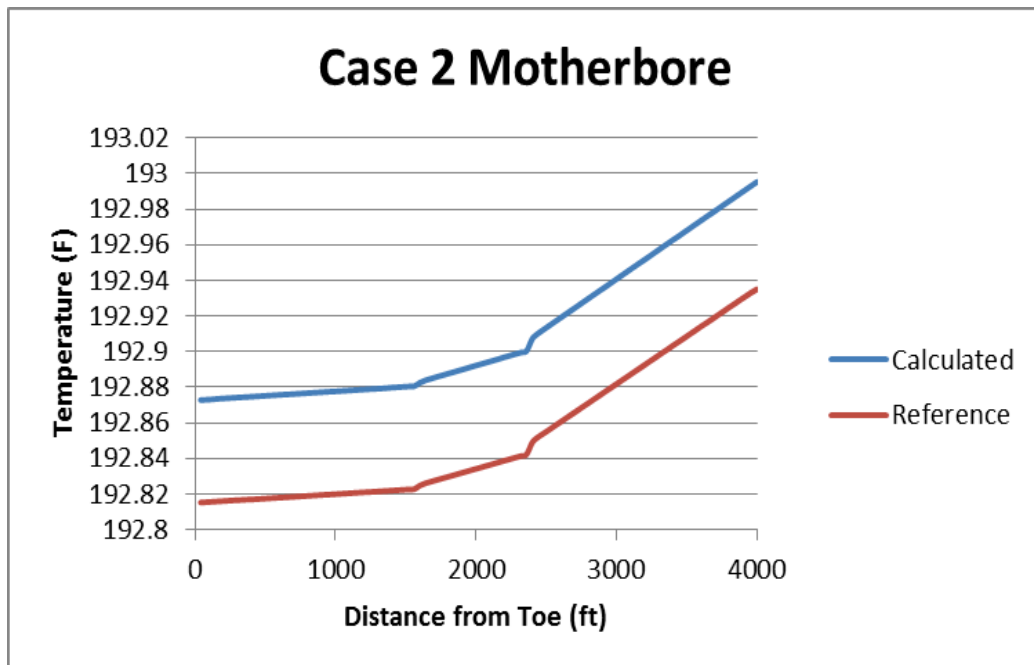


Fig. 5.8 Case 2 Temperature Profiles in Motherbore

5.3.3 Case Three

In this case, lateral 1 was extended by 2000 ft while laterals 2 and 3 were kept the same at 4753 ft and 4802 ft respectively. That increase contributed an increase of production by 4720 bbl/d in total production rate.

Corresponding temperature profiles can be seen in the figures 5.9 to 5.12.

Temperature profiles in the laterals showed an expected behavior as production rates increased compared to the previous case.

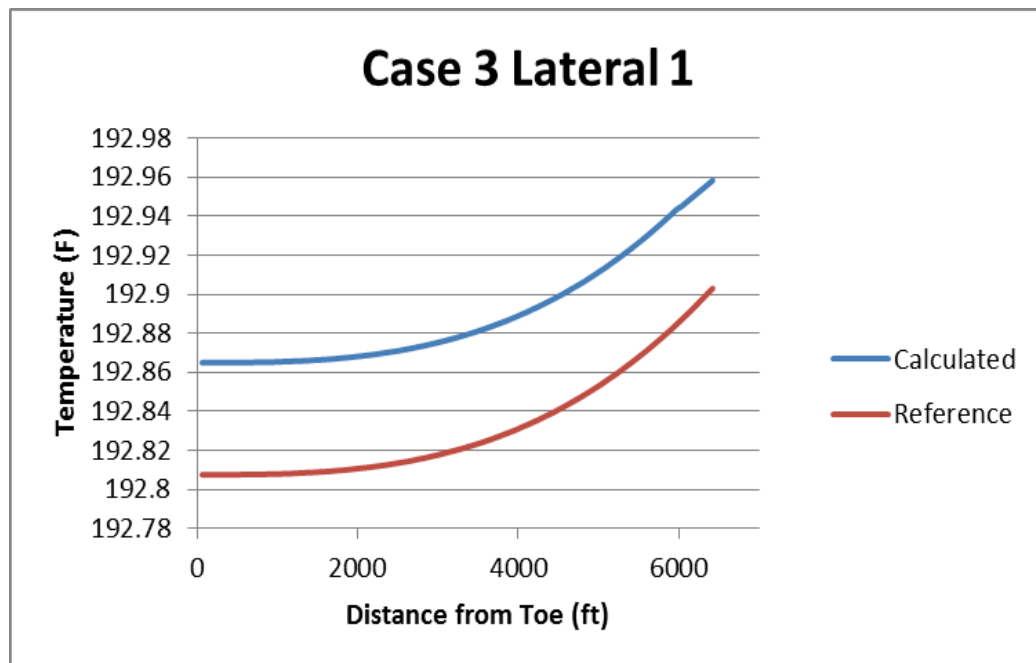


Fig. 5.9 Case 3 Temperature Profiles in Lateral 1

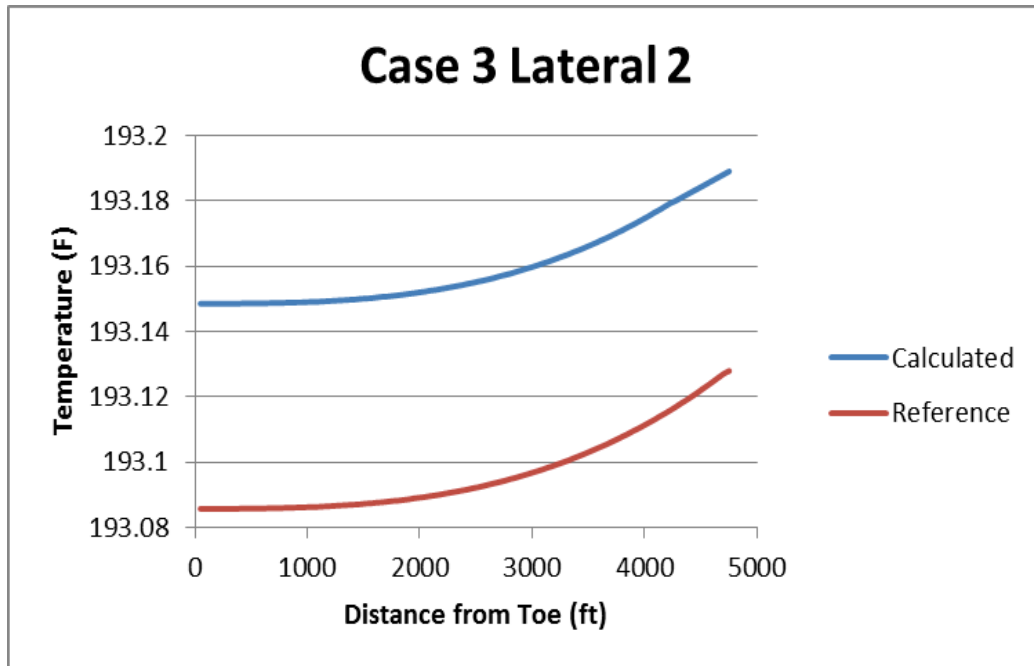


Fig. 5.10 Case 3 Temperature Profiles in Lateral 2

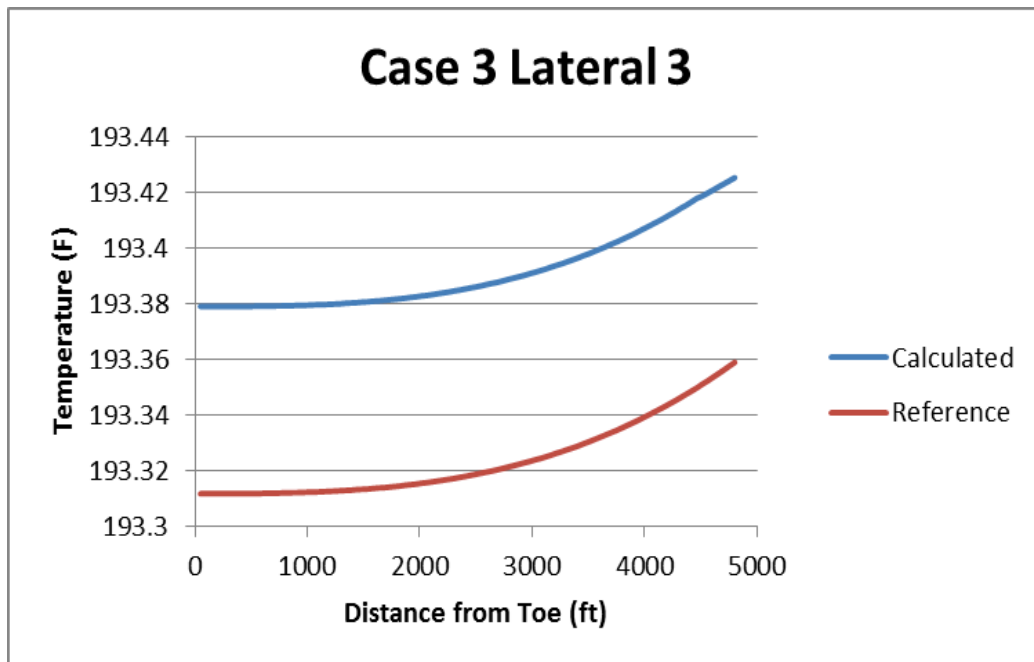


Fig. 5.11 Case 3 Temperature Profiles in Lateral 3

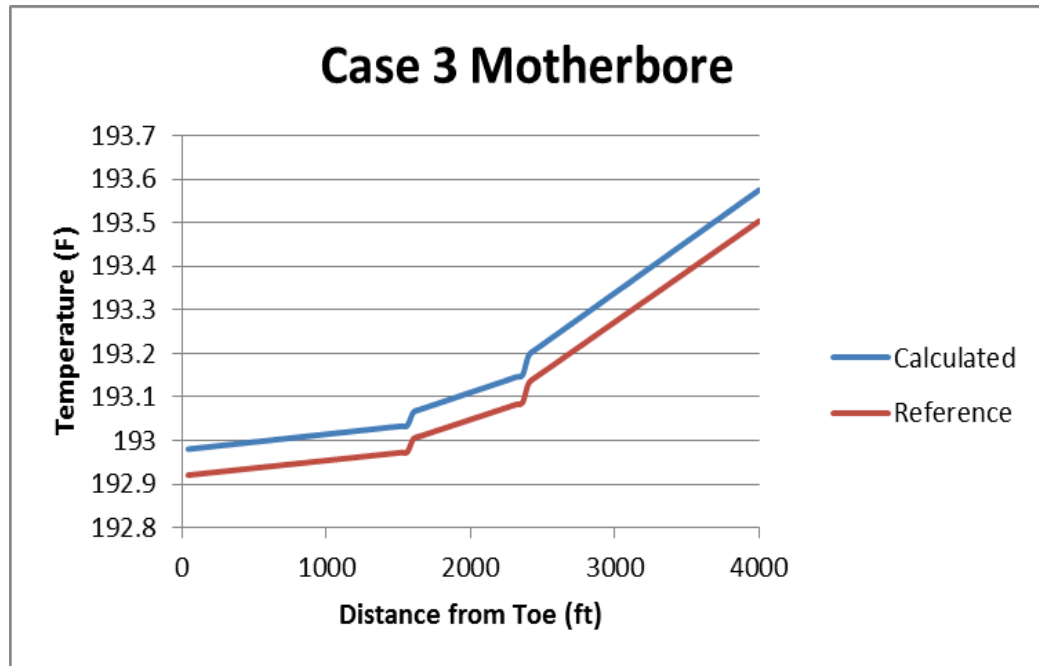


Fig. 5.12 Case 3 Temperature Profiles in Motherbore

5.3.4 Case Four

Lateral 1 was retained to its original length of 4423 ft while lateral 2 was extended by 2000 ft. Similarly to the previous case, the production rate of lateral 2 increased proportionally to the increase in length while lateral 1 rate dropped back to what it was like prior to the length extension. Figures 5.13 to 5.16 show the temperature distribution in all laterals for case 4.

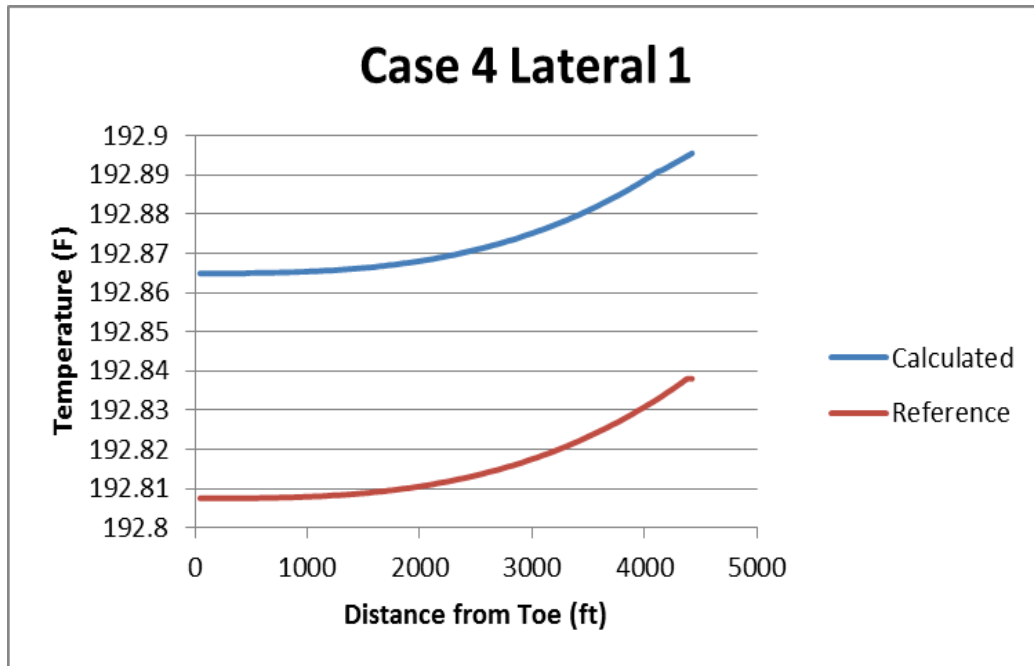


Fig. 5.13 Case 4 Temperature Profiles in Lateral 1

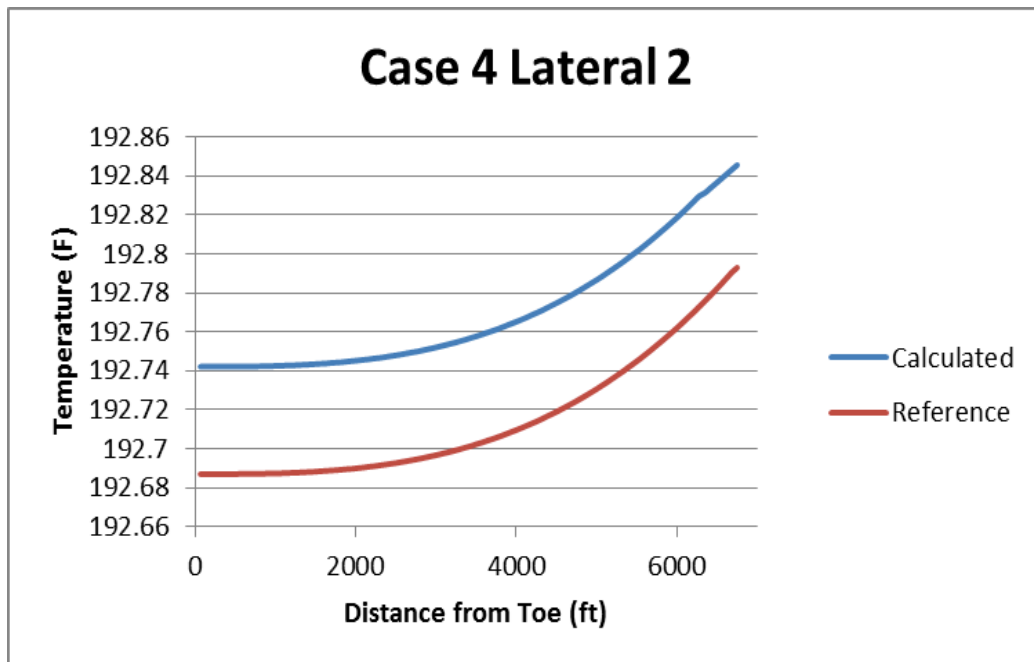


Fig. 5.14 Case 4 Temperature Profiles in Lateral 2

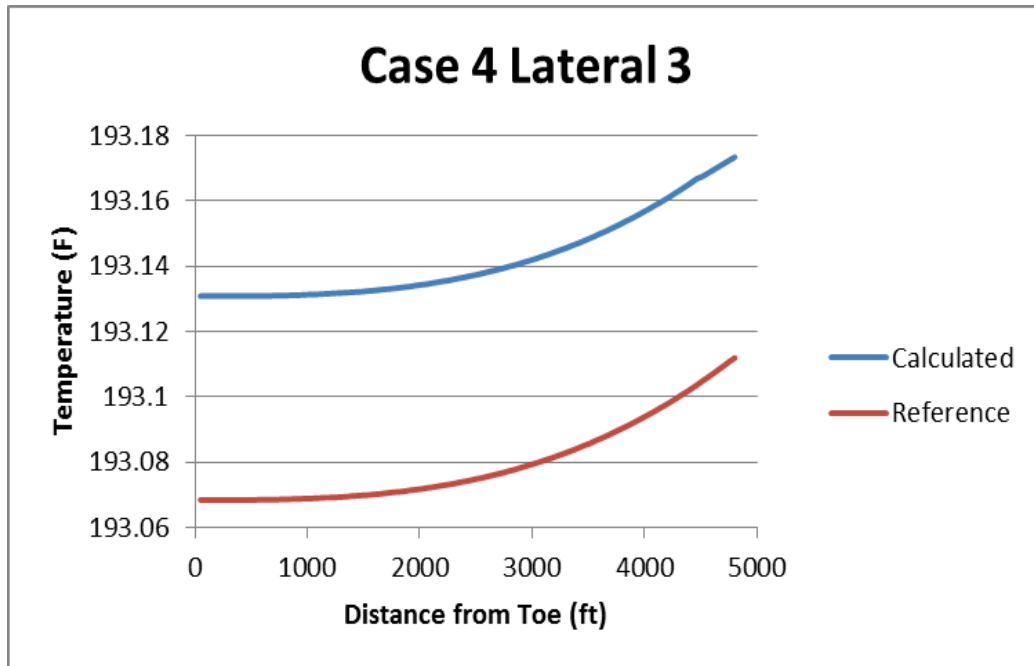


Fig. 5.15 Case 4 Temperature Profiles in Lateral 3

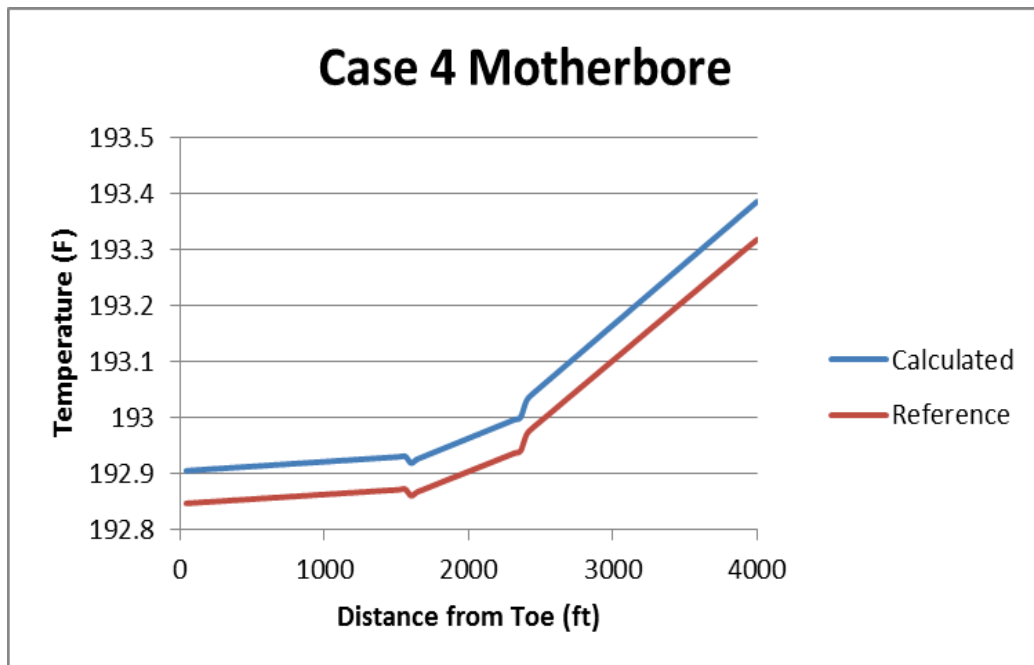


Fig. 5.16 Case 4 Temperature Profiles in Motherbore

5.3.5 Case Five

In the last case, lateral 3 was extended by 2000 ft while the other two were back to the original design lengths. Total production rate in this case according to the model is 31,323 bbl/d.

Figures 5.17 to 5.20 show the temperature profiles generated by the model for this case.

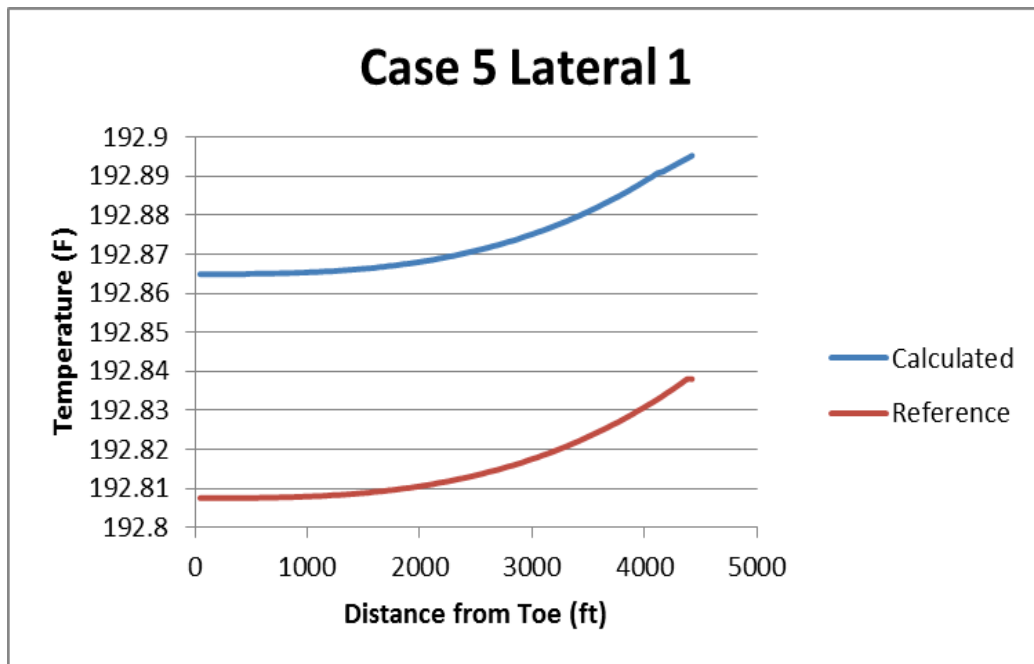


Fig. 5.17 Case 5 Temperature Profiles in Lateral 1



Fig. 5.18 Case 5 Temperature Profiles in Lateral 2

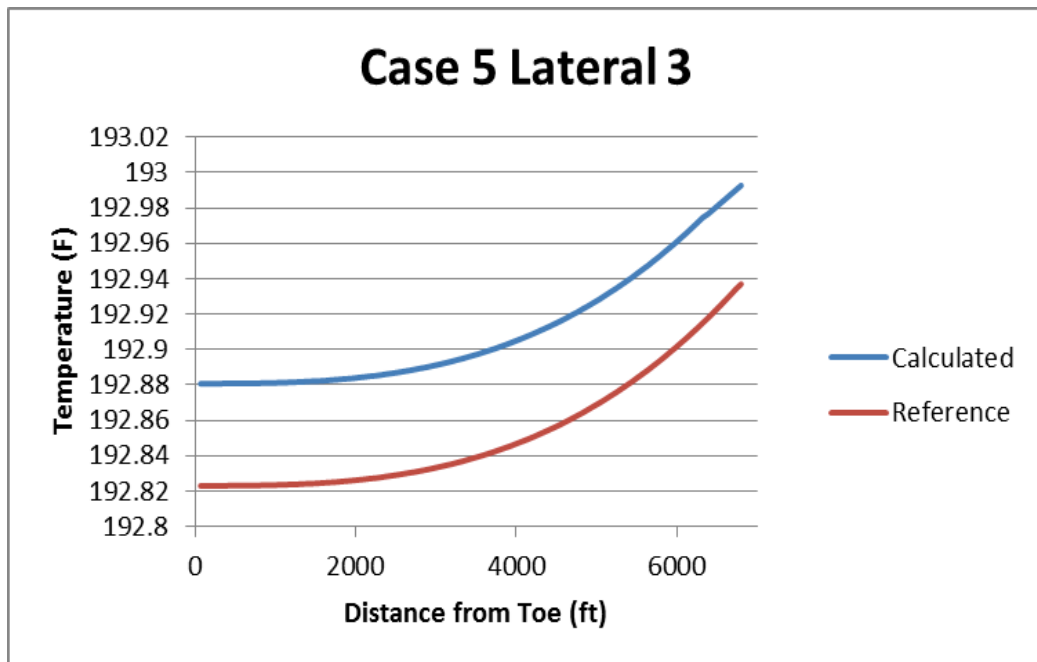


Fig. 5.19 Case 5 Temperature Profiles in Lateral 3

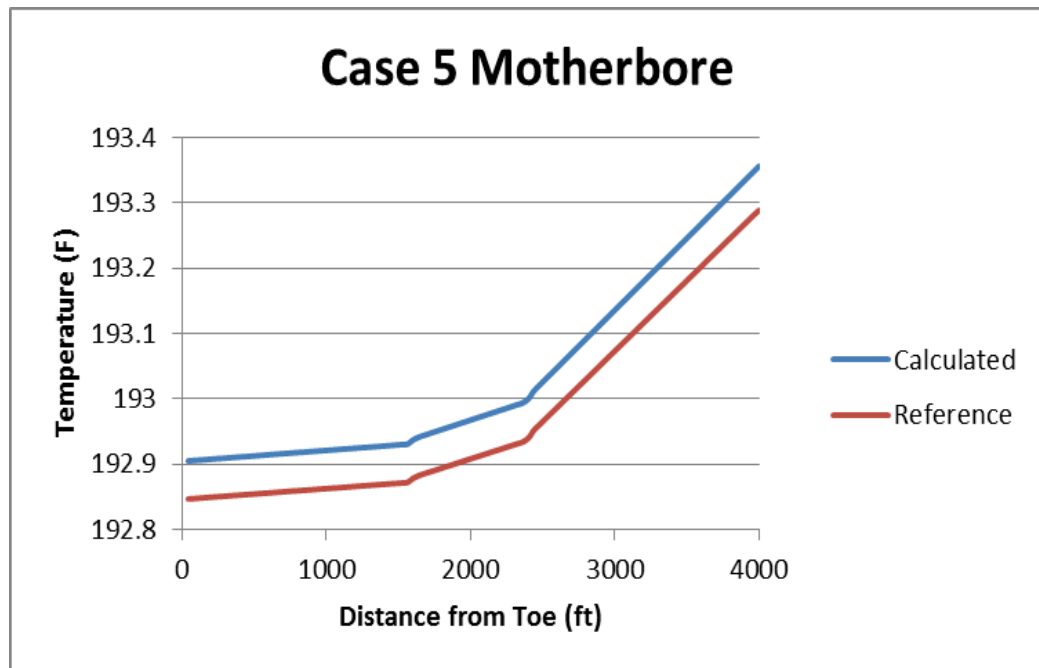


Fig. 5.20 Case 5 Temperature Profiles in Motherbore

5.4 Discussion

All five cases when run using the model have yielded reasonable results. Case one, with all laterals extended showed the highest increase in total production rate. Upon further investigation of results, extending lateral 1 showed better potential than extending laterals 2 or 3 if extending just one lateral was to be considered. Reason behind that is when extending lateral 1, production rate showed an increase at a rate of 2.36 bbl/d/ft compared to 1.82 bbl/d/ft for lateral 2 and 1.80 bbl/d/ft for lateral 3.

Results of all cases were reasonable. There is no reason to deem the model undependable. Temperature behavior reacted favorably to rates produced and completion designs.

CHAPTER VI

CONCLUSION

The amount of data available via downhole sensors can be overwhelming. Pressure and temperature data is available real-time in many newly drilled wells that are equipped with such gauges. There have always been challenges to get the most out of the available data stream. One of the challenges is to predict flow rate in real-time based on pressure and temperature. This challenge is even more daunting when dealing with complex multilateral wells with horizontal laterals. In this study a model capable of predicting flow rates in multilateral wells have been developed. The model consists of two main parts; forward model and inverse model.

The forward model is a steady-state model that is used to calculate temperature and pressure profiles in all laterals and motherbore. It consists of a wellbore model and a reservoir model. The wellbore model is developed using a flow model that deals with mass and momentum balance in pipe flow and a thermal model that deals with energy balance in pipe flow. The reservoir model also has a flow model and a thermal model. The flow model deals with calculating flow rate out of the reservoir while the thermal model deals with energy balance in porous media. The main purpose of developing the forward model is to show the type of pressure and temperature behavior associated with certain flow rates.

After building the forward model, several cases were run and favorable results were obtained. A sensitivity analysis have been run as well to see the effect of changing horizontal permeability, k_h , and lateral length has on flow rate generated by the forward model. When running the forward model using the base case that was developed, a

production rate of 27,431 bbl/d was predicted. That rate dropped to 26,798 bbl/d when the lengths of the laterals were changed while keeping the total length constant.

Changing permeability also changed predicted flow rates accordingly. When the permeability was dropped from 400 mD in the base case to 100 mD the production rate dropped to 14,375 bbl/d.

The second part of the model is the inverse model. The inverse model is designed to estimate flow rate using data provided by downhole sensors. The inverse model problem is a nonlinear least-square regression problem. The method used is to apply an objective function that calculates the discrepancy between measured and simulated data. The solution is found by minimizing the objective function as much as possible. We introduced two inversion methods which were the stochastic and the Gauss-Newton. In our model, the two methods were combined so we could have a fast inversion method that is able to find the global minimum instead of local minima. We ran the model using the same case that were tested using the forward model and the resulting profiles and flow rates were close enough to be considered dependable (Within 10%). The model was then used to simulate temperature profiles and flow rate after being fed real field input data. The resulting simulation showed a production rate of 27,719 bbl/d compared to the actual rate that was measured in the field of 25,091 bbl/d. That is a difference of 10% in production rate. That proved the dependability of the model.

The value of the model approach for production optimization for trilateral wells is illustrated through parametric study. For that study, we designed five different well

cases in the same field. The model then was used to estimate flow rates for each design.

The results reflected the expected outcome given each design.

REFERENCES

Achnivu, Ochi I., Zhu, D., and Furui, Kenji. 2008. Field Application of an Interpretation Method of Downhole Temperature and Pressure Data for Detecting Water Entry in Inclined Gas Wells. Paper SPE 115753 presented at the SPE Annual Technical Conference and Exhibition, Denver, Colorado, 21-24 September.

Al Zahrani, Rashad. 2010. Utilizing Distributed Temperature and Pressure Data to Evaluate the Production Distribution in Multilateral Wells. Master Thesis, Texas A&M University, College Station, Tx.

Babu, D.K. and Odeh, A. S. 1989. Productivity of a Horizontal Well (includes associated papers 20306, 20307, 20394, 20403, 20799, 21307, 21610, 21611, 21623, 21624, 25295, 25408, 26262, 26281, 31025 and 31035). *SPE Reservoir Engineering* **4** (4): 417-421.

Bird, R.B., Stewart, W.E., and Lightfoot, E.N. 2002. *Transport Phenomena*, New York: John Wiley and Sons.

Dikken, Ben J. 1990. Pressure Drop in Horizontal Wells and Its Effect on Production Performance. *J. Pet Tech* **42** (11): 1426-1433. SPE-19824-PA.

Economides, M.J., Hill, A.D., and Ehlig-Economides, C. 1994. *Petroleum Production Systems*, New Jersey: Prentice Hall Inc.

Ehlig-Economides, C.A. and Joseph, Jeffrey. 1987. A New Test for Determination of Individual Layer Properties in a Multilayer Reservoir. *SPE Form Eval* **2** (3): 261-283. SPE-14167-PA.

Gilbert, C.J. 1996. Pressure Transient Analysis in Horizontal Wells in Some Sole Pit Area Fields, U.K. 1996. *SPE Reservoir Engineering* **11** (2): 101-108. SPE-30439-PA.

Hill, A.D. and Society of Petroleum Engineers (U.S.). 1990. *Production Logging: Theoretical and Interpretive Elements*. Monograph/SPE. Richardson, Tex.: Henry L. Doherty Memorial Fund of AIME, Society of Petroleum Engineers. Original edition. ISBN 9781555630300.

Hill, A.D., Zhu, Ding, and Economides, Michael J. 2008. *Multilateral Wells*. Texas: Society of Petroleum Engineering.

Izgec, B., Kabir, C.S., and Zhu, D. et al. 2007. Transient Fluid and Heat Flow Modeling in Coupled Wellbore/Reservoir Systems. *SPE Reservoir Evaluation & Engineering* **10** (3): 294-301. SPE-102070-PA.

Jayawardena, S.S. et al. 2001. A New Model for Dispersed Multi-Layer Oil-Water Flow. Presented at the 2001 Proceedings of the Engineering Technology Conference on Energy, Houston, Texas, 5-7 February.

Kabir, C.S., Izgec, B., and Hasan, A.R., et al. 2008. Real-Time Estimation of Total Flow Rate and Flow Profiling in DTS-Instrumented Wells. Paper IPTC 12343 presented at the International Petroleum Technology Conference, Kuala Lumpur, Malaysia, 3-5 December.

Kamkom, R. and Zhu, D. 2005. Two-Phase Correlation for Multilateral Well Deliverability. Paper SPE 95652-MS presented at the SPE Annual Technical Conference and Exhibition, Dallas, Texas, 9-12 October.

Kragas, T.K., Williams, B.A., and Mayers, G.A. 2001. The Optic Oil Field: Deployment and Application of Perminant In-Well Fiber Optic Sensing Systems for Production and Reservoir Monitoring. Paper SPE presented at the SPE Annual Technical Conference and Exhibition, New Orleans, Louisiana, 30 September-3 October.

Kuchuk, F., Karakas, M., and Ayestaran, L. 1986a. Well Testing and Analysis Techniques for Layered Reservoirs. *SPE Form Eval* **1** (4): 342-354. SPE-13081-PA.

Kuchuk, F. J. and Habashy, Tarek. 1996. Pressure Behavior of Horizontal wells in Multilayer Reservoirs with Crossflow. *SPE Form Eval* **11** (1): 55-64. SPE-22731-PA.

Kuchuk, F.J., Goode, P.A., and Wilkinson, D.J. et al. 1991. Pressure-Transient Behavior of Horizontal Wells with and Without Gas Cap or Aquifer. *SPE Formation Evaluation* **6** (1): 86-94.

Kuchuk, F. J., Shah, P.C., and Ayestaran, L. et al. 1986b. Application of Multilayer Testing and Analysis: A Field Case. Paper SPE 15419 presented at the SPE Annual Technical Conference and Exhibition, New Orleans, Louisiana, 5-8 October.

Lefkovits, H.C. 1961. A Study of the Behavior of Bounded Reservoirs Composed of Stratified Layers. *SPE J.* **1** (1): 43-58. SPE-1329-G.

Ma, X., Al-Harbi, M., Datta-Gupta, A., and Efendiev, Y. 2008. An Efficient Two-Stage Sampling Method of Uncertainty Quantification in History Matching Geological Models. *SPE Journal* **13** (1): 77-87. SPE-102476-PA.

Metropolis, N., Rosenbluth, A., and Rosenbluth, M.N et al. 1953. Equations of State Calculations by Fast Computing Machines. *Journal of Chemical Physics* **21** (6): 1087-1092.

- Nowak, T. J. 1953. The Estimation of Water Injection Profiles from Temperature Surveys. SPE-953203-G. Trans., AIME **198**: 203-212.
- Oliver, D.S., Reynolds, A.C., and Liu, N. 2008. Inverse Theory for Petroleum Reservoir Characterization and History Matching. Cambridge, UK: Cambridge University Press.
- Ouyang, Liang-Biao. 1998. Single-Phase and Multiphase Fluid Flow in Horizontal Wells. PhD Dissertation, Stanford University, Stanford, Ca.
- Ouyang, Liang-Biao and Aziz, Khalid. 2000. A Homogeneous Model for Gas-Liquid Flow in Horizontal Wells. *J. Pet. Sci. and Eng* **27** (9):119-128
- Ouyang, Liang-Biao and Belanger, Dave. 2006. Flow Profiling by Distributed Temperature Sensor (DTS) System-Expectation and Reality. *SPE Production & Operations* **21** (2): 269-281. SPE-90541-PA.
- Ramey, H.J. Jr. 1962. Wellbore Heat Transmission. *J. Pet Tech* **14** (4): 427-435; Trans., AIME, 225. SPE-96-PA.
- Sagar Rajiv, D.R. Doty and Schmidt, Zellmer. 1991. Predicting Temperature Profiles in a Flowing Well. *SPE Production Engineering* **6** (4): 441-448. SPE-19702-PA

Sandal, Hugo M., Horne, Roland N., and Ramey, Henry J. Jr. et al. 1978. Interference Testing with Wellbore Storage and Skin Effect at the Produced Well. Paper SPE 7454 presented at the SPE Annual Fall Technical Conference and Exhibition, Houston, Texas, 1-3 October.

Shah, Plyush C., Karakas, Metin, and Kuchuk, Fikri. et al. 1988. Estimation of the Permeabilities and Skin Factors in Layered Reservoirs with Downhole Rate and Pressure Data. *SPE Form Eval* 3 (3): 555-565. SPE-14131-PA.

Shi, H., Holmes, J.A., Durlofsky, L.J. et al. 2005. Drift-Flux Modeling of Two-Phase Flow in Wellbores. *SPE Journal* 10 (1): pp. 24-33. DOI: 10.2118/84228-pa

Stehfest, H. 1970. Algorithm 368, Numerical Inversion of Laplace Transforms. D-5 communications, *ACM* 13 (1): 47-49.

Sui, Weibo. 2009. Determining Multilayer Formation Properties from Transient Temperature and Pressure Measurements. PhD dissertation, Texas A&M University, College Station, TX.

Sui, W., Zhu, D., and Hill, A.D. et al. 2008. Model for Transient Temperature and Pressure Behavior in Commingled Vertical Wells. Paper SPE 115200 presented the SPE

Russian Oil & Gas Technical Conference and Exhibition, Moscow, Russia, 28-30 October.

Tabtabaei, Mohammad. 2011. Real-Time Evaluation of Stimulation and Diversion in Horizontal Wells. PhD dissertation, Texas A&M University, College Station, TX.

Tariq, Syed M., and Ramey, Henry J. Jr. 1978. Drawdown Behavior of a Well with Storage and Skin Effect Communicating with Layers of Different Radii and Other Characteristics. Paper SPE 7453-MS presented at the SPE Annual Fall Technical Conference and Exhibition, Houston, Texas, 1-3 October.

Vogel, J. V. 1968. Inflow Performance Relationships for Solutions-Gas Drive Wells. *SPE Journal of Petroleum Technology* **20** (1): 83-92.

Wells, K.L. and Ehlig-Economides, C.A. 2005. Average Reservoir Pressure from a Horizontal Well Pressure Buildup Test. Paper IPTC 10096 presented at the International Petroleum Technology Conference, Doha, Qatar, 21-23 November.

Yoshioka, K. 2007. Detection of Water or Gas Entry into Horizontal Wells by Using Permanent Downhole Monitoring Systems. PhD dissertation, Texas A&M University, College Station, TX.

Yoshioka, K., Zhu, D., and Hill, A.D. 2007. A New Inversion Method to Interpret Profiles from Distributed Temperature and Pressure Measurements in Horizontal Wells. Paper SPE 109749 presented at the SPE Annual Technical Conference and Exhibition, Anaheim, California, 11-14 November.

Zarea, Marwan. 2010. A Comprehensive Evaluation of Reservoir Inflow and Wellbore Behavior in Intelligent Wells. Master Thesis, Texas A&M University, College Station, Tx.

VITA

NAME: Jassim Mohammed A. Almulla

PERMANENT ADDRESS: Saudi Aramco
P.O. Box 11451
Dhahran, 31311
Saudi Arabia

EDUCATION: B.S., Petroleum Engineering
University of Louisiana at Lafayette,
Lafayette, Louisiana
December, 2000

M.S., Petroleum Engineering
Texas A&M University,
College Station, Texas
May, 2007

Ph.D., Petroleum Engineering
Texas A&M University,
College Station, Texas
May, 2012